ELSEVIER

Advances in Colloid and Interface Science
81 (1999) 167–249

ADVANCES IN COLLOID AND INTERFACE SCIENCE

Contact angle measurement and contact angle interpretation

D.Y. Kwok[1], A.W. Neumann*

Department of Mechanical and Industrial Engineering, University of Toronto, 5 King's College Road, Toronto, Ontario, Canada M5S 3G8

Abstract

Recent progress in the correlation of contact angles with solid surface tensions are summarized. The measurements of meaningful contact angles in terms of surface energetics are also discussed. It is shown that the controversy with respect to measurement and interpretation of contact angles are due to the fact that some (or all) of the assumptions made in all energetic approaches are violated when contact angles are measured and processed. For a large number of polar and non-polar liquids on different solid surfaces, the liquid–vapor surface tension times cosine of the contact angle, $\gamma_{lv}\cos\theta$, is shown to depend only on the liquid–vapor surface tension γ_{lv}, and the solid–vapor surface tension γ_{sv} when the appropriate experimental techniques and procedures are used. Equations which follow these experimental patterns and which allow the determination of solid surface tensions from contact angles are discussed. Universality of these experimental contact angle patterns is illustrated; other reasons which may cause data to deviate from the patterns slightly are discussed. It is found that surface tension component approaches do not reflect physical reality. Assuming the fact that solid surface tension is constant for one and the same solid surface, experimental contact angle patterns are employed to deduce a functional relationship to be used in conjunction with Young's equation for determining solid surface tensions. The explicit form of such a relation is obtained by modifying Berthelot's rule together with experimental data; essentially constant solid surface tension values are obtained, independent of liquid surface tension and molecular structure. A new combining rule is also derived based on an expression similar to one used in molecular theory; such a combining rule

* Corresponding author. Tel.: +1-416-978-1270; fax: +1-416-978-7753.
E-mail address: neumann@me.utoronto.ca (A.W. Neumann)
[1] This paper represents, in part, the Ph.D. thesis of D.Y. Kwok. Present address: Department of Chemical Engineering Massachusetts Institute of Technology, Cambridge, MA 02139, USA. Tel.: +1-617-253-6482; fax: +1-617-258-5042; e-mail: dykwok@mit.edu

PII: S0001-8686(99)00087-6

should allow a better understanding of the molecular interactions between unlike solid–liquid pairs from like pairs. Existing static contact angles for 34 different types of solid surfaces from Zisman et al. are evaluated in terms of their solid surface tensions using experimental contact angle patterns. A FORTRAN computer program has been implemented to automate these procedures. It is found that literature contact angles do not have to be discarded completely; they can be used to determine solid surface tensions, with caution. The surface tensions for the 34 solid surfaces from Zisman et al. are also reported.

Keywords: Contact angle; Solid surface tension; Surface tension component; Combining rule; Drop shape method

Contents

1. Introduction

The determination of solid–vapor (γ_{sv}) and solid–liquid (γ_{sl}) interfacial tensions is of importance in a wide range of problems in pure and applied science. Because of the difficulties involved in measuring directly the surface tension involving a solid phase, indirect approaches are called for: Several independent approaches have been used to estimate solid surface tensions, including direct force measurements [1–9]; contact angles [10–17]; capillary penetration into columns of particle powder [18–21]; sedimentation of particles [22–25]; solidification front interaction with particles [26–33]; film flotation [34–38]; gradient theory [39–42]; Lifshitz theory of van der Waals forces [42–45]; and theory of molecular interactions [46–49]. Among these methods, contact angle measurements are believed to be the simplest.

Contact angle measurement is easily performed by establishing the tangent (angle) of a liquid drop with a solid surface at the base. The attractiveness of using contact angles θ to estimate the solid–vapor and solid–liquid interfacial tensions is due to the relative ease with which contact angles can be measured on suitably prepared solid surfaces. It will become apparent later that this seeming simplicity is, however, very misleading.

The possibility of estimating solid surface tensions from contact angles relies on a relation which has been recognized by Young [50] in 1805. The contact angle of a liquid drop on a solid surface is defined by the mechanical equilibrium of the drop under the action of three interfacial tensions (Fig. 1): solid–vapor, γ_{sv}, solid–liquid, γ_{sl}, and liquid–vapor, γ_{lv}. This equilibrium relation is known as Young's equation:

$$\gamma_{lv}\cos\theta_Y = \gamma_{sv} - \gamma_{sl} \tag{1}$$

where θ_Y is the Young contact angle, i.e. a contact angle which can be inserted

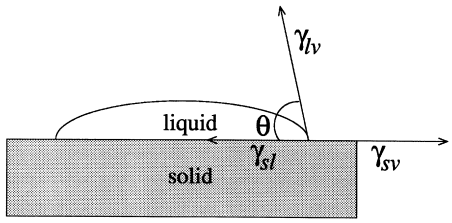

Fig. 1. Schematic of a sessile-drop contact angle system.

into Young's equation. It will become apparent later that the experimentally accessible contact angles may or may not be equal to θ_Y.

Young's Eq. (1) contains only two measurable quantities, the contact angle θ and the liquid–vapor surface tension, γ_{lv}. In order to determine γ_{sv} and γ_{sl}, an additional relation relating these quantities must be sought. Nevertheless, Eq. (1) suggests that the observation of the equilibrium contact angles of liquids on solids may be a starting point for investigating the solid surface tensions, γ_{sv} and γ_{sl}. This has inspired many studies which attempt to develop methodologies for determining solid surface tensions. A common feature of these approaches is the assumption that contact angle measurement is a trivial task.

Since γ_{lv}, γ_{sv} and γ_{sl} are thermodynamic properties of the liquid and solid, Eq. (1) implies a single, unique contact angle; in practice, however, contact angle phenomena are complicated [51–53]. In particular, the contact angle made by an advancing liquid (θ_a) and that made by a receding liquid (θ_r) are not identical; nearly all solid surfaces exhibit contact angle hysteresis, H (the difference between θ_a and θ_r):

$$H = \theta_a - \theta_r \tag{2}$$

Contact angle hysteresis can be due to roughness and heterogeneity of a solid surface. If roughness is the primary cause, then the measured contact angles are meaningless in terms of Young's equation. On very rough surfaces, contact angles are larger than on chemically identical, smooth surfaces [21]. Obviously, interpreting such angles in terms of Eq. (1) would lead to erroneous results because the contact angle would inevitably reflect surface topography, rather than exclusively surface energetics.

Because of these various complexities, models have been employed to gain a deeper understanding of the thermodynamic status of contact angles. In general, it has been found that the experimentally observed apparent contact angle, θ, may or may not be equal to the Young contact angle, θ_Y [51,52]:

1. On ideal solid surfaces, there is no contact angle hysteresis and the experimentally observed contact angle is equal to θ_Y.
2. On smooth, but chemically heterogeneous solid surfaces, θ is not necessarily equal to the thermodynamic equilibrium angle. Nevertheless, the experimental advancing contact angle, θ_a, can be expected to be a good approximation of θ_Y. This has been illustrated using a model of a vertical surface consisting of heterogeneous and smooth strips [51,52]. Therefore, care must be exercised to ensure that the experimental apparent contact angle, θ, is the advancing contact angle in order to be inserted into the Young equation. While the receding angle on a heterogeneous and smooth surface can also be a Young angle, it is usually found to be non-reproducible often because of sorption of the liquid into the solid and swelling of the solid by the liquid [54].
3. On rough solid surfaces, no such equality between θ_a and θ_Y exists: all contact angles on rough surfaces are meaningless in terms of Young's equation.

The thermodynamic equilibrium angles on rough and heterogeneous surfaces are the so-called Wenzel [55] and Cassie [56–58] angles, respectively. They are not equal to θ_Y [51,52]; furthermore, they are not experimentally accessible quantities.

There are as yet no general criteria to answer the question of how smooth a solid surface has to be for surface roughness not to have an effect on the contact angle. This and similar problems can be linked to line tension, which has its own complexities [59]. It is, therefore, of utmost importance to prepare solid surfaces as smooth as possible so that the experimental advancing angles can be a good approximation of θ_Y. In addition to these complexities, penetration of the liquid into the solid, swelling of the solid by the liquid, and chemical reactions can all play a role. For example, swelling of a solid by a liquid [54] can change the chemistry of the solid in an unknown manner and hence affect the values of γ_{sv}, and/or γ_{sl}. Therefore, it is also important to ensure that the solid surfaces are as inert as possible, in order to minimize such effects, by appropriate choice of the liquid.

Several contact angle approaches [10–17], of current interest, were largely inspired by the idea of using Young's equation for the determination of surface energetics. While these approaches are, logically and conceptually, mutually exclusive, they share, nevertheless, some basic assumptions:

1. All approaches rely on the validity and applicability of Young's equation for surface energetics from experimental contact angles.
2. Pure liquids are always used; surfactant solutions or mixtures of liquids should not be used, since they would introduce complications due to preferential adsorption.
3. The values of γ_{lv}, γ_{sv} (and γ_{sl}) are assumed to be constant during the experiment, i.e. there should be no physical or chemical reaction between the solid and the liquid.
4. The liquid surface tensions of the testing liquids should be higher than the anticipated solid surface tension.
5. The values of γ_{sv} going from liquid to liquid are also assumed to be constant, i.e. independent of the liquids used.

With respect to the first assumption, one requires the solid surfaces to be rigid, smooth and homogeneous so that Young's equation is the appropriate equilibrium condition; the experimentally observed contact angles should also be advancing contact angles. However, many attempts have been made in the literature to interpret surface energetics of solids, which are not rigid (e.g. gels [60]) and not smooth (e.g. biological surfaces [61]), in conjunction with Young's equation. Clearly, these results are open to question, since Young's equation may not be valid or applicable in these situations. With respect to the other assumptions, the solid surfaces should be as inert as possible so that effects, such as swelling and chemical reactions are minimized.

In order to assure that the experimentally measured contact angles do not violate any of the above assumptions, one requires careful experimentation and suitable methodology. However, contact angles are typically measured simply by depositing a drop of liquid on a given solid surface, and manually placing a tangent

to the drop at its base using a so-called goniometer–sessile drop technique [62,63]. Apart from the subjectivity of the technique, it normally yields contact angle accuracy of no better than $\pm 2°$. More important, the technique cannot be expected to reflect the complexities of solid–liquid interactions. It will become apparent in this paper that much of the controversy with respect to the interpretation of contact angles in terms of surface energetics lies in the fact that not enough attention is given to the readily accepted assumptions.

In this paper, the correlation of contact angles with solid surface tensions will be discussed. Section 2.1 illustrates the experimental contact angle patterns on inert solid surfaces using an automated axisymmetric drop shape analysis; these results will be contrasted with the patterns obtained on non-inert solid surfaces using a conventional goniometer–sessile drop technique in Section 2.2. By using the automated axisymmetric drop shape analysis — profile (ADSA-P) and the appropriate experimental procedures described in Section 2.3, the discrepancy between the two contact angle-patterns is shown to come from the fact that some (or all) of the widely accepted assumptions are violated, because the goniometer procedure does not have a built-in quality control mechanism. Section 2.3 illustrates the low-rate dynamic contact angle results for various solid surfaces, as obtained by ADSA-P. The universality of the contact angle patterns will be discussed in Section 2.4. and 2.5 presents a detailed discussion of the criteria for calculations of surface energetics. Equations which follow these experimental patterns and which allow the determination of solid surface tensions from contact angles will be sought in Section 3. Applications of the equation developed in Section 3 will be discussed in Section 4; contact angle data from Zisman et al. [10] on several solid surfaces will be evaluated for energetic calculations. A summary, perspective, and future development will be given, respectively, in Sections 5–7.

2. Contact angle measurement

2.1. Experimental contact angle patterns

On carefully prepared solid surfaces, Li et al. [64,65] have performed static (advancing) contact angle experiments using an automated axisymmetric drop shape analysis — profile (ADSA-P). ADSA-P [66] is a technique to determine liquid–fluid interfacial tensions and contact angles from the shape of axisymmetric menisci, i.e. from sessile as well as pendant drops. Assuming that the experimental drop is Laplacian and axisymmetric, ADSA-P finds the theoretical profile that best matches the drop profile extracted from the image of a real drop, from which the surface tension, contact angle, drop volume, surface area and three-phase contact radius can be computed. The strategy employed is to fit the shape of an experimental drop to a theoretical drop profile according to the Laplace equation of capillarity, using surface/interfacial tension as an adjustable parameter. The best fit identifies the correct surface/interfacial tension from which the contact angle can be determined by a numerical integration of the Laplace equation. Details can

be found elsewhere [67–69]. It has been found [64,65] that a contact angle accuracy of better than $\pm 0.3°$ can be obtained on well-prepared solid surfaces.

In the experiments of Li et al. [64,65], static (advancing) contact angles were measured by supplying test liquids from below the surface into the sessile drop, using a motor-driven syringe device. A hole of approximately 1 mm in the centre of each solid surface was required to facilitate such procedures. Liquid was pumped slowly into the drop from below the surface until the three-phase contact radius was approximately 0.4 cm. After the motor was stopped, the sessile drop was allowed to relax for approximately 30 s to reach equilibrium. Then three pictures of this sessile drop were taken successively at intervals of 30 s. More liquid was then pumped into the drop until it reached another desired size, and the above procedure was repeated [64]. These procedures ensure that the measured static contact angles are indeed the advancing contact angles.

Three carefully prepared solid surfaces were used in Li et al.'s study: they are FC-721-coated mica, Teflon FEP (fluorinated ethylene propylene) heat-pressed against quartz glass slides and poly(ethylene terephthalate) PET. FC-721 is a 3M 'Fluorad' brand antimigration coating designed to prevent the creep of lubricating oils out of bearings. The FC-721-coated mica was prepared by a dip-coating technique. Teflon FEP (fluorinated ethylene propylene) surfaces were prepared by a heat-pressing method. The material was cut to 2×4 cm, sandwiched between two glass slides, and heat-pressed by a jig in an oven. Poly(ethylene terephthalate) PET is the condensation product of ethylene glycol and terephthalic acid. The surface of PET films were exceedingly smooth as received and were cleaned before measurement. Details of the solid surface preparation can be found elsewhere [64].

Fig. 2 shows these contact angle results in a plot of $\gamma_{lv}\cos\theta$ vs. γ_{lv}, for a large number of pure liquids with different molecular properties. It can be seen that, for a given solid surface, $\gamma_{lv}\cos\theta$ changes smoothly and systematically with γ_{lv}. Since the solid surface tension, γ_{sv}, of a given solid surface is expected to be constant, i.e. independent of the choice of the testing liquid used, Fig. 2 implies that $\gamma_{lv}\cos\theta$ depends only on γ_{lv} at constant γ_{sv}. Replacing the solid surface from the hydrophobic FC-721 surface to the hydrophilic PET surface shifts the curve in a very regular manner. Thus, one has to conclude that the values of $\gamma_{lv}\cos\theta$ depend only on γ_{lv} and γ_{sv}, independent of any specific intermolecular forces of the liquids and solids [64,65,70]:

$$\gamma_{lv}\cos\theta = f(\gamma_{lv}, \gamma_{sv}) \tag{3}$$

where f is an as yet unknown function. Because of Young's equation, the experimental contact angle patterns in Fig. 2 imply, in light of Eq. (3), that the solid–liquid interfacial tension γ_{sl} depends only on the liquid–vapor γ_{lv} and solid–vapor γ_{sv} surface tensions: combining Young's equation with Eq. (3) yields

$$\gamma_{sv} - \gamma_{sl} = f(\gamma_{lv}, \gamma_{sv}) \tag{4}$$

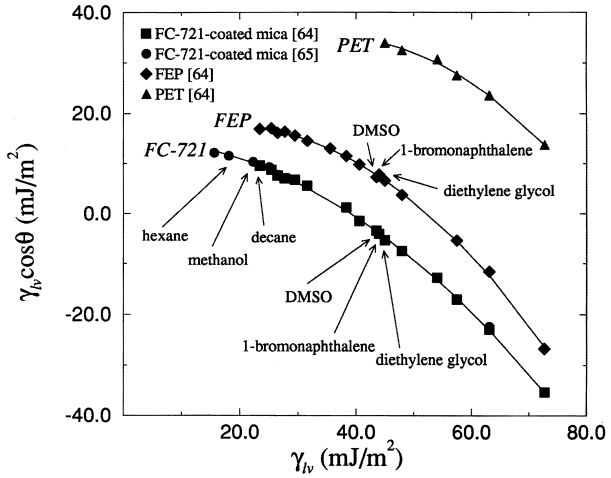

Fig. 2. $\gamma_{lv}\cos\theta$ vs. γ_{lv} for three well-prepared inert solid surfaces: FC-721-coated mica, heat-pressed Teflon FEP (fluorinated ethylene propylene), and poly(ethylene terephthalate) PET [64,65]. The smoothness suggests that $\gamma_{lv}\cos\theta$ depends only on γ_{lv} and γ_{sv}.

and hence

$$\gamma_{sl} = \gamma_{sv} - f(\gamma_{lv}, \gamma_{sv}) = F(\gamma_{lv}, \gamma_{sv}) \tag{5}$$

where F is as yet another unknown function. This is indeed in agreement with thermodynamics [71] and the thermodynamic phase rule for capillary systems [72–75] which states that there are only two degrees of freedom for such solid–liquid systems. Thus, one can simply change the contact angle by changing either γ_{lv} or γ_{sv}. While the specific intermolecular forces determine the primary surface tensions of liquids and solids, they do not have any additional and independent effects on the contact angles, in the context of Young's equation. In principle, a plot of $\cos\theta$ vs. γ_{lv}, rather than $\gamma_{lv}\cos\theta$ vs. γ_{lv}, can also be used to deduce the functional dependence of Eq. (5). Historically, a plot of $\gamma_{lv}\cos\theta$ vs. γ_{lv} has been used in conjunction with Young's equation to argue the fact that as $\gamma_{lv}\cos\theta$ increases and approaches γ_{sv}, γ_{sl} approaches zero [13,14].

It is to be noted that the experimental contact angle patterns shown in Fig. 2 do not always appear in the literature: curves far less smooth or no unique curves at all are very frequently reported (see later). Such patterns can have a variety of causes. Accurate contact angle measurements require extreme experimental care. Even very minor vibrations can cause advancing contact angles to decrease, resulting in errors of several degrees. Surface roughness can affect the contact angles and make Young's equation inapplicable. Swelling of a solid by a liquid [54] can change the chemistry of the solid and hence the values of γ_{sv} and θ in an unpredictable manner. Non-constancy of γ_{lv}, γ_{sv} and γ_{sl} during the experiment, and non-constancy of γ_{sv} from liquid to liquid can produce scatter in plots of the type of Fig. 2 easily.

It will be shown below that the present controversy with respect to the experimental contact angle patterns arises from the fact that these patterns are often complex, and cannot be unraveled by the simple goniometer techniques: an example of the experimental patterns, which are very different from those of Fig. 2 will be illustrated, simply by measuring advancing contact angles by a goniometer technique.

2.2. Experimental contact angle patterns from a goniometer

In order to compare the experimental contact angle patterns obtained by a goniometer with those by an automated ADSA-P technique shown in Fig. 2, two well-defined copolymers were selected. These copolymers were selected purposely to be not as inert as the FC-721-coated mica, Teflon FEP, and PET surfaces used by Li et al. [64,65].

Two copolymers, poly(propene-*alt*-*N*-(*n*-propyl)maleimide) and poly(propene-*alt*-*N*-(*n*-hexyl)maleimide), i.e. copolymers with different side chains [76], were used for contact angle measurements. For each copolymer, a 2% solution was prepared using tetrahydrofuran as the solvent. Silicon wafers ⟨100⟩ were selected as the substrate for the copolymer coating. The silicon wafer surfaces were obtained as circular discs of approximately 10 cm diameter and were cut into rectangular shapes of approximately 2×3 cm^2. Each rectangular silicon wafer surface was first cleaned with ethanol, acetone, and then soaked in chromic acid for at least 24 h. The cleaned wafer surfaces were rinsed with doubly-distilled water, and dried under a heat lamp before the copolymer coating. A few drops of the 2% copolymer/tetrahydrofuran solution were deposited on the dried silicon wafers inside petri glass dishes overnight; the solution spread and a thin layer of the copolymer formed on the wafer surface after tetrahydrofuran evaporated. This preparation produced good quality coated surfaces, as manifested by light fringes, due to refraction at these surfaces, suggesting that roughness is in the order of nanometers or less. It should be noted that if preparation of the solid surfaces and liquids for contact angle measurements is less careful, impurities can easily contaminate the testing liquids and solids. This would inevitably result in the contact angle measurements of contaminated liquids and solids, rather than the presumed pure liquids and solids.

Thirteen liquids were chosen in this study. Selection of these liquids was based on the following criteria: (1) liquids should include a wide range of intermolecular forces; (2) liquids should be non-toxic; and (3) the liquid surface tension should be higher than the anticipated solid surface tension [10,13,21]. They are, in the order of increasing surface tension, *cis*-decalin, 2,5-dichlorotoluene, ethyl cinnamate, dibenzylamine, dimethyl sulfoxide (DMSO), 1-bromonaphthalene, diethylene glycol, ethylene glycol, diiodomethane, 2,2′-thiodiethanol, formamide, glycerol and water.

The procedures to measure the advancing contact angles using a goniometer–sessile drop technique are the same as those typically used in the literature: a sessile drop of approximately 0.4–0.5 cm radius was formed from

above through a Teflon capillary. The three-phase contact line of the drop was then slowly advanced by supplying more liquid from above through the capillary which was always kept in contact with the drop. The maximum (advancing) contact angles were measured carefully from the left and right side of the drop and subsequently averaged. The above procedures were repeated for five drops on five new surfaces. All readings were then averaged to give an averaged contact angle.

Fig. 3 shows the contact angle results for the two copolymers from the goniometer–sessile drop measurements in a plot of $\gamma_{lv}\cos\theta$ vs. γ_{lv}. Contrary to the contact angle patterns shown in Fig. 2, considerable scatter is apparent. On a given solid, say the poly(propene-*alt*-*N*-(*n*-hexyl)maleimide) copolymer, γ_{sv}, is expected to be constant; since the values of $\gamma_{lv}\cos\theta$ here do not appear to give a smooth and systematic change with γ_{lv}, one might argue that $\gamma_{lv}\cos\theta$ cannot be a simple function g of only γ_{lv} and γ_{sv}, but has to depend also on the various specific intermolecular forces of the liquids and solids:

$$\gamma_{lv}\cos\theta = g(\gamma_{lv}, \gamma_{sv}, \text{dipole–dipole, hydrogen bonding, etc.}) \tag{6}$$

Thus, because of Young's equation, this scatter would seem to favor the stipulation of the surface tension component approaches [11,15–17,77–79] that γ_{sl} depends not only on γ_{lv} and γ_{sv}, but also on the specific intermolecular forces:

$$\gamma_{sv} - \gamma_{sl} = g(\gamma_{lv}, \gamma_{sv}, \text{dipole–dipole, hydrogen bonding, etc.}) \tag{7}$$

and hence

$$\begin{aligned}\gamma_{sl} &= \gamma_{sv} - g(\gamma_{lv}, \gamma_{sv}, \text{dipole–dipole, hydrogen bonding, etc.}) \\ &= G(\gamma_{lv}, \gamma_{sv}, \text{dipole–dipole, hydrogen bonding, etc.})\end{aligned} \tag{8}$$

where G is an unknown function. It is to be noted that while the contact angle patterns in Fig. 3 can be easily found in the literature, they do not really support the above stipulation of the surface tension component approaches [11,15–17,77–79]. In the next section, it will be shown that this scatter indeed comes from the fact that many of the experimental contact angles in Fig. 3 have violated some (or all) assumptions usually made and summarized in the Introduction. Thus, the apparent additional degrees of freedom (inferred from the scatter) do not come from the putative independent effect of intermolecular forces on the contact angles: $\gamma_{lv}\cos\theta$ can be shown to change smoothly and systematically with γ_{lv} if suitable experimental techniques and procedures are employed, such as those described below, to delete measurements which violate any of the above assumptions.

2.3. Low-rate dynamic (advancing) contact angles by ADSA-P

2.3.1. Experimental procedures

Sessile drop contact angle measurements using ADSA-P were performed dynamically, by using a motor-driven syringe to pump liquid steadily into the sessile

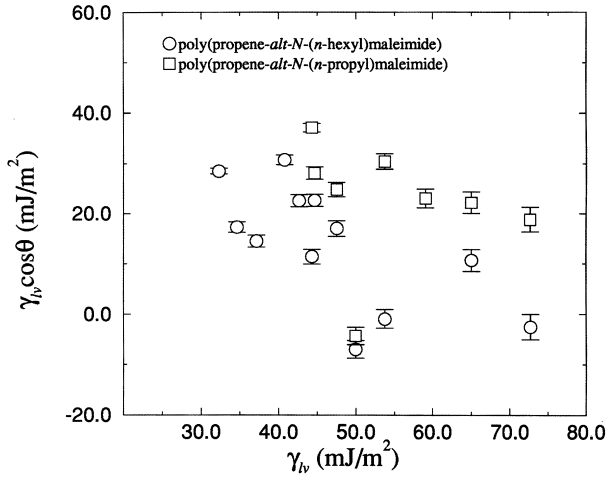

Fig. 3. $\gamma_{lv}\cos\theta$ vs. γ_{lv} for poly(propene-*alt*-*N*-(*n*-propyl)maleimide) and poly(propene-*alt*-*N*-(*n*-hexyl)maleimide) copolymers. These angles are advancing contact angles measured by a conventional goniometer technique [76]. Due to the scatter, one might argue that $\gamma_{lv}\cos\theta$ cannot be a simple function of γ_{lv} and γ_{sv}.

drop from below the surface [80]. A quartz cuvette ($5 \times 5 \times 5$ cm^3) was used to isolate the drop from its environment. It has been found that there are virtually no difference between the measured contact angles with or without a cuvette. The dynamic advancing and receding contact angle measurements can be performed, respectively, by pushing or pulling the syringe plunger of a motorized syringe mechanism, leading to an increase or decrease in drop volume. A schematic of this mechanism is shown in Fig. 4. Normally, at least five and up to 10 dynamic contact angle measurements were performed on a new solid surface each time, at velocities of the three-phase contact line in the range from 0.1 to 1.5 mm/min. It will become apparent later that low-rate dynamic contact angles in this velocity range are essentially identical to the static contact angles for relatively smooth surfaces.

In these dynamic procedures, liquid is supplied into the sessile drop from below the solid surface using a motorized-syringe device [80]. In order to facilitate such an experimental procedure, a hole of approximately 1 mm diameter in the solid surface is required. The strategy of pumping liquid from below the surface was pioneered by Oliver et al. [81,82] because of its potential for avoiding drop vibrations and for measuring true advancing contact angles without disturbing the drop profile. In order to avoid leakage between a stainless steel needle and the hole (on the surface), Teflon tape was wrapped around the end of the needle before insertion into the hole. In the literature, it is customary to first deposit a drop of liquid on a given solid surface using a syringe or a Teflon needle; the drop is then made to advance by supplying more liquid from above using a syringe or a needle in contact with the drop. Such experimental procedures cannot be used for

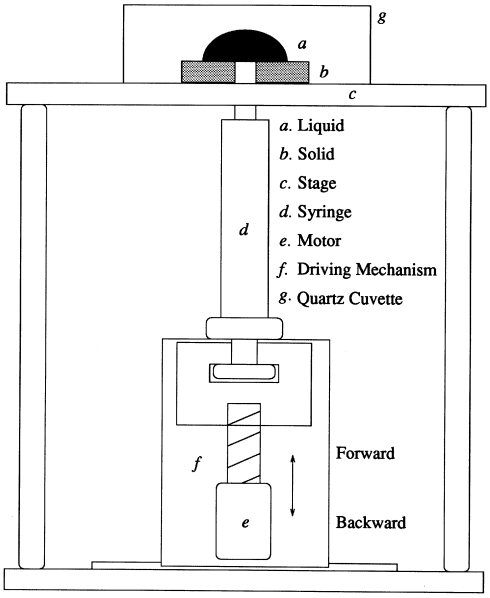

Fig. 4. Schematic of a motorized-syringe mechanism for dynamic contact angle measurements.

ADSA-P since ADSA determines the contact angles and surface tensions based on the complete and undisturbed drop profile.

In actual experiments, an initial liquid drop of approximately 0.3 cm radius was carefully deposited from above using a gas-tight Hamilton syringe with a stainless steel needle, covering the hole in the surface. This is to ensure that the drop will increase axisymmetrically in the centre of the image field when liquid is supplied from the bottom of the surface and will not hinge on the lip of the hole. The motor in the motorized-syringe mechanism was then set to a specific speed, by adjusting the voltage from a voltage controller. Such a syringe mechanism pushes the syringe plunger, leading to an increase in drop volume and hence the three-phase contact radius. A sequence of pictures of the growing drop was then recorded by the computer typically at a rate of one picture every 2 s, until the three-phase contact radius was approximately 0.5 cm or larger. For each low-rate dynamic contact angle experiment, at least 50 and up to 500 images were normally taken. Since ADSA-P determines the contact angle and the three-phase contact radius simultaneously for each image, the advancing dynamic contact angles as a function of the three-phase contact radius (i.e. location on the surface) can be obtained. In addition, the change in the contact angle, drop volume, drop surface area, and the three-phase contact radius can also be studied as a function of time. The actual rate of advancing can be determined by linear regression, by plotting the three-phase contact radius over time. For each liquid, different rates of advancing were studied, by adjusting the speed of the pumping mechanism [80].

It should be noted that measuring contact angles as a function of the three-phase contact radius has an additional advantage: the quality of the surface is observed indirectly in the measured contact angles. If a solid surface is not very smooth, irregular and inconsistent contact angle values will be seen as a function of the three-phase contact radius. When the measured contact angles are essentially constant as a function of surface location, the mean contact angle for a specific rate of advancing can be obtained by averaging the contact angles, after the three-phase contact radius reaches 0.3–0.5 cm (see later). The purpose of choosing these relatively large drops is to avoid any possible line tension effects on the measured contact angles [59,83,84].

2.3.2. Inert (non-polar) surfaces: FC-722-coated mica surface

A fluorocarbon, FC-722, dip-coated onto mica surfaces was chosen as the substrate for the dynamic contact angle experiments. FC-722 is a fluorochemical coating available from 3M and is chemically very similar to the FC-721 used in earlier studies. They were prepared by the same dip-coating procedures described elsewhere [64,65], using freshly cleaved mica surfaces. The mica surfaces were obtained originally as sheets.

Before dip-coating, the mica surfaces were prepared in the following procedures: (1) mica sheets were cut into small mica plates of approximately 2×3 cm^2; (2) a hole of approximately 1 mm in diameter was made, by drilling, in the centre of each mica surface; (3) each mica surface was then cleaved by a sharp knife, cleaned with ethanol, and acetone, and dried in the air before dip-coating.

Seventeen liquids were chosen for the contact angle measurements [80]. The surface tensions of these liquids were determined independently by applying ADSA-P to pendant drops at room temperature, 23.0 ± 0.5°C. Selection of these liquids was based on the criteria described in the preceding section.

Fig. 5 shows a typical example of a low-rate dynamic contact angle experiment: water on a FC-722 surface. As can be seen in this figure, increasing the drop volume V linearly from 0.18 cm^3 to 0.22 cm^3, by the motorized-syringe mechanism, increases the contact angle θ from approximately 108° to 119° at essentially constant three-phase contact radius R. This is due to the fact that even carefully putting an initial drop from above on a solid surface can result in a contact angle somewhere between advancing and receding. Therefore, it takes addition of a certain amount of liquid for the initial drop front to start advancing. Further increase in the drop volume causes the three-phase contact line to advance, with θ essentially constant as R increases. Increasing the drop volume in this manner ensures the measured θ to be an advancing contact angle. The rate of advancing for this experiment can be determined by linear regression from the linear region of the plot of the three-phase contact radius over time: It was found that the drop periphery was being advanced at a rate of 0.14 mm/min, in the specific example given in Fig. 5. The regression coefficient for the rate of advancing was found to be 0.999; this indicates that the rate of change of the three-phase contact line was very constant, even though it was controlled simply by manipulating the drop volume.

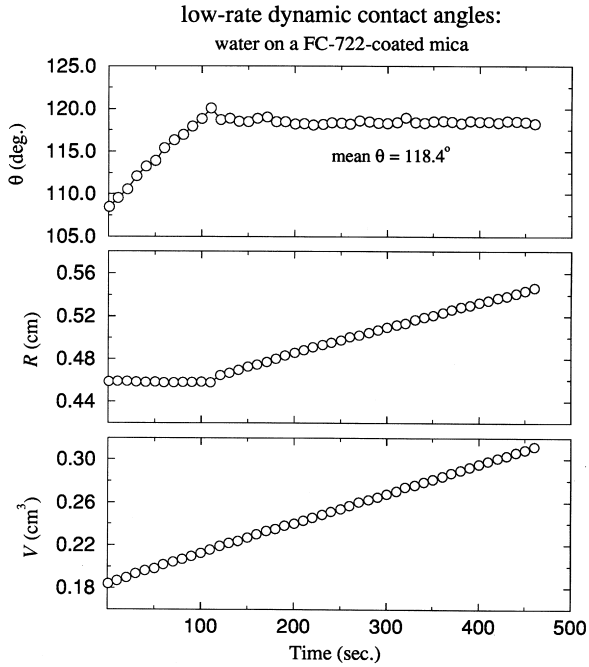

Fig. 5. Low-rate dynamic contact angles of water on a FC-722-coated mica [80].

As can be seen in Fig. 5, the measured contact angles are essentially constant as R increases. This indicates good surface quality of the solid used in this experiment. It turns out that averaging the measured contact angles after R reaches 0.50 cm is convenient, since the drop is guaranteed to be in the advancing mode and that line tension effects are negligible [59,83,84]. Averaging the measured contact angles, after R reaches 0.50 cm, yields a mean contact angle of 118.4° for water. While a three-phase contact radius of 0.50 cm may seem to be an arbitrary value, it turns out that there is virtually no difference between averaging θ for R larger than 0.48 cm and 0.54 cm; the contact angles are essentially constant after $R = 0.50$ cm. Similar results were also obtained for other liquids [80].

Dynamic/static contact angle experiments have also been performed: A liquid drop is first selected to advance at a specific rate of advancing and then stopped, while a sequence of images is recorded. A typical experiment is shown in Fig. 6 for *cis*-decalin. As drop volume increases from 0.05 cm^3 to 0.07 cm^3, the three-phase contact line advances from approximately 0.36 cm to 0.41 cm at a rate of 0.41 mm/min. A sequence of drop images was acquired after the motor was stopped at $R = 0.41$ cm. As can be seen in Fig. 6, the contact angle is independent of the slow rate of advancing, suggesting that the low-rate dynamic contact angle θ_{dyn} is identical to the static contact angle θ_{stat}. This result re-confirms validity of the experimental protocol used by Li et al. [64,65] to measure static contact angles and

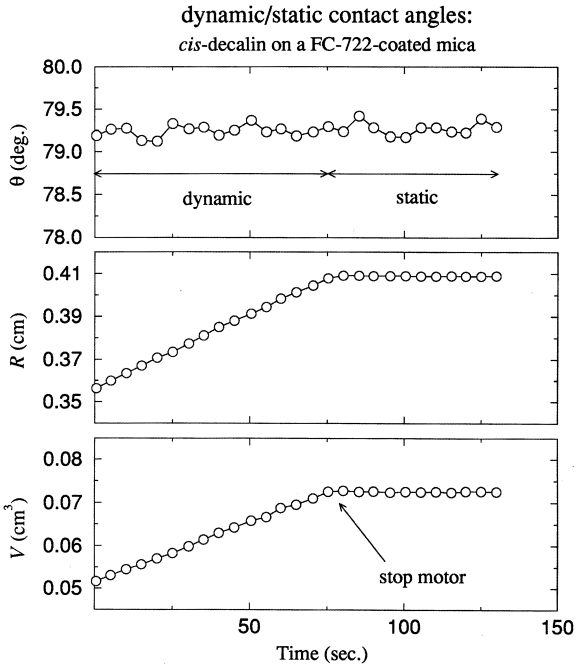

Fig. 6. Dynamic and static contact angles of *cis*-decalin on a FC-722-coated mica [80]. This result suggests that the low-rate dynamic contact angle is identical to the static angle.

is also in good agreement with recent work to determine low-rate dynamic contact angles by the automated capillary rise technique [85,86].

With each liquid, ten different measurements (i.e. ten different rates of advancing on ten new surfaces) were performed [80]. It was found that these dynamic contact angles are essentially independent of the velocity of the three-phase contact line, as is, in principle, obvious from Fig. 6. Since the low-rate dynamic contact angles are essentially independent of the velocity of the three-phase contact line, a mean dynamic contact angle for each pure liquid was determined by averaging the contact angles at the ten different rates of advancing.

Fig. 7 shows all experimental contact angle results at very slow motion of the three-phase contact line in a plot of $\gamma_{lv}\cos\theta$ vs. γ_{lv}. This result reconfirms the finding of Li et al. [64,65] shown in Fig. 2 that, at constant γ_{sv}, $\gamma_{lv}\cos\theta$ changes smoothly with γ_{lv}, independent of the liquid properties. Clearly, if there were any additional and independent effects of intermolecular forces on the contact angles, the data points for the polar liquids (1-pentanol, 1-decanol, DMSO, 2,2′-thiodiethanol, diethylene glycol, ethylene glycol, glycerol, and water) in Fig. 7 would not fall completely on a smooth curve along with the non-polar liquids. It can be seen that the data point for 1-pentanol is slightly below the curve; 1-decanol is again slightly below; DMSO is above and ethylene glycol is on the curve: there is

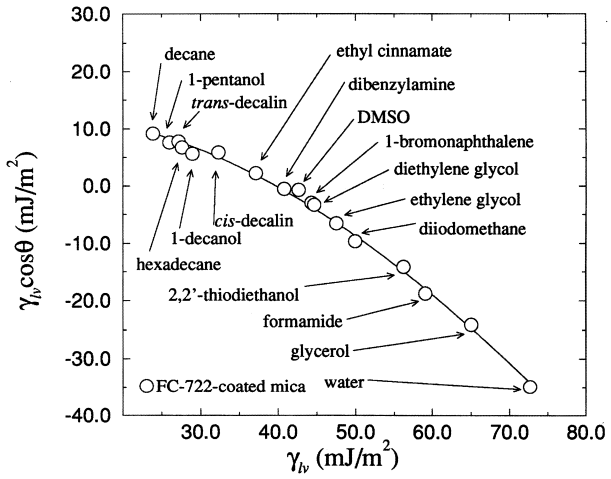

Fig. 7. $\gamma_{lv}\cos\theta$ vs. γ_{lv} for the dynamic contact angles of the 17 liquids on a FC-722-coated mica. This result reconfirms the finding of Li et al. shown in Fig. 2 that at constant γ_{sv}, $\gamma_{lv}\cos\theta$ changes smoothly with γ_{lv}, independent of other liquid properties.

no evidence of any systematic deviation of the polar liquids away from such a curve. This question will also be addressed in Section 2.4.1.

It should be noted that in these low-rate dynamic contact angle experiments, images of an advancing drop (and hence information, such as surface tension and contact angle) are recorded continuously as drop volume is steadily increased from below the surface. The procedures used here are different from those by Li et al. [64,65] in that the contact angles measured by Li et al. were static angles, i.e. contact angles at zero velocity of the three-phase contact line.

2.3.3. Non-inert (polar) surfaces: poly(propene-alt-N-(n-hexyl)maleimide) and poly(propene-alt-N-(n-propyl)maleimide)

Experience has shown that non-polar surfaces, such as Teflon and fluorocarbons, often are quite inert with respect to many liquids; however, polar surfaces often are less inert and hence may show different contact angle patterns, due to such causes as chemical reaction and/or swelling and dissolution of the solid by the liquid. Since low-rate dynamic contact angle experiments when interpreted by ADSA-P have many advantages over the conventional way of manually putting tangents to the sessile drops, ADSA-P is employed here to measure low-rate dynamic contact angles on the copolymers, poly(propene-*alt*-*N*-(*n*-propyl)maleimide) and poly(propene-*alt*-*N*-(*n*-hexyl)maleimide), in order to elucidate the discrepancies between the results in Figs. 2 and 7 on the one hand, and those in Fig. 3 by a goniometer on the other. It will become apparent that a goniometer technique is liable to produce a mixture of meaningful and meaningless angles, with no criteria to distinguish between the two. If one disregards the meaningless angles to be identified by dynamic ADSA measurements, the results are in harmony with those patterns shown in Figs. 2 and 7, as will be shown below.

Eight liquids were selected for the contact angle measurements on poly(propene-*alt*-*N*-(*n*-propyl)maleimide) and 13 liquids on poly(propene-*alt*-*N*-(*n*-hexyl)maleimide). The chemical structure of these copolymers has been described elsewhere [76]. Silicon wafer ⟨100⟩ was again selected as the substrate. They were obtained as circular discs of approximately 10 cm diameter and were cut into rectangular size of approximately 2×3 cm^2. The general procedures to prepare the solid surfaces are similar to those described in Section 2.2. Before soaking the rectangular wafer surfaces into chromic acid, a hole of approximately 1 mm diameter was made by drilling, using a diamond drill bit from Lunzer (New York; SMS-0.027). For each copolymer, a 2% solution was prepared using tetrahydrofuran as the solvent. A few drops of the 2% copolymer/tetrahydrofuran solution were deposited on the dried silicon wafers inside petri glass dishes overnight; the solution spread and a thin layer of the copolymer formed on the wafer surface after tetrahydrofuran evaporated. This procedure produced good quality coated surfaces. Such polymer-coated surfaces have been studied by Atomic Force Microscopy [87]. It was found that surface roughness of the surfaces prepared by this procedure is in the order of nanometer.

Fig. 8 shows a typical example of water on the poly(propene-*alt*-*N*-(*n*-propyl)maleimide) copolymer. As described above, in order to avoid that the drop

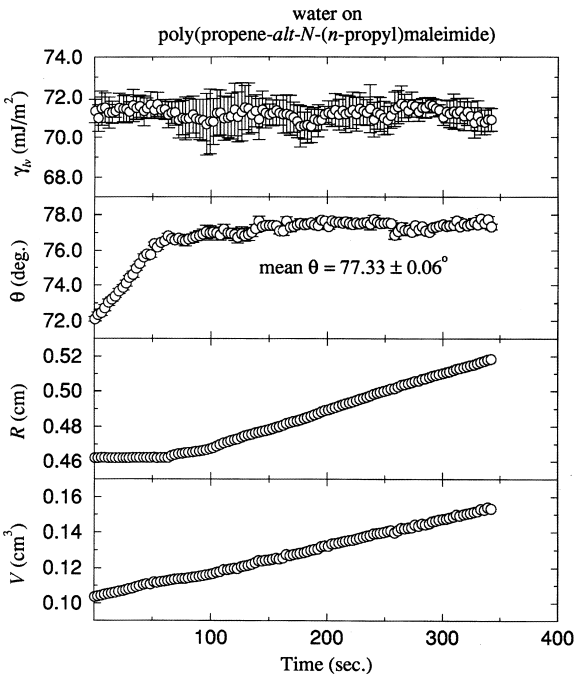

Fig. 8. Low-rate dynamic contact angles of water on a poly(propene-*alt*-*N*-(*n*-propyl)maleimide) copolymer [76].

hinges at the edge of the hole, a small drop is deposited from above, covering the hole completely. This leads to an initial contact angle different from the advancing angle: increasing the drop volume, V, linearly from 0.10 cm^3 to approximately 0.12 cm^3 increases the apparent contact angle, θ, from approximately 72° to 77° at essentially constant three-phase radius, R. This is due to the fact that even carefully putting an initial water drop from above on a solid surface can result in a contact angle somewhere between advancing and receding. This effect can be pronounced for liquids, such as water, which evaporate fast. Thus, it takes time for the initial drop front to start advancing. Further increase in the drop volume causes the three-phase contact line to advance, with θ essentially constant as R increases. Increasing the drop volume in this manner ensures the measured θ to be an advancing contact angle. In this specific example, the measured contact angles are essentially constant as R increases. This indicates good quality of the surfaces used. A mean contact angle of 77.33 $\pm$ 0.06° was obtained for this experiment. A total of nine experiments at different rates of advancing were performed, each on a newly prepared surface. Since the contact angle results of water at different rates of advancing were found to be essentially constant [76], they were averaged and resulted in a final value of 77.51 $\pm$ 0.27°.

Another contact angle result is shown in Fig. 9 for glycerol on the same

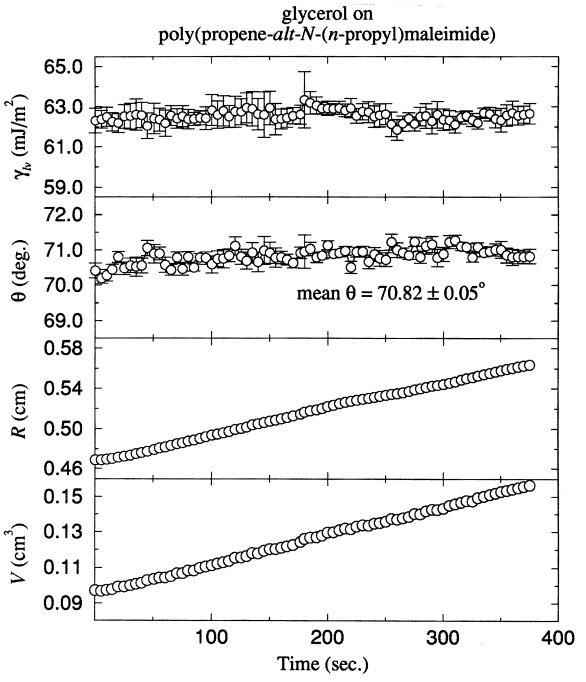

Fig. 9. Low-rate dynamic contact angles of glycerol on a poly(propene-*alt*-*N*-(*n*-propyl)maleimide) copolymer [76].

copolymer. Because the contact angles are essentially constant for all experiments, they can be averaged, resulting in a mean contact angle of 70.82 ± 0.05° at a rate of advancing of 0.16 mm/min. Similar results were also obtained for 2,2′-thiodiethanol and 1-bromonaphthalene [76]. For each liquid, at least 5 and up to 10 different experiments (for different rates of advancing) were performed.

Unfortunately, not all liquids yield essentially constant advancing contact angles. Fig. 10 shows the results of formamide on the same copolymer. It can be seen that as drop volume increases initially, contact angle increases from 60° to 63° at essentially constant three-phase radius. As the drop volume continues to increase, θ suddenly decreases to 60° and the three-phase contact line starts to move. As R increases further, the contact angle decreases slowly from 60° to 54°. The surface tension-time plot indicates that the surface tension of formamide decreases with time. This suggests that dissolution of the copolymer occurs, causing γ_{lv} and to change from that of the pure liquid. Similar behavior can also be observed in other experiments [76]. It is an important question to ask which contact angles one should use for the interpretation in terms of surface energetics. Since chemical or physical reactions, such as polymer dissolution change the liquid–vapor, solid–vapor and solid–liquid interface (interfacial tensions) in an unknown manner, the contact angle data in Fig. 10 should be disregarded for the interpretation in terms of

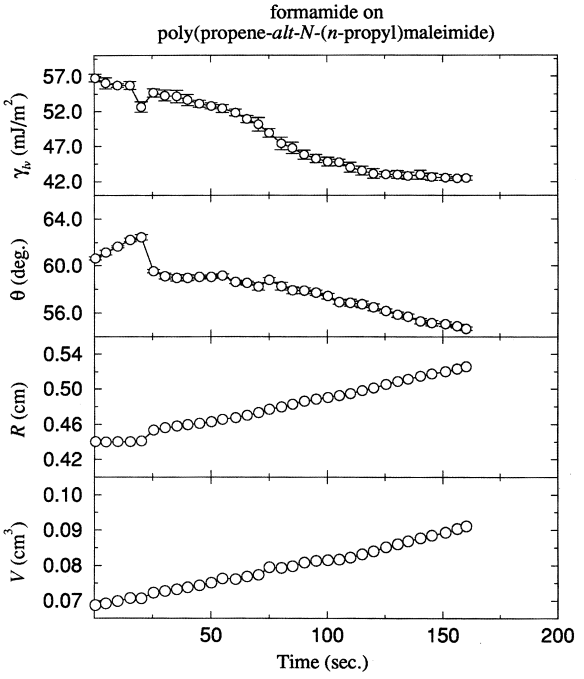

Fig. 10. Low-rate dynamic contact angles of formamide on a poly(propene-*alt*-*N*-(*n*-propyl)maleimide) copolymer [76].

surface energetics. The criteria for rejecting angles for calculations of solid surface tensions will be discussed in detail in Section 2.5. Obviously, it is virtually impossible for goniometer measurements to detect the complexities shown in Fig. 10, e.g. the decrease in γ_{lv}. Thus, the contact angle obtained from a goniometer for this and similar solid–liquid systems cannot be meaningful.

The results of ethylene glycol are shown in Fig. 11. It can be seen that the contact angle increases slowly from 54° to 57° as the three-phase contact line advances from 0.46 cm to 0.54 cm. While the cause of this increase in the contact angle is unclear, it is suspected that the operative solid–liquid interfacial tension is changed slowly due to physico-chemical reaction: according to Young's equation, if the values of γ_{lv} and γ_{sv}, are constant, a change in the contact angle must be a consequence of a change in γ_{sl}. It should be noted that the observed trends in the contact angle may well start immediately after drop formation, not only after the measurement procedure was set in motion. Also, there is no reason to suspect that the change of contact angle with time (or radius) would cease once the measurement was terminated. More likely, such trends would continue. Because there is no unique apparent contact angle and it is unclear whether or not the solid–liquid interfacial tension will remain constant and whether Young's equation is applicable, these angles should be excluded from the interpretation in terms of surface

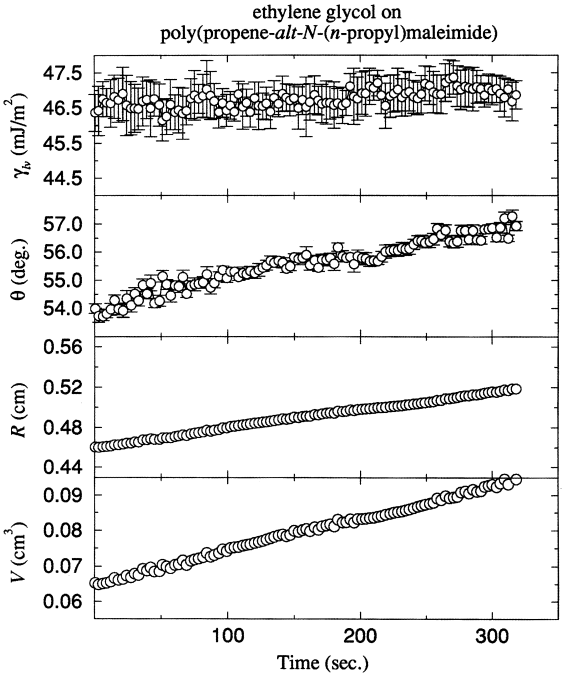

Fig. 11. Low-rate dynamic contact angles of ethylene glycol on a poly(propene-*alt*-*N*-(*n*-propyl)maleimide) copolymer [76].

energetics. However, one might consider averaging the contact angles larger than $R = 0.48$ cm, since γ_{lv} seems to be constant and since the contact angle error after averaging would not be very large, i.e. $\theta = 55.74 \pm 0.63°$. It should be noted that such averaging is not allowed: apart from the experimental reasons given above, the question of whether averaging over some data is allowed or not has firm quantitative answers based on the laws of statistics. The main fact is that the statistical analysis rejects 'averaging' of the above contact angle data over time by a very large margin [76].

While the contact angle data of formamide, diiodomethane, ethylene glycol, and diethylene glycol for poly(propene-*alt*-*N*-(*n*-propyl)maleimide) should be disregarded, the contact angles of water, glycerol, 2,2′-thiodiethanol, and 1-bromonaphthalene can be used for the interpretation in terms of surface energetics.

A similar study was conducted for a second copolymer, poly(propene-*alt*-*N*-(*n*-hexyl)maleimide). It was found that only the advancing contact angles of water, glycerol, diethylene glycol, and *cis*-decalin are essentially constant [76]. The remaining liquids, formamide, 2,2′-thiodiethanol, diiodomethane, ethylene glycol, 1-bromonaphthalene, dimethyl sulfoxide (DMSO), dibenzylamine, ethyl cinnamate, and 2,5-dichlorotoluene all show very complex contact angle patterns which have to be excluded from the interpretation in terms of surface energetics and testing of approaches for interfacial tensions.

A different contact angle experiment is shown in Fig. 12 for diiodomethane on the poly(propene-*alt*-*N*-(*n*-hexyl)maleimide): initially the apparent drop volume, as perceived by ADSA-P, increases linearly, and the contact angle increases from 88° to 96° at essentially constant three-phase radius. Suddenly, the drop front jumps to a new location as more liquid is supplied into the sessile drop. The resulting contact angle decreases sharply from 96° to 88°. As more liquid is supplied into the sessile drop, the contact angle increases again. Such slip/stick behavior could be due to non-inertness of the surface. Phenomenologically, an energy barrier for the drop front exists, resulting in sticking, which causes θ to increase at constant R. However, as more liquid is supplied into the sessile drop, the drop front possesses enough energy to overcome the energy barrier, resulting in slipping, which causes θ to decrease suddenly. It should be noted that as the drop front jumps from one location to the next, it is unlikely that the drop will remain axisymmetric. Such a non-axisymmetric: drop will obviously not meet the basic assumptions underlying ADSA-P, causing possible errors, e.g. in the apparent surface tension and drop volume. This can be seen from the discontinuity of the apparent drop volume and apparent surface tension with time as the drop front sticks and slips. Similar behavior can also be observed in other experiments [76,88]. Obviously, the observed contact angles cannot all be Young contact angles, since γ_{lv}, γ_{sv} (and γ_{sl}) are constants, so that because of Young's equation, θ ought to be a constant. In addition, it is difficult to decide unambiguously at this moment whether or not Young's equation is applicable at all because of lack of understanding of the slip/stick mechanism. Therefore, these contact angles should not be used for the interpretation in terms of surface energetics.

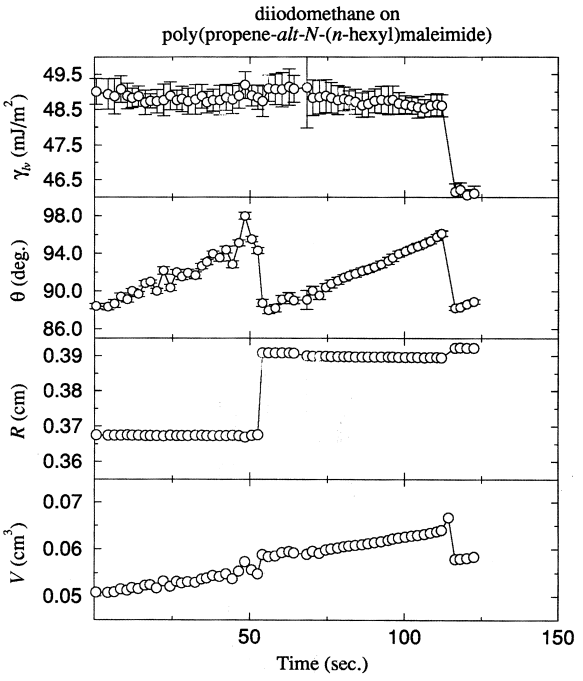

Fig. 12. Low-rate dynamic contact angles of diiodomethane on a poly(propene-*alt*-*N*-(*n*-hexyl)maleimide) copolymer [76].

While pronounced cases of slip/stick behavior can indeed be observed by the goniometer, it is virtually impossible to record the entire slip/stick behavior manually. In this case, the goniometer contact angle can be very subjective, depending on the skill of the experimentalist. It is expected that a contact angle thus recorded by the goniometer should agree with the maximum angles obtained by ADSA-P. Indeed, a contact angle of 98° was observed, in reasonable agreement with the maxima in the entire slip/stick pattern of the ADSA-P results ($\theta \approx 96°$ in Fig. 12). In cases where the liquid–vapor surface tension of the sessile drop decreases due to, e.g. dissolution of the surface, only ADSA can detect changes in the liquid–vapor surface tension. The distinctions and differentiations made by ADSA-P are not possible in a goniometer study. Thus, circumspection is necessary in the decision whether or not experimental contact angles can be used in conjunction with Young's equation; contact angles from a conventional goniometer–sessile drop technique may produce contact angles which do not fulfil the basic assumptions made in all surface energetic approaches [10–17], e.g. constancy of γ_{lv} and applicability of Young's equation already mentioned in the Introduction. These various assumptions will be discussed in detail in Section 2.5.

A comparison of the angles measured here and those by the goniometer technique had been made. It was found that the goniometer angles correspond very

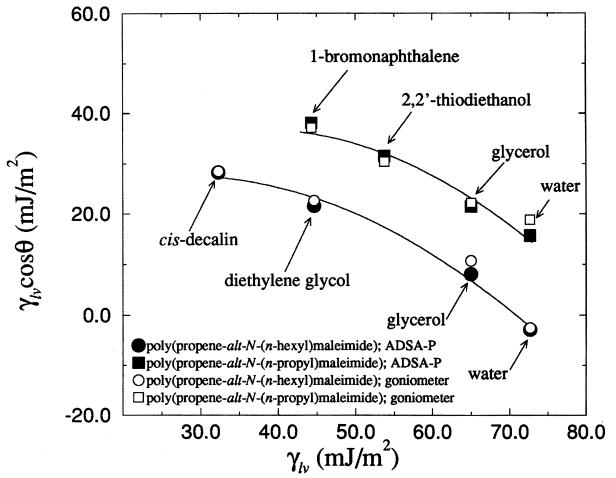

Fig. 13. $\gamma_{lv}\cos\theta$ vs. γ_{lv} for the poly(propene-*alt*-*N*-(*n*-propyl)maleimide) and poly(propene-*alt*-*N*-(*n*-hexyl)maleimide) copolymers [76]. Fig. 3 changes drastically upon elimination of the angles shown to be meaningless using the dynamic contact angle procedures by ADSA-P.

well with those of ADSA-P only in situations where the contact angles are constant; in cases where complexities of contact angles arise, the goniometer contact angles correspond only to the maxima of the angles from ADSA-P. The picture emerging in Fig. 3 changes drastically upon elimination of the angles shown to be meaningless in the ADSA-P study, see Fig. 13. The curves in Fig. 13 are in harmony with the results obtained for more inert polar and non-polar surfaces in Figs. 2 and 7. Again, it can be concluded that $\gamma_{lv}\cos\theta$ changes smoothly and systematically with γ_{lv} at constant γ_{sv}. Because of Young's equation, a relation of the form of Eq. (5) can be deduced:

$$\gamma_{sl} = F(\gamma_{lv}, \gamma_{sv}) \tag{5'}$$

Thus, the experimental procedures and techniques used are crucial in the collection of contact angle data for surface energetics; conventional goniometer techniques may produce contact angles which violate the basic assumptions made in all surface energetic approaches. In other words, the most serious shortcoming of goniometer studies is not subjectivity and lack of accuracy, but inability to distinguish between meaningful and meaningless contact angle measurements. A recent study [89] has shown that using the above dynamic procedures with a simple polynomial fit to sessile drop images may also allow one to identify meaningless and meaningful contact angles.

2.3.4. Other non-polar and polar surfaces

Similarly, low-rate dynamic contact angles of a large number of liquids were studied extensively on various solid surfaces. They are FC-722-coated silicon wafer [89], FC-725-coated silicon wafer [90], poly(*n*-butyl methacrylate) P*n*BMA [91],

polystyrene PS [92], poly(styrene-*alt*-(hexyl/10-carboxydecyl(90/10)maleimide)) [93], poly(methyl methacrylate/*n*-butyl methacrylate) P(MMA/*n*BMA) [94], poly(methyl methacrylate) PMMA [95], poly(propene-*alt*-*N*-methylmaleimide) [89]. Details with respect to solid surface preparation and experimental results have been given elsewhere [89–95].

Again, it was found that not all contact angles can be used for energetic purposes. For example, slip/stick of the three-phase contact line, γ_{lv} decreases, and θ decreases or increases as the drop front advances, and dissolution of the polymers by the liquids were observed. The meaningful angles for these polymers

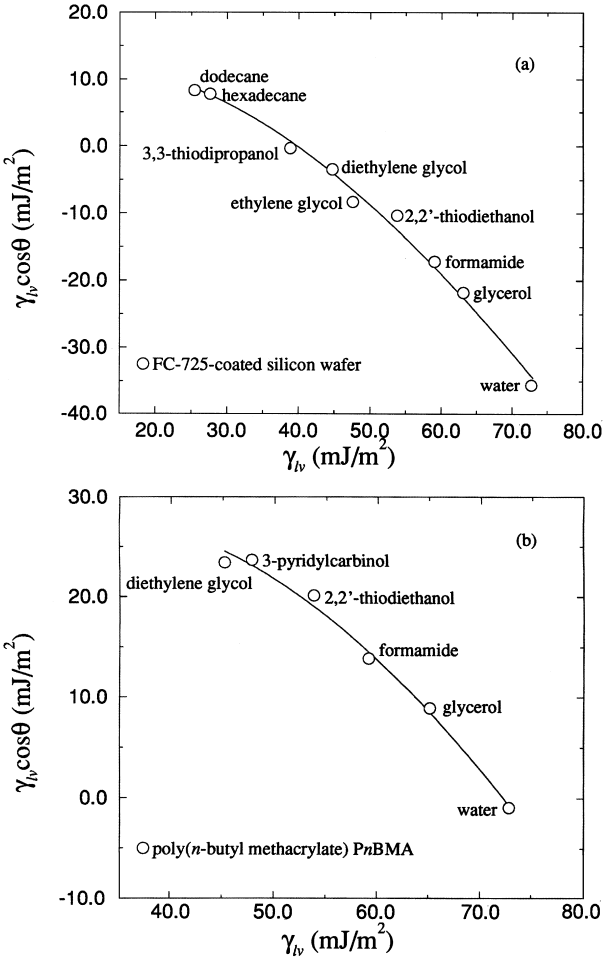

Fig. 14. $\gamma_{lv}\cos\theta$ vs. γ_{lv} for (a) FC-725-coated. silicon wafer [90], (b) poly(*n*-butyl methacrylate) P*n*BMA [91], (c) polystyrene PS [92], (d) poly(styrene-*alt*-(hexyl/10-carboxydecyl(90/10)maleimide)) [93], (e) poly(methyl methacrylate/*n*-butyl methacrylate) P(MMA/*n*BMA) [94], (f) poly(methyl methacrylate) PMMA [95], and (g) poly(propene-*alt*-*N*-(*n*-alkyl)maleimide) [89].

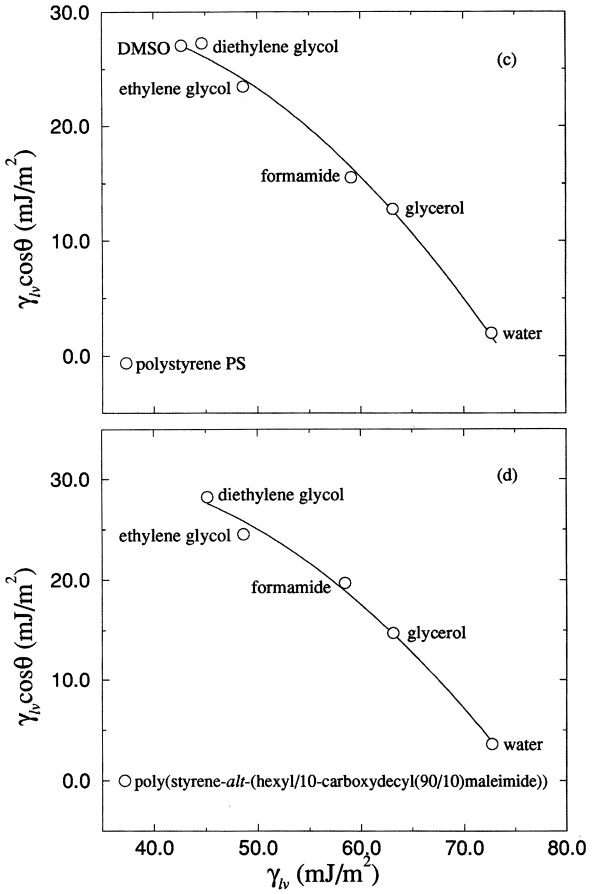

Fig. 14. Continued

(copolymers) are plotted in Fig. 14, in plots of $\gamma_{lv}\cos\theta$ vs. γ_{lv}. For a given solid surface, γ_{sv} is expected to be constant and these results suggest that $\gamma_{lv}\cos\theta$ changes smoothly and systematically with γ_{lv}. Changing the solid surface (and hence γ_{sv}) shifts the curves in a regular manner: intermolecular forces do not have any additional and independent effects on the contact angles. The universality of these contact angle patterns will be discussed in the next section.

2.4. Universality of contact angle patterns

In addition to ADSA-P, the capillary rise at a vertical plate technique [85,86,96] is also suitable for the determination of low-rate dynamic contact angles. Since the capillary rise at a vertical plate technique has been automated [96] to perform various dynamic advancing and receding contact angle measurements at immersion

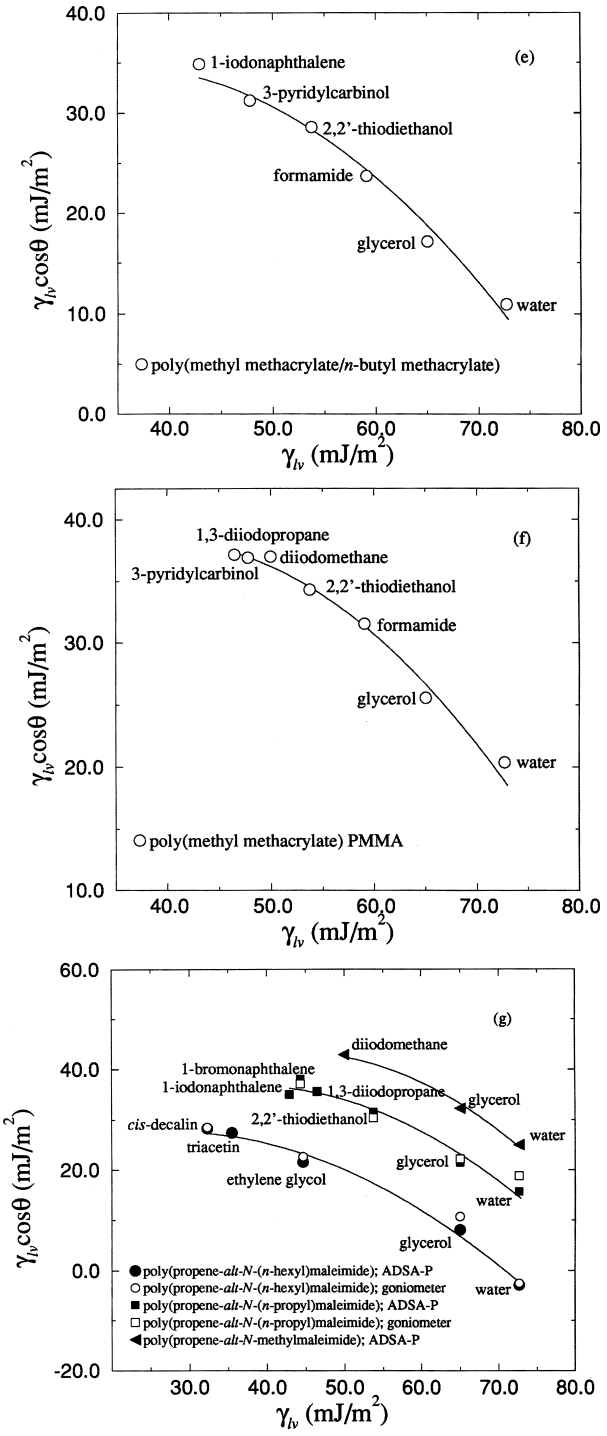

Fig. 14. Continued

speeds ranging from 0.008 to 0.9 mm/min, measurements can be and have been performed [85,86] under dynamic conditions closely resembling those in the ADSA-P experiments. The capillary rise experiments are performed by immersing a vertical (plate) solid surface into the liquid, at a constant (slow) speed; during the immersion, motion of the three-phase contact line along the vertical solid surface is always monitored. The task of measuring a contact angle is reduced to the measurement of a length (capillary rise), which can be performed optically with a high degree of accuracy. In several instances, the capillary rise technique has been employed on relatively inert and well-prepared surfaces: FC-721-coated mica [86], heat-pressed Teflon FEP [86], hexatriacontane [51,97], and cholesteryl acetate [51,98]. The FC-721 and FEP surfaces were prepared, respectively, by a dip-coating technique and a heat-pressing technique [64]. Hexatriacontane and cholesteryl acetate were produced by vapor deposition in a vacuum [51,97,98]; the surface quality was found to be so good that there was no contact angle hysteresis when water was used. It has been found that the contact angles determined from ADSA-P and the capillary rise at a vertical plate technique are virtually identical for the same solid–liquid systems [85,86].

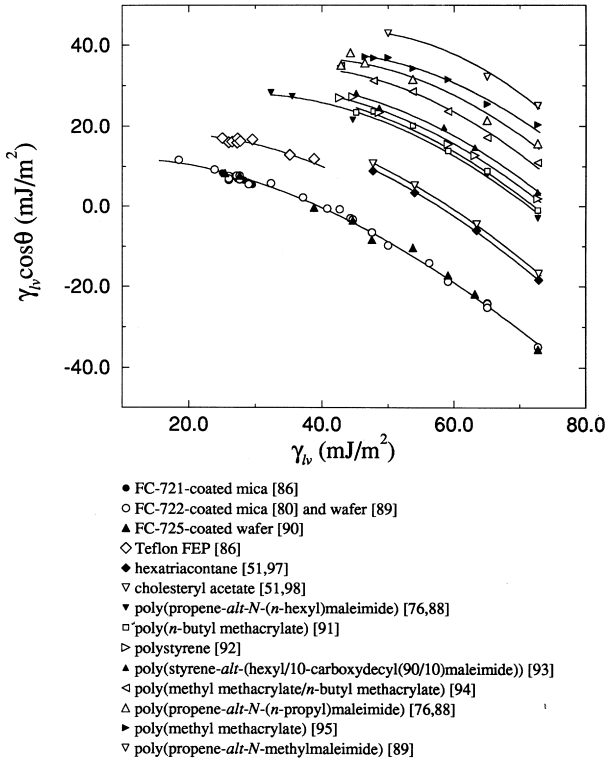

Fig. 15. $\gamma_{lv}\cos\theta$ vs. γ_{lv} for various solid surfaces.

In order to illustrate the universality of the contact angle patterns, Fig. 15 shows recent dynamic contact angles for various solids measured by the capillary rise technique and those by ADSA-P: FC-721-coated mica [86], FC-722-coated mica [80] and silicon wafer [89], FC-725-coated silicon wafer [90], heat-pressed Teflon FEP [86], hexatriacontane [51,97], cholesteryl acetate [51,98], poly(propene-*alt*-*N*-(*n*-hexyl)maleimide) [76,88], poly(*n*-butyl methacrylate) P*n*BMA [91], polystyrene PS [92], poly(styrene-*alt*-(hexyl/10-carboxydecyl(90/10)maleimide)) [93], poly(methylmethacrylate/*n*-butyl methacrylate) P(MMA/*n*BMA) [94], poly(propene-*alt*-*N*-(*n*-propyl)maleimide) [76,88], poly(methyl methacrylate) PMMA [95] and poly(propene-*alt*-*N*-methylmaleimide) [89]. Details of the solid surface preparation can be found elsewhere [51,76,80,86,88–95,97,98]. The ADSA-P (low-rate) dynamic contact angles were established also by the procedures developed in the preceding section. Again, the results in Fig. 15 suggest that the values of $\gamma_{lv}\cos\theta$ change systematically with γ_{lv} in a very regular fashion, from the hydrophobic hydrocarbon surfaces to the hydrophilic poly(propene-*alt*-*N*-methylmaleimide) surface, and that the patterns are independent of the experimental technique on the one hand and liquid structure on the other. Overall, the regularity of the contact angle patterns is remarkable.

For a given solid surface, γ_{sv} is assumed — reasonably — to be constant; the results suggest that $\gamma_{lv}\cos\theta$ depends only on γ_{lv}. Changing the solid surface (and hence γ_{sv}) shifts the curve in a very regular manner. Overall, these experimental results suggest that $\gamma_{lv}\cos\theta$ depends only on γ_{lv} and γ_{sv} [see Eq. (3)] where f is as yet an unknown function. The specific intermolecular forces of the liquids and solids, which give rise to the surface tensions, do not have additional and independent effects on the contact angles. Thus, one can change the contact angle, and because of Young's equation, the solid–liquid interfacial tension, by the simple mechanism of changing either the liquid or the solid. Combining Eq. (3) with Young's equation, we can express γ_{sl} as another unknown function F of only γ_{lv} and γ_{sv}, allowing a search for an equation in the form of Eq. (5). This is called an equation-of-state relation, as a relation involving intensive properties [99]. It should be noted that equations of this form have been in the literature for a long time, e.g. Antonow's [100] and Berthelot's [101] rules (see later).

2.4.1. Reasons of deviation from smoothness

As Fig. 15 stands, on one and the same solid surface, there are minor deviations of some contact angle data from the curves and one might wish to argue that intermolecular forces could still have some independent effects on the contact angles. This question will be addressed here, by focusing on the contact angle data of three chemically similar methacrylate polymers.

Fig. 16 shows a plot of $\gamma_{lv}\cos\theta$ vs. γ_{lv} curves for the P*n*BMA, P(MMA/*n*BMA), and PMMA polymers. As can be seen in this figure, there are slight deviations of the data points from the curves; however, it is not apparent that these deviations are systematic and are caused by any independent effects of intermolecular forces on the contact angles: For example, in the case of 3-pyridylcarbinol with γ_{lv} of approximately 48.0 mJ/m^2, the data point on the PMMA curve appears to be

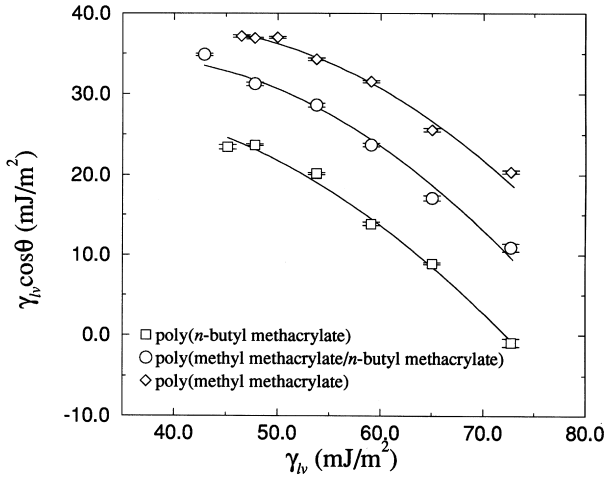

Fig. 16. $\gamma_{lv}\cos\theta$ vs. γ_{lv} for three methacrylate polymer-coated silicon wafer surfaces.

slightly higher, while the point on the P(MMA/*n*BMA) is slightly lower and the one for P*n*BMA slightly higher again. There is no evidence for any systematic variation, for this and other liquids. Clearly, if there were a deviation due to specific intermolecular forces, one would, at the most, expect a monotonous change of the deviation when going from PMMA to P(MMA/*n*BMA) to P*n*BMA. Obviously, this does not mean that intermolecular forces are irrelevant; they determine the primary surface tensions of the liquids and solids.

To keep matters in perspective, it has to be realized that the curves in Fig. 16 would have to be considered completely smooth if a conventional goniometer technique with $\pm 2°$ contact angle accuracy had been used. Furthermore, the fact that an equilibrium spreading pressure π_e

$$\pi_e = \gamma_s - \gamma_{sv} \tag{9}$$

of as low as 1 mJ/m^2 would easily contribute to such a variation should not be overlooked; γ_s is the surface tension of a solid in a vacuum. On one and the same solid surface, γ_{sv} is expected to be constant when vapor adsorption is negligible, however, if vapor adsorption of liquids does play a role, then γ_{sv}, can be different from liquid to liquid even on one and the same type of solid surface. The answer to the question of whether or not vapor adsorption has an effect on the contact angle patterns in Fig. 16 (and similar figures) would require general criteria to distinguish this from all other effects, such as swelling of a solid surface. As Fig. 16 stands, it does not appear that vapor adsorption plays a significant role in the contact angles presented here; otherwise, one would expect such an effect to manifest itself as random variations of the contact angles, rather than the remarkable regularity. Nevertheless, minor adsorption which causes the equilibrium spreading pressure π_e, to vary by as much as 1 mJ/m^2 has been considered possible for low-energy solid surfaces [102].

Although the liquids and solids (polymers) selected are of high purity, e.g. $> 99\%$, minute impurities presented in either the liquids or the solids are unavoidable and finding liquids and solids (polymers) which contain absolutely no impurities is unrealistic. There is no guarantee that such matters could not have caused the apparent minor deviations of the points in Fig. 16 (and similar figures). It is worth mentioning that even very minor swelling of the polymer [54] or creeping of the liquid could easily introduce a slight deviation of some points away from such curves. Therefore, only after considering all such possibilities would the need or justification arise for explanations in terms of direct effects of intermolecular forces [45]. There is no reason to suppose that intermolecular forces have any additional and independent effects on the contact angles beyond the fact that intermolecular forces determine the primary interfacial tensions, γ_{lv}, γ_{sv} (and γ_{sl}); the interfacial tensions then determine the contact angle, as given by Young's equation. This fact is most easily understood in terms of the experimental contact angle patterns shown in Figs. 2, 7 and 13–16.

2.5. Criteria for calculations of surface energetics

In Section 2.3.3, it has been shown that there exist a large number of contact angle complexities which prevent use of the measurements for energetic calculations. To arrive at the curves shown in Fig. 15, several assumptions already mentioned before were used to eliminate the meaningless contact angles. However, there remains one last assumption which has not been used and discussed: the constancy of γ_{sv}, going from liquid to liquid. It will be apparent in this section that such an assumption is indeed needed for energetic calculations; the importance of the various underlying assumptions in the determination of solid surface tensions will be discussed in detail. They will be addressed further in Section 3.1, in conjunction with the surface tension component approaches [11,15–17].

2.5.1. Accepted assumptions for calculations of surface energetics

1. It has to be realized that Young's equation Eq. (1) is the only thermodynamic relation to inter-relate the three surface tensions, γ_{lv}, γ_{sv}, γ_{sl}, with the experimental contact angle θ. Therefore, the expectation of the applicability of Young's equation has to be fulfilled. As in the case of slip/stick of the three-phase contact line shown in Fig. 12, Young's equation cannot be applicable: Since γ_{lv}, γ_{sv}, and γ_{sl} are material properties and are expected to be constant, Young's equation implies a unique contact angle. Thus, contact angles from slip/stick of the three-phase contact line have to be discarded.
2. Obviously, contact angle interpretation of surfactant solutions or mixtures of liquids is expected to be more complicated than that of the pure liquid. It has been found that if one measures contact angles of mixture solutions on one and the same solid surface, scatter, or patterns different from those in plots of the type in Fig. 15 would arise [103]. Thermodynamically, such systems have three degrees of freedom [72–75]. The additional degree of freedom comes from the

effect of an additional liquid component. While Young's equation may still be applicable in this case, no contact angle approach as yet allows the determination of solid surface tensions from such angles. Therefore, pure liquids are always used in contact angle measurements. However, even if this is the case, one has to ensure that γ_{lv} remains constant during the experiment. In an example shown earlier in Fig. 10, polymer dissolution occurs, causing the liquid surface tension to differ from that of the pure liquid. This reflects the fact that the presumed pure liquid has been changed to a mixture of liquid/polymer solution. If a conventional goniometer technique had been used instead, the change in the operative γ_{lv} might not be detected. Such goniometer measurements would inevitably reflect a solid–liquid system with a changed γ_{lv}, rather than the γ_{lv} of the presumed pure liquid. Thus, contact angle interpretation from such angles would be in error.

3. If a chemical/physical reaction takes place, any of γ_{lv}, γ_{sv}, and γ_{sl} could change during the experiment, and because of Young's Eq. (1), the contact angle θ would also change. Therefore, changes in θ suggest that at least one of γ_{lv}, γ_{sv}, and γ_{sl} is changing. In an example shown in Fig. 11, the contact angle increases as the drop front advances with essentially constant γ_{lv}. While there is no reason to question the applicability of Young's equation, γ_{sl} is suspected to change; from Young's equation, if γ_{lv} and γ_{sv} are constant, changes in θ must be a consequence of a change in γ_{sl}. While such cases might be very interesting in a different context, they have to be discarded because our goal is to deduce solid surface tension from the simplest possible situations.
4. If $\gamma_{lv} \approx \gamma_{sv}$ or $\gamma_{lv} < \gamma_{sv}$, complete wetting occurs, or a change in γ_{sv} induced by the solid/liquid contact (autophobicity). In order to illustrate this, a plot of $\gamma_{lv}\cos\theta$ vs. γ_{lv} is shown in Fig. 17 for a PET surface. In this figure, liquids

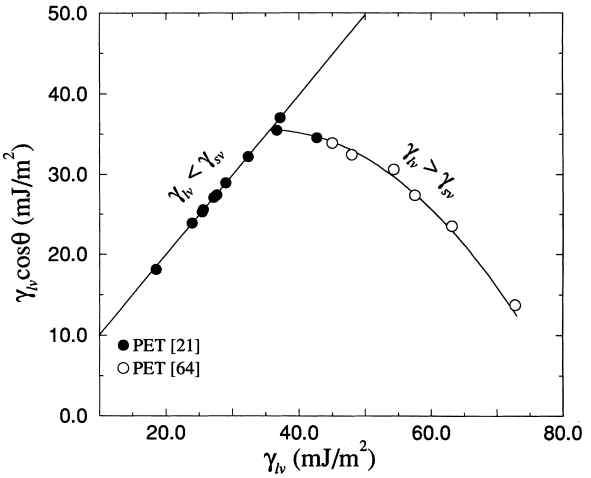

Fig. 17. $\gamma_{lv}\cos\theta$ vs. γ_{lv} for a PET surface.

having surface tensions less than that of the anticipated PET surface tension are included, i.e. $\gamma_{lv} < \gamma_{sv}$. As can be seen, the values of $\gamma_{lv}\cos\theta$ increase as γ_{lv} decreases, reaching a global maximum. Further decrease in γ_{lv} causes the data point to fall on a straight line. Thus, the liquid surface tensions of the testing liquids should be higher than that of the anticipated solid surface tension, by the appropriate choice of the liquids. Another possible effect of $\gamma_{lv} < \gamma_{sv}$ is liquid adsorption, which could cause γ_{sv} to be different from liquid to liquid. Therefore, the testing liquids used in this study were selected to fulfil the condition $\gamma_{lv} > \gamma_{sv}$.

5. One last assumption which has not been used to identify meaningful contact angles in Section 2.3 is the assumption of the constancy of γ_{sv} going from liquid to liquid. This assumption is needed for reasons of procedure in deducing solid surface tensions. Between the three variables, γ_{lv}, γ_{sv}, and γ_{sl}, only γ_{lv} is measurable; an additional measurable quantity is, however, the contact angle θ which can be inter-related to these quantities only by Young's equation. Therefore, it is impossible to study the direct effect of changing γ_{lv} on a second (non-measurable) quantity γ_{sl}, through θ, unless the third (non-measurable) quantity, γ_{sv}, is kept constant. Otherwise, interpretation of the data showing implicitly the effect of changes of γ_{lv} on γ_{sl} would not be possible by any of the contact angle approaches of current interest. The assumption of constant γ_{sv} will be used to deduce solid surface tensions from contact angles in Section 3.

2.5.2. Experimental criteria

The experimental results in Section 2.3.3 illustrate that there are three apparent contact angle complexities;

1. slip/stick of the three-phase contact line;
2. contact angle increases/decreases as the drop front advances; and
3. liquid surface tension changes as the drop front advances.

These contact angles should not be used for the determination of solid surface tensions. With respect to the first point, slip/stick of the three-phase contact line indicates that Young's equation is not applicable. Increase/decrease in the contact angle and change in the liquid surface tension as the drop front advances violate the expectation of no physical/chemical reaction. Therefore, when the experimental contact angles and liquid surface tensions are not constant, they should be disregarded. However, the question arises as to whether the reverse is true, i.e. whether constancy of θ and γ_{lv} in the dynamic measurements described in Section 2.3 will always guarantee that the above contact angle assumptions (in the preceding section) are fulfilled. This question will be explored below.

In practice, many solids are not truly inert with respect to many liquids; even swelling of fluorocarbon surfaces by alkanes has been reported [54]. For example, if swelling of a solid surface occurs quickly upon the contact with a liquid as the drop front advances, θ will change to reflect the changed energetics. If the time scale of such an effect is much less than that of the contact angle measurements, θ could reflect the changed γ_{sl}. This might result in a rather constant contact angle,

although the energetics would have changed. If this mechanism would not affect the liquid, γ_{lv} would remain constant, i.e. be independent of time. However, such constant contact angles would reflect only the energetics of the already swollen solid surface in contact with the liquid. Furthermore, one and the same solid surface could swell differently by different test liquids in an unknown manner. This effect would manifest itself in scatter of the plots of $\gamma_{lv}\cos\theta$ vs. γ_{lv} because

$$\gamma_{sl} \neq F(\gamma_{lv}, \gamma_{sv}) \tag{10}$$

In this case, a systematic study of the effect of surface energetics is not possible since the energetics have changed in an unknown, more complex manner. Obviously, such angles would have to be disregarded even if the measured liquid surface tensions and contact angles are constant, because the assumption of no chemical/physical reaction would have been violated. Unfortunately, the strategies employed here will not allow identification of such matters, and it remains a possibility that such effects contribute to the minor deviations of some data points from a smooth curve.

An example for this more complex pattern is self-assembled monolayers (SAMs), which have been widely used to produce monolayer surfaces of different chemical compositions and wettabilities [104–107]. For this type of surfaces, it is expected that penetration of liquids into the SAMs is inevitable; different liquids would have different effects on such surfaces. Because penetration of liquid is expected to occur almost instantly as the liquid contacts the solid, the observed advancing angle might reflect a γ_{sl} value caused by a modification of the solid surface.

Low-rate dynamic contact angles of water on a octadecanethiol ($HS(CH_2)_{17}CH_3$) SAM on a gold substrate are shown in Fig. 18. It can be seen that the advancing contact angles and liquid surface tension are quite constant. A plot of $\gamma_{lv}\cos\theta$ vs. γ_{lv} and of various liquids for this surface is shown in Fig. 19 (solid symbols). These contact angles were determined dynamically by ADSA-P in another study [84]. Contrary to the patterns shown in Figs. 2 and 7, and Figs. 13–16, no smooth curve results in Fig. 19. The reason for the difference in pattern is believed to be the effect of liquid penetration into the monolayer SAMs. Such mechanism is believed to be absent or negligible for the relatively thick polymer films used in Section 2.

It is instructive to compare this contact angle pattern with that obtained from the hexatriacontane surface [51,97,98,108] (also plotted in Fig. 19). Since both surfaces are expected to consist entirely of CH_3 groups, their solid surface tensions should be similar; one would then expect the two contact angle patterns to be essentially the same. However, the hexatriacontane data follow a smooth curve. From the point of view of surface energetics, the only difference for the two surfaces is that the SAM is a monolayer, whereas the hexatriacontane is a relatively thick crystallized layer. Obviously, it is the effect of liquid penetration and possible contact with the substrate of the SAMs which causes γ_{sl} to change in a pattern different from that which would prevail in the absence of liquid penetration. In this case, there is no reason to question the validity and applicability of Young's equation; however, different liquids are expected to penetrate

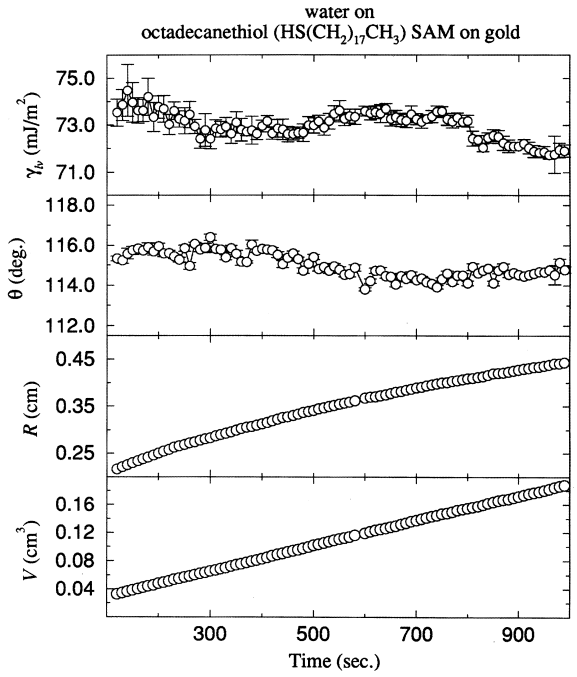

Fig. 18. Low-rate dynamic contact angles of water on a octadecanethiol ($HS(CH_2)_{17}CH_3$) SAM on a gold substrate.

differently even on one and the same solid surface (in an unknown manner) and hence the energetics could be very different from liquid to liquid. Since nothing is known about the changed energetics and the systems have violated the assumption of no physical reaction, use of these contact angles in any contact angle approach naively could be meaningless [109]. Although the interpretation of contact angles on SAMs in terms of surface energetics could be misleading, wettability studies of SAMs can be very interesting [107,110].

3. Contact angle interpretation

The calculation of solid surface tension γ_{sv}, from the contact angle of a liquid of surface tension γ_{lv} starts with Young's equation, Eq. (1). Of the four quantities in Young's equation, only γ_{lv} and θ are readily measurable. Thus, in order to determine γ_{sv}, further information is necessary. Conceptually, an obvious approach is to seek one more relation among the parameters of Eq. (1), such as an equation-of-state relation, of the form of Eq. (5) which is now known to exist from experimental facts. The simultaneous solution of Eqs. (1) and (5) would solve the problem.

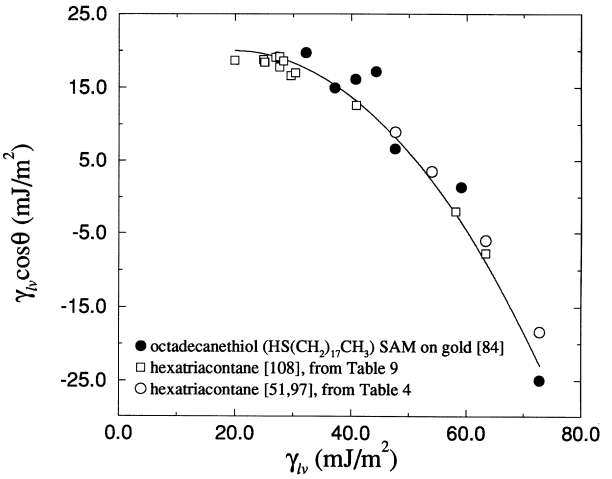

Fig. 19. $\gamma_{lv}\cos\theta$ vs γ_{lv} for a octadecanethiol ($HS(CH_2)_{17}CH_3$) SAM on a gold substrate, and on a hexatriacontane surface.

Historically, the interpretation of contact angles in terms of solid surface energetics started with the pioneering work of Zisman and co-workers [10]; the key observation they made was that for a given solid the measured contact angles did not vary randomly as the liquid was varied; rather, $\cos\theta$ changed smoothly with the liquid surface tension γ_{lv} within a band in a fashion that may suggest a straight-line relationship.

Subsequent to Zisman's work, two major schools of thought evolved: one is the surface tension component approach [11,15–17]; the other is the equation of state approach [12–14] which can be understood as a further development of Zisman's approach. The former approach stipulates that γ_{lv} depends not only on γ_{lv} and γ_{sv}, but also on the specific intermolecular forces; the latter approach is based on an equation-of-state relation which has been shown to exist from thermodynamics [71–75] and the experimental results in Figs. 2, 7 and 13–16.

From the experimental results shown in Figs. 2, 7 and 13–16, the curves for all solid surfaces with very different chemical properties are effectively very smooth, independent of intermolecular forces and liquid structures. This point has been addressed elsewhere [70,76,80,88–95]. Within the framework of all surface tension component approaches [11,15–17], it stands to reason that, for a given solid surface, the values of $\gamma_{lv}\cos\theta$ would have to depend not only on γ_{lv}, but also the various intermolecular forces of the liquids. This expectation, however, clashes directly with the experimental results shown in Figs. 2, 7 and 13–16. The only possible conclusion is that surface tension component approaches [11,15–17] contradict physical reality [70,76,80,88–95]. Only equation of state type approaches can be used: two well-known equation-of-state relations are those of Antonow [100] and Berthelot [101]. Nevertheless, surface tension component approaches will be briefly discussed and tested in the next section.

3.1. Surface tension component approaches

3.1.1. Fowkes approach

The approach of surface tension components was pioneered by Fowkes [11]. He postulated that the total surface tension can be expressed as a sum of different surface tension components, each of which arises due to a specific type of intermolecular forces:

$$\gamma = \gamma^d + \gamma^h + \gamma^{di} + \cdots \tag{11}$$

where γ, γ^d, γ^h, and γ^{di} are, respectively, the total surface tension, dispersive surface tension component, and surface tension components due to hydrogen and dipole–dipole bonding. Eq. (11) is often rearranged into

$$\gamma = \gamma^d + \gamma^n \tag{12}$$

i.e. the total surface tension γ is a sum of only the dispersive γ^d and non-dispersive γ^n surface tension components. The former is claimed to result from molecular interaction due to London forces, the latter from all other interactions due to non-London forces. A geometric mean relationship was postulated both of the solid–liquid and liquid–liquid interfacial tensions:

$$\gamma_{12} = \gamma_1 + \gamma_2 - 2(\gamma_1^d \gamma_2^d)^{1/2} \tag{13}$$

For solid–liquid systems, combining Eq. (13) with Young's Eq. (1) yields

$$\gamma_l \cos\theta_Y = -\gamma_l + 2(\gamma_s^d \gamma_l^d)^{1/2} \tag{14}$$

Typically, experimental contact angles of different liquids with known γ_l^d on a dispersive solid surface ($\gamma_s = \gamma_s^d$) are employed to determine the surface tension of a solid. In these procedures, the applicability of Young's equation and the constancy of solid surface tension from liquid to liquid stated in the Section 2.5.1 are, obviously, implied.

The Fowkes approach, Eq. (13) and hence Eq. (14), can be easily tested using the contact angle results in Section 2. For simplicity, two liquids of nearly the same surface tension but very different intermolecular forces are selected on the FC-722-coated mica surface; the polar (non-dispersive) liquid is 1-pentanol (γ_l = 26.0 mJ/m^2) and the dispersive one is *trans*-decalin ($\gamma_l = \gamma_l^d$ = 27.2 mJ/m^2). From Eq. (14), the $\gamma_s (= \gamma_s^d)$ value determined using the contact angle (73.4°) of *trans*-decalin is 11.2 mJ/m^2. Since 1-pentanol is a polar liquid, γ_l^d is expected to be very different (smaller) than the total surface tension γ_l; assuming for the moment that dispersion force contributes 75% to the total surface tension of 1-pentanol. This corresponds to γ_l^d = 19.5 mJ/m^2 for γ_l = 26.0 mJ/m^2. From the experimental contact angle (73.0°) of 1-pentanol, Eq. (14) predicts the γ_s value to be 14.5 mJ/m^2. This value is almost 30% larger than that calculated using *trans*-decalin; a γ_s value of 11.2 mJ/m^2 would imply γ_l^d of 1-pentanol to be 25.2 mJ/m^2. This is clearly absurd: 1-pentanol would have to be classified as a non-polar liquid, i.e.

$\gamma_l \approx \gamma_l^d$. Similar calculations can be performed for other dispersive/non-dispersive liquid pairs, with similar results. This result simply illustrates the fact that the perceived 'surface tension components' in Fowkes' sense do not reflect physical reality. In principle, this is obvious from the experimental results that $\gamma_{lv}\cos\theta$ changes smoothly with γ_{lv}, independent of intermolecular forces and liquid structures. Thus, the basic postulate of the Fowkes approach is false and any generalization of this approach must suffer from the same deficiency.

3.1.2. Owens–Wendt–Kaelble approach

Owens and Wendt [15] extended Fowkes' concept to cases where both dispersion and hydrogen bonding forces may operate. They regarded the surface tension as being composed of two components such that

$$\gamma = \gamma^d + \gamma^h \tag{15}$$

where γ^h denotes the component of surface tension due to both hydrogen bonding and dipole–dipole interactions. They postulated

$$\gamma_{sl} = \gamma_s + \gamma_l - 2\sqrt{\gamma_s^d \gamma_l^d} - 2\sqrt{\gamma_s^h \gamma_l^h} \tag{16}$$

Combining this equation with Young's Eq. (1) yields

$$\gamma_l(1 + \cos\theta_Y) = 2\sqrt{\gamma_s^d \gamma_l^d} + 2\sqrt{\gamma_s^h \gamma_l^h} \tag{17}$$

Nearly at the same time, Kaelble [77] also published a very similar equation in terms of dispersion and polar forces. Thus, Eq. (16) is often called the Owens–Wendt–Kaelble equation.

Clearly, the applicability of Young's equation discussed in Section 2.5.1 is implied in Eq. (17). Since Eq. (17) contains two unknowns (γ_s^d and γ_s^h) of the solid, it is suggested to use contact angle measurements of at least two different liquids on one and the same solid surface, by solving two simultaneous equations. Such procedures also imply constancy of the solid surface tension from liquid to liquid; if the operative solid surface tension is not constant from one liquid to the next, simultaneous solution of different equations (from contact angles of different liquids) would be meaningless.

Equation (17) can be easily tested using the contact angles of *trans*-decalin and 1-pentanol on the FC-722 surface in Fig. 7. Assuming the polarity of the (dispersive) FC-722 surface to be unknown and that γ_l^d of 1-pentanol to be again 19.5 mJ/m^2, two simultaneous equations can be used to determine the two unknowns (γ_s^d and γ_s^h) from the experimental contact angles of 1-pentanol and *trans*-decalin. Eq. (17) predicts γ_s^d and γ_s^h to be, respectively, 11.2 mJ/m^2 and 0.6 mJ/m^2. Since diiodomethane is claimed to be a dispersive liquid [16,17] ($\gamma_l = \gamma_l^d = 50.0$ mJ/m^2) and water is a non-dispersive liquid [11] ($\gamma_l = 72.7$ mJ/m^2 and $\gamma_l^d = 21.8$ mJ/m^2), two additional simultaneous equations can be obtained by insertion of the experimental contact angles from Fig. 7. This procedure yields γ_s^d and γ_s^h to be 8.1 mJ/m^2 and 2.8 mJ/m^2, respectively. Clearly, different choices of the liquid pairs

yield different surface tension components of the solid surface: if nothing were known about the dispersive property of the FC-722 surface, Eq. (17) would have predicted this dispersive surface to be non-dispersive; the relative magnitudes would depend on the choice of the liquid pairs. Similar calculations can be performed for other pairs of liquids, with similar results.

3.1.3. Lifshitz–van der Waals / acid–base (van Oss) approach

The Lifshitz–van der Waals / acid–base (van Oss) approach [16,17] was claimed to be a generalization of the Fowkes approach, by considering perceived acid–base interactions at the interface. van Oss et al. divided the surface tension into different perceived components, i.e. the so-called Lifshitz–van der Waals (LW), acid ($+$), and base ($-$) components, such that the total surface tension is given by

$$\gamma_i = \gamma_i^{LW} + 2\sqrt{\gamma_i^+ \gamma_i^-} \tag{18}$$

where i denotes either the solid or liquid phase. The interfacial tension was postulated both of solid–liquid and liquid–liquid systems as

$$\gamma_{12} = \gamma_1 + \gamma_2 - 2(\gamma_1^{LW}\gamma_2^{LW})^{1/2} - 2(\gamma_1^+\gamma_2^-)^{1/2} - 2(\gamma_1^-\gamma_2^+)^{1/2} \tag{19}$$

For solid–liquid systems, combining Eq. (19) with Young's equation yields

$$\gamma_l(1 + \cos\theta_Y) = 2(\gamma_l^{LW}\gamma_s^{LW})^{1/2} + 2(\gamma_l^+\gamma_s^-)^{1/2} + 2(\gamma_l^-\gamma_s^+)^{1/2} \tag{20}$$

Eq. (20) is often used to determine the solid surface tension components (γ_s^{LW}, γ_s^+, and γ_s^-) from contact angles, using three simultaneous equations by inserting properties of calibration liquids. These procedures also imply the applicability of Young's equation and constancy of the solid surface tension from one liquid to the next, as discussed in Section 2.5.1. The failure of this approach can be easily illustrated, by employing the postulated liquid surface tension components from van Oss et al. [16,17] and experimental contact angles of liquid triplets; three simultaneous equations of Eq. (20) (from contact angles of three different polar liquids) will yield the three unknown solid properties. Table 1 illustrates the solid surface tension components of the FC-721-coated mica surface [111]. It can be seen that the calculated γ_s, value varies from -30.0 to 107.0 mJ/m^2, depending on the choice of the liquid triplets; the resulting 'surface tension components' vary by a very large margin. However, it was recently suggested [112] that at least one non-polar liquid should be used for the above calculations, such as 1-bromonaphthalene. It is the contention of the proponents of this acid–base approach that 1-bromonaphthalene is a non-polar compound. No reason was given for the necessity of including a non-polar liquid. For this reason, the solid surface tension components of the same surface were recalculated using 1-bromonaphthalene and shown in Table 2. Again, the calculated γ_s values are not consistent, varying from -36.0 to 9.5 mJ/m^2. If nothing were known about the properties of the non-polar FC-721 surface, and if only a small number of measurements were available, this approach would predict all kinds of different molecular properties:

Table 1
Calculated solid surface tension components for FC-721 using three simultaneous equations of the acid–base approach, Eq. (20), from contact angles of three polar liquids [111]

	$(\gamma_s^{LW})^{1/2}$ (mJ/m^2)	$(\gamma_s^{+})^{1/2}$ (mJ/m^2)	$(\gamma_s^{-})^{1/2}$ (mJ/m^2)	γ_s (mJ/m^2)
Fo-Gl-Wa	2.56	0.46	0.87	7.38
Fo-Gl-DM	2.33	1.30	−1.60	1.27
Fo-Gl-EG	2.08	2.17	−4.23	−14.02
Fo-Wa-DM	7.08	−4.07	1.24	40.12
Fo-Wa-EG	1.14	1.90	0.75	4.15
Fo-DM-EG	1.66	2.05	−2.00	−5.44
Gl-Wa-DM	3.38	−0.10	0.68	11.31
Gl-Wa-EG	9.96	−4.72	−0.78	106.6
Gl-DM-EG	0.87	3.23	−4.76	−30.0
Wa-DM-EG	2.39	0.97	0.53	6.73

DM: dimethyl sulfoxide (DMSO); EG: ethylene glycol; FO: formamide; Gl: glycerol; Wa: water.

non-polar, monopolar, bipolar acidic and basic as well as 'negative' solid and solid–liquid interfacial tensions. Thus, the ability of the approach to explain, e.g. 'negative' interfacial tensions does not imply its validity. The reason that the scatter of the results is not as bad as those in Table 1 is due to the use of Berthelot's rule (see later). Clearly, this approach is just as erroneous as the earlier surface tension component approaches.

3.2. Equation of state approach

In this, and the following sections, an equation of state approach will be

Table 2
Calculated solid surface tension components for FC-721 using three simultaneous equations of the acid–base approach, Eq. (20), from contact angles of one non-polar and two polar liquids [111]

	$(\gamma_s^{LW})^{1/2}$ (mJ/m^2)	$(\gamma_s^{+})^{1/2}$ (mJ/m^2)	$(\gamma_s^{-})^{1/2}$ (mJ/m^2)	γ_s (mJ/m^2)
Fo-Gl-Br	9.07	−1.10	5.58	−3.21
Fo-Wa-Br	9.07	0.02	0.90	9.11
Fo-DM-Br	9.07	0.53	−1.19	7.81
Fo-EG-Br	9.07	2.44	−9.16	−35.63
Gl-Wa-Br	9.07	1.60	0.76	9.31
Gl-DM-Br	9.07	0.39	−0.13	8.97
Gl-EG-Br	9.07	1.36	−3.82	− 1.32
Wa-DM-Br	9.07	0.30	0.63	9.45
Wa-EG-Br	9.07	0.50	0.42	9.49
DM-EG-Br	9.07	0.04	2.70	9.29

DM: dimethyl sulfoxide (DMSO); EG: ethylene glycol; FO: formamide; Gl: glycerol; Wa: water, Br: 1-bromonaphthalene.

discussed, as such a relation has been inferred from the experimental results in Section 2. In the literature, two well-known equation-of-state relations are Antonow's [100] and Berthelot's [101] rules.

3.2.1. Antonow's rule

An old equation of state is that of Antonow [100]. Antonow's rule relates γ_{sl} with γ_{lv} and γ_{sv} for solid–liquid systems in the following simple manner:

$$\gamma_{sl} = |\gamma_{lv} - \gamma_{sv}| \tag{21}$$

This equation, although never having been derived in any fashion, appears in the literature from time to time. Combining this relation with Young's equation gives

$$\cos\theta_Y = -1 + 2\frac{\gamma_{sv}}{\gamma_{lv}} \tag{22}$$

Thus, assuming, for the sake of the argument, the validity of Eq. (22), γ_{sv} can be determined when γ_{lv} and θ_Y are known. Once γ_{sv} is known, γ_{sl} can be found either from Young's Eq. (1) or from Eq. (21).

3.2.2. Berthelot's (geometric mean) combining rule

Another equation-of-state relation can be obtained from the Berthelot combining rule [101]. Unlike Antonow's rule, Berthelot's rule has a theoretical background; based on molecular interactions of like pairs; from the London theory of dispersion [113,114], the long range dispersion energy function for two identical molecules is given by

$$U_{\text{disp}} = \frac{C_6}{r^6} \tag{23}$$

where C_6 is a negative constant, so that the energy contribution is attractive. A more general form [114] of the long range dispersion energy function including electrostatic and induction interactions can be expressed as

$$U_{\text{disp}} = \frac{C_6}{r^6} + \frac{C_8}{r^8} + \frac{C_{10}}{r^{10}} + \cdots \tag{24}$$

where C_8 and C_{10} are all negative constants. It has been shown [113,114] that the energy coefficient C_6 for two identical molecules can be expressed as

$$C_6 = -\frac{3}{4}\frac{E_I\alpha^2(0)}{(4\pi\varepsilon_o)^2} \tag{25}$$

where ε_o is the permittivity of free space, $\alpha(0)$ is the static polarizability, and E_I, is the ionization energy.

From Eq. (25), the dispersion energy coefficient of a pair of molecules of species

i is given by

$$C_6^{ii} = -\frac{3}{4}\frac{E_{I_i}\alpha_i^2(0)}{(4\pi\varepsilon_o)^2} \tag{26}$$

and similarly, for a pair of molecules of species j,

$$C_6^{jj} = -\frac{3}{4}\frac{E_{I_j}\alpha_j^2(0)}{(4\pi\varepsilon_o)^2} \tag{27}$$

It has been shown [114] that the interaction C_6^{ij} between two dissimilar molecules i and j can be related by the following expression:

$$C_6^{ij} = -\frac{3}{2}\frac{E_{I_i}E_{I_j}}{E_{I_i}+E_{I_j}}\frac{\alpha_i(0)\alpha_j(0)}{(4\pi\varepsilon_o)^2} \tag{28}$$

Because the ionization energies vary only slightly from molecule to molecule, i.e. $E_{I_i} \approx E_{I_j}$, the dispersion energy coefficient C_6^{ij} of Eq. (28) can be written in terms of C_6^{ii} and C_6^{jj} as

$$C_6^{ij} = \sqrt{C_6^{ii}C_6^{jj}} \tag{29}$$

This relation indeed forms a basis of the Berthelot (geometric mean) combining rule [101]:

$$\varepsilon_{ij} = \sqrt{\varepsilon_{ii}\varepsilon_{jj}} \tag{30}$$

where ε_{ij} is the potential energy parameter (well depth) of unlike-pair interactions; ε_{ii} and ε_{jj} are the potential energy parameters (well depth) of like-pair interactions.

Thermodynamically, a relation of the free energy of adhesion per unit area of a solid–liquid pair is equal to the work required to separate unit area of the solid–liquid interface [115]:

$$W_{sl} = \gamma_{lv} + \gamma_{sv} - \gamma_{sl} \tag{31}$$

From the geometric mean combining rule (i.e. the Berthelot rule, Eq. (30)) the free energy of adhesion W_{sl} can be approximated in terms of the free energy of cohesion of the solid, W_{ss}, and the free energy of cohesion of the liquid, W_{ll} [101,114,116,117], i.e.

$$W_{sl} = \sqrt{W_{ll}W_{ss}} \tag{32}$$

By the definitions $W_{ll} = 2\gamma_{lv}$ and $W_{ss} = 2\gamma_{sv}$, Eq. (32) becomes

$$W_{sl} = 2\sqrt{\gamma_{lv}\gamma_{sv}} \tag{33}$$

By combining Eq. (33) with Eq. (31), the solid–liquid interfacial tension γ_{sl} can be

Table 3
Calculated γ_{sv} values (mJ/m^2) of the FC-722-coated mica surface from Antonow's and Berthelot's rules. The contact angles are low-rate dynamic angles measured by ADSA-P

Liquid	γ_{lv} (mJ/m^2)	θ (degree)	γ_{sv}	
			Antonow's rule, Eq. (22)	Berthelot's rule, Eq. (35)
Decane	23.88	67.36	16.5	11.5
1-Pentanol	26.01	72.95	16.8	10.9
trans-Decalin	27.19	73.38	17.5	11.2
Hexadecane	27.62	75.94	17.2	10.7
1-Decanol	28.99	78.84	17.3	10.3
cis-Decalin	32.32	79.56	19.1	11.3
Ethyl cinnamate	37.17	86.54	19.7	10.5
Dibenzylamine	40.80	90.70	20.1	10.0
Dimethyl sulfoxide (DMSO)	42.68	90.95	21.0	10.3
1-Bromonaphthalene	44.31	93.81	20.7	9.7
Diethylene glycol	44.68	94.22	20.7	9.6
Ethylene glycol	47.55	97.87	20.5	8.9
Diiodomethane	49.98	101.18	20.1	8.1
2,2′-Thiodiethanol	56.26	104.56	21.1	7.9
Formamide	59.08	108.49	20.2	6.9
Glycerol	65.02	111.73	20.5	6.5
Water	72.70	118.69	18.9	4.9

written as

$$\gamma_{sl} = \gamma_{lv} + \gamma_{sv} - 2\sqrt{\gamma_{lv}\gamma_{sv}} = \left(\sqrt{\gamma_{lv}} - \sqrt{\gamma_{sv}}\right)^2 \tag{34}$$

Combining this equation with Young's Eq. (1) yields

$$\cos\theta_Y = -1 + 2\sqrt{\frac{\gamma_{sv}}{\gamma_{lv}}} \tag{35}$$

Thus, the solid–vapor surface tension can be determined when experimental (Young) contact angle and liquid–vapor surface tension are known.

The question then arises as to what to expect when such an equation-of-state relation, in conjunction with Young's equation, is used to calculate solid surface tensions. There is one immediate criterion that the results obtained with this equation (or, for that matter, any other equation) must satisfy; when measuring contact angles with a number of liquids on a low-energy solid, the solid–vapor surface tension γ_{sv} is expected to be constant, independent of the liquid surface tension γ_{lv}. In other words, different pairs of θ and γ_{lv} for one and the same solid should yield sensibly constant values of γ_{sv}. The γ_{sv} values obtained from Eq. (35) and Eq. (22) are given in Table 3 for the FC-722-coated mica from Fig. 7. It can be seen that the γ_{sv} values obtained from Antonow's and Berthelot's rule are not

constant; rather, the former tends to increase as γ_{lv} increases; the latter tends to decrease as γ_{lv} increases.

As mentioned above, Antonow's rule does not have a theoretical basis. But, in the theory of intermolecular interactions and the theory of mixtures, combining rules are used to evaluate the parameters of unlike-pair interactions in terms of those of the like interactions [118,119]. However, as for many other combining rules, the Berthelot rule [101], i.e. Eq. (34), is only a useful approximation and does not provide a secure basis for the understanding of unlike-pair interactions. For the interactions between two very dissimilar types of molecules or materials, where there is an apparent difference between ε_{ii} and ε_{jj}, it has been demonstrated [44,120] that the geometric mean combining rule generally over-estimates the strength of the unlike-pair interaction, i.e. the geometric mean value is too large an estimate. Clearly, this is why the geometric mean combining rule does not work for situations of large differences $|W_{ll} - W_{ss}|$ or $|\gamma_{lv} - \gamma_{sv}|$, as can be seen in Table 3. This fact is indeed well-known [46–49,114].

In general, ε_{sl}, the minimum of the solid–liquid interaction potential, is often expressed in the following manner [45–49]:

$$\varepsilon_{sl} = g(\sigma_s/\sigma_l)\sqrt{\varepsilon_{ss}\varepsilon_{ll}} \tag{36}$$

where ε_{ss} and ε_{ll} are, respectively, the minima in the solid–solid and liquid–liquid potentials; σ_s and σ_l, are the appropriate core diameters for the molecules of the solid and liquid, respectively. It should be noted that many explicit forms of $g(\sigma_s/\sigma_l)$ have been suggested. For example, Matyushov and Schmid [49] proposed

$$g(\sigma_s/\sigma_l) = \left(\frac{4\sigma_s/\sigma_l}{(1 + \sigma_s/\sigma_l)^2} \right)^3 \tag{37}$$

and Sullivan [48] set

$$g(\sigma_s/\sigma_l) = \frac{1}{4}\left(1 + \frac{\sigma_s}{\sigma_l}\right)^2 \tag{38}$$

in attempts to give a better representation of solid–liquid interactions from solid–solid and liquid–liquid interactions. In general, these functions are normalized such that $g(\sigma_s/\sigma_l) = 1$ when $\sigma_s = \sigma_l$. In this case, they revert to Berthelot's geometric mean combining rule, Eq. (30). Therefore, a modification of Berthelot's rule is called for, leading to an equation of state approach for solid–liquid interfacial tensions.

3.2.3. Equation of state approach: modified Berthelot's rule

In the study of mixtures [118,119] it has become common practice to introduce a factor $(1 - K_{ij})$ to the geometric mean combining rule,

$$\varepsilon_{ij} = (1 - K_{ij})\sqrt{\varepsilon_{ii}\varepsilon_{jj}} \tag{39}$$

where K_{ij} is an empirical parameter quantifying deviations from the geometric mean combining rule. Since the geometric mean combining rule overestimates the strength of the unlike-pair interactions, the modifying factor $(1 - K_{ij})$ should be a decreasing function of the difference $\varepsilon_{ii} - \varepsilon_{jj}$ and be equal to unity when the difference $\varepsilon_{ii} - \varepsilon_{jj}$ is zero.

On the basis of this thought, Li et al. [121] have considered a modified combining rule of the form

$$\varepsilon_{ij} = \sqrt{\varepsilon_{ii}\varepsilon_{jj}}\, e^{-\alpha(\varepsilon_{ii}-\varepsilon_{jj})^2} \tag{40}$$

where α is an empirical constant; the square of the difference $(\varepsilon_{ii} - \varepsilon_{jj})$, rather than the difference itself, reflects the symmetry of this combining rule, and hence the anticipated symmetry of the equation of state. Correspondingly, for the cases of large differences $|W_{ll} - W_{ss}|$ or $|\gamma_{lv} - \gamma_{sv}|$, the combining rule for the free energy of adhesion of a solid–liquid pair can be written as

$$W_{sl} = \sqrt{W_{ll}W_{ss}}\, e^{-\alpha(W_{ll}-W_{ss})^2} \tag{41}$$

or, more explicitly, by using $W_{ll} = 2\gamma_{lv}$, and $W_{ss} = 2\gamma_{sv}$,

$$W_{sl} = 2\sqrt{\gamma_{lv}\gamma_{sv}}\, e^{-\beta(\gamma_{lv}-\gamma_{sv})^2} \tag{42}$$

In the above, α and β are as yet unknown constants. Clearly, when the values of γ_{lv} and γ_{sv} are close to each other, Eq. (42) reverts to Eq. (33), the geometric mean combining rule. By combining Eq. (42) with Eq. (31), an equation of state for solid–liquid interfacial tensions can be written as

$$\gamma_{sl} = \gamma_{lv} + \gamma_{sv} - 2\sqrt{\gamma_{lv}\gamma_{sv}}\, e^{-\beta(\gamma_{lv}-\gamma_{sv})^2} \tag{43}$$

Combining Eq. (43) with Young's Eq. (1) yields

$$\cos\theta_Y = -1 + 2\sqrt{\frac{\gamma_{sv}}{\gamma_{lv}}}\, e^{-\beta(\gamma_{lv}-\gamma_{sv})^2} \tag{44}$$

Thus, the solid surface tensions can be determined from experimental (Young) contact angles and liquid surface tensions when β is known, e.g. by the Newton method [122]. Obviously, for a given set of γ_{lv} and θ data measured on one and the same type of solid surface, the constant β and γ_{sv} values can be determined by a least-square analysis technique [64,123,124]. Starting out with arbitrary values for γ_{sv} and β, iterative procedures can be used to identify that pair of γ_{sv} and β values which provides the best fit of the experimental data to the set of experimental γ_{lv} and θ_Y pairs belonging to one and the same solid surface. From the experimental contact angles on the FC-721-coated mica, heat-pressed Teflon FEP, and poly(ethylene terephthalate) PET surfaces (not used here), an averaged β value of 0.0001247 $(m^2/mJ)^2$ was obtained [14,64].

Table 4
Summary of the dynamic contact angles of various solids by ADSA-P and capillary rise techniques. The γ_{sv} values (mJ/m^2) were calculated from the equation of state approach

Solid surface/technique	Liquid	γ_{lv} (mJ/m^2)	θ (degree)	γ_{sv} Equation of state, Eq. (44)
FC-721-coated mica/ capillary rise [86]	Dodecane	25.03	70.4	11.7
	2-Octanol	26.00	73.5	11.3
	Tetradecane	26.50	73.5	11.6
	1-Octanol	27.28	75.1	11.5
	Hexadecane	27.31	75.6	11.3
	1-Hexadecene	27.75	74.0	12.0
	1-Decanol	28.29	76.6	11.5
	1-Dodecanol	29.53	79.2	11.3
FC-722-coated mica/ ADSA-P [80]	Decane	23.88	67.36	11.9
	1-Pentanol	26.01	72.95	11.5
	trans-Decalin	27.19	73.38	11.9
	Hexadecane	27.62	75.94	11.4
	1-Decanol	28.99	78.84	11.2
	cis-Decalin	32.32	79.56	12.4
	Ethyl cinnamate	37.17	86.54	12.2
	Dibenzylamine	40.80	90.70	12.2
	Dimethyl sulfoxide (DMSO)	42.68	90.95	12.9
	1-Bromonaphthalene	44.31	93.81	12.4
	Diethylene glycol	44.68	94.22	12.4
	Ethylene glycol	47.55	97.87	12.1
	Diiodomethane	49.98	101.18	11.7
	2,2′-Thiodiethanol	56.26	104.56	12.7
	Formamide	59.08	108.49	12.0
	Glycerol	65.02	111.73	12.8
	Water	72.70	118.69	12.2
FC-722-coated silicon wafer/ADSA-P [89]	Hexane	18.50	50.83	12.4
	2-Octanol	26.42	74.74	11.2
	Hexadecane	27.62	75.64	11.5
	Glycerol	65.02	111.89	12.7
FC-725-coated silicon wafer/ADSA-P [90]	Dodecane	25.64	71.02	11.8
	Hexadecane	27.62	73.41	12.1
	3,3-Thiodipropanol	39.83	90.48	11.9
	Diethylene glycol	45.16	94.47	12.5
	Ethylene glycol	48.66	100.05	11.6
	2,2′-Thiodiethanol	53.77	101.07	13.2
	Formamide	59.08	106.89	12.7
	Glycerol	63.13	110.21	12.7
	Water	72.70	119.31	11.9

Table 4 (*Continued*)

Solid surface/technique	Liquid	γ_{lv} (mJ/m^2)	θ (degree)	γ_{sv} Equation of state, Eq. (44)
Teflon (FEP)/capillary rise [86]	Dodecane	25.03	47.8	17.7
	2-Octanol	26.00	52.3	17.2
	Tetradecane	26.50	52.6	17.5
	1-Octanol	27.28	54.4	17.5
	Hexadecane	27.31	53.9	17.7
	1-Hexadecene	27.75	54.2	17.9
	1-Dodecanol	29.53	55.7	18.6
	Dimethylformamide	35.21	68.6	17.7
	Methyl salicylate	38.85	72.2	18.4
Hexatriacontane/capillary rise [51,97]	Ethylene glycol	47.7	79.2	20.3
	2,2′-Thiodiethanol	54.0	86.3	20.3
	Glycerol	63.4	95.4	20.6
	Water	72.8	104.6	20.3
Cholesteryl acetate/ capillary rise [51,98]	Ethylene glycol	47.7	77.0	21.3
	2,2′-Thiodiethanol	54.0	84.3	21.3
	Glycerol	63.4	94.0	21.3
	Water	72.8	103.3	21.1
Poly(propene-*alt*-*N*-(*n*-hexyl)maleimide)/ ADSA-P [76,88]	*cis*-Decalin	32.32	28.81	28.5
	Triacetin	35.52	39.45	28.3
	Diethylene glycol	44.68	61.04	26.7
	Glycerol	65.02	82.83	28.6
	Water	72.70	92.26	27.8
Poly(*n*-butyl methacrylate) /ADSA-P [91]	Diethylene glycol	45.16	58.73	28.0
	3-Pyridylcarbinol	47.81	60.30	29.2
	2,2′-Thiodiethanol	53.77	68.00	29.4
	Formamide	59.08	76.41	28.5
	Glycerol	65.02	82.11	29.0
	Water	72.70	90.73	28.7
Polystyrene/ADSA-P [92]	Dimethyl sulfoxide (DMSO)	42.68	50.67	29.7
	Diethylene glycol	44.68	52.41	30.5
	Ethylene glycol	48.66	61.20	29.3
	Formamide	59.08	74.76	29.4
	Glycerol	63.11	78.38	30.0
	Water	72.70	88.42	30.2
Poly(styrene-*alt*-(hexyl/ 10-carboxydecyl(90/10) maleimide))/ ADSA-P [93]	Diethylene glycol	45.16	51.32	31.3
	Ethylene glycol	48.66	59.72	30.2
	Formamide	58.45	70.28	31.4
	Glycerol	63.13	76.51	31.0
	Water	72.70	87.13	31.0

Table 4 (*Continued*)

Solid surface/technique	Liquid	γ_{lv} (mJ/m^2)	θ (degree)	γ_{sv} Equation of state, Eq. (44)
Poly(methyl methacrylate/ *n*-butyl methacrylate)/ ADSA-P [94]	1-Iodonaphthalene	42.92	35.67	35.7
	3-Pyridylcarbinol	47.81	49.22	34.2
	2,2′-Thiodiethanol	53.77	57.84	34.6
	Formamide	59.08	66.33	34.0
	Glycerol	65.02	74.72	33.3
	Water	72.70	81.33	34.6
Poly(propene-*alt*-*N*-(*n*-propyl)maleimide)/ ADSA-P [76,88]	1-Iodonaphthalene	42.92	35.19	35.9
	1-Bromonaphthalene	44.31	30.75	38.6
	1,3-Diiodopropane	46.51	39.98	37.1
	2,2′-Thiodiethanol	53.77	54.04	36.5
	Glycerol	65.02	70.67	35.7
	Water	72.70	77.51	37.0
Poly(methyl methacrylate) /ADSA-P [95]	1,3-Diiodopropane	46.51	36.95	38.3
	3-Pyridylcarbinol	47.81	39.47	38.4
	Diiodomethane	49.98	42.25	39.0
	2,2′-Thiodiethanol	53.77	50.35	38.3
	Formamide	59.08	57.73	38.6
	Glycerol	65.02	66.84	37.9
	Water	72.70	73.72	39.3
Poly(propene-*alt*-*N*-methylmaleimide) /ADSA-P [89]	Diiodomethane	49.98	30.71	43.7
	Glycerol	65.02	60.25	41.7
	Water	72.70	69.81	41.8

The γ_{sv}, values calculated from Eq. (44) with the above β value are given in Table 4, for all solid surfaces shown in Fig. 15. It can be seen that the γ_{sv} values calculated from the equation of state approach [14,64] are quite constant, essentially independent of the choice of the liquids. This reconfirms the validity of the approach to determine solid surface tensions from contact angles. A FORTRAN computer program to calculate γ_{sv} from γ_{lv} and θ, using Eq. (44) with $\beta = 0.0001247$ (m^2/mJ)^2, is given in Appendix A.

It should be noted that the above calculations were based on a constant β value of 0.0001247 (m^2/mJ)^2. Alternatively, the γ_{sv} values of various solids can be determined by the two-variable least-square analysis [64,123,124], by assuming γ_{sv} and β in Eq. (44) to be constant, as described above. This leads to a β value and a γ_{sv} value for every given solid surface. The results, together with those obtained using the β value of 0.0001247 (m^2/mJ)^2, are given in Table 5. It is evident that there is good agreement between the γ_{sv} values determined from the two strategies, and the slight difference in the β values have very little effect on the calculated γ_{sv}, values. Since the β values do not appear to change systematically

Table 5
Averaged γ_{sv} values reproduced from Table 4; the γ_{sv} (mJ/m^2) and β (m^2/mJ)^2 values determined by a two-variable least-square fit are also given

Solid surface/technique	No. of system	Table 4 γ_{sv}[a]	Least-square fit	
			β	γ_{sv}
FC-721-coated mica/capillary rise [86]	8	11.5 ± 0.2	0.000124	11.7
FC-722-coated mica/ADSA-P [80]	17	12.1 ± 0.3	0.000111	11.8
FC-722-coated silicon wafer/ADSA-P [89]	4	12.0 ± 1.1	0.000111	11.8
FC-725-coated silicon wafer/ADSA-P [90]	9	12.3 ± 0.4	0.000114	11.9
Teflon FEP/capillary rise [86]	9	17.8 ± 0.3	0.000142	18.0
Hexatriacontane/capillary rise [51,97]	4	20.4 ± 0.2	0.000124	20.3
Cholesteryl acetate/capillary rise [51,98]	4	21.3 ± 0.2	0.000128	21.5
Poly(propene-*alt*-*N*-(*n*-hexyl)maleimide)/ADSA-P [76,88]	5	28.0 ± 1.0	0.000122	27.9
Poly(*n*-butyl methacrylate)/ADSA-P [91]	6	28.8 ± 0.5	0.000124	28.8
Polystyrene/ADSA-P [92]	6	29.9 ± 0.5	0.000120	29.7
Poly(styrene-*alt*-(hexyl/10-carboxydecyl(90/10)maleimide))/ ADSA-P [93]	5	31.0 ± 0.6	0.000120	30.8
Poly(methyl methacrylate/*n*-butyl methacrylate)/ADSA-P [94]	6	34.4 ± 0.8	0.000136	34.7
Poly(propene-*alt*-*N*-(*n*-propyl)maleimide)/ADSA-P [76,88]	6	36.8 ± 1.1	0.000133	36.9
Poly(methyl methacrylate)/ADSA-P [95]	7	38.5 ± 0.4	0.000113	38.3
Poly(propene-*alt*-*N*-methylmaleimide)/ADSA-P [89]	3	42.4 ± 2.8	0.000167	43.4

[a] Error limits are 95% confidence limits.

with the solid surface (and hence γ_{sv}), a weighted β value can be calculated. Alternatively, a statistical analysis can be used to decide whether or not averaging of β over γ_{sv} is allowed [76,123–126]. This procedure yields a correlation coefficient r_{cal} of 0.477 for the 14 observations in Table 5. A tabulated correlation coefficient r_{tab} at 99% is 0.623. Since, $r_{cal} < r_{tab}$, there is no correlation between β and γ_{sv} at over 99% confidence, for the results given in Table 5. Thus, averaging of β is allowed. Remarkably, this procedure together with the new experimental data yield a weighted β value of 0.0001234 (m^2/mJ)^2, which is in excellent agreement with that (β = 0.0001247 (m^2/mJ)^2) obtained by Li et al. [64] from contact angles on only three solid surfaces not considered here.

It should be noted that other forms of the modified Berthelot's rule (or any other equation in the form of Eq. (5)) can also be used, as long as they are capable of describing the experimental contact angle patterns in Figs. 2 and 7, and Figs. 13–16. A different form of the modified-Berthelot's rule will be proposed and discussed in the next section, which yields essentially the same γ_{sv} values as Eq. (44) does.

3.2.4. Equation of state approach: alternative formulation

Following the arguments leading to Eq. (39), we propose an alternative formulation [125,126] of the equation of state approach, i.e. a modified Berthelot's rule with a different modifying factor similar to the (1-K_{ij}) used in Eq. (39),

$$1 - \kappa_1(\varepsilon_{ii} - \varepsilon_{jj})^2 \tag{45}$$

so that $(1 - \kappa_1(\varepsilon_{ii} - \varepsilon_{jj})^2)$ is also a decreasing function of the difference $(\varepsilon_{ii} - \varepsilon_{jj})$ and is equal to unity when $\varepsilon_{ii} = \varepsilon_{jj}$; κ_1 is an unknown constant. Thus, Eq. (39) can then be written as

$$\varepsilon_{ij} = \left(1 - \kappa_1(\varepsilon_{ii} - \varepsilon_{jj})^2\right)\sqrt{\varepsilon_{ii}\varepsilon_{jj}} \tag{46}$$

The square of the difference $(\varepsilon_{ii} - \varepsilon_{jj})$, rather than the difference itself, reflects again the symmetry of this combining rule, and hence the anticipated symmetry of the equation of state. Because the free energy is directly proportional to the energy parameter ε [116,117], i.e. $W \propto \varepsilon$, and for the cases of large differences $|W_{ll} - W_{ss}|$ or $|\gamma_{lv} - \gamma_{sv}|$, the combining rule for the free energy of adhesion of a solid–liquid pair can be written as

$$W_{sl} = \left(1 - \alpha_1(W_{ll} - W_{ss})^2\right)\sqrt{W_{ll}W_{ss}} \tag{47}$$

where α_1 is an empirical constant which is in general different from κ_1 in Eq. (46); more explicitly, by using $W_{ll} = 2\gamma_{lv}$ and $W_{ss} = 2\gamma_{sv}$,

$$W_{sl} = 2\left(1 - \beta_1(\gamma_{lv} - \gamma_{sv})^2\right)\sqrt{\gamma_{lv}\gamma_{sv}} \tag{48}$$

In the above, α_1 and β_1 $(= 4\alpha_1)$ are as yet unknown constants. Clearly, when the values of γ_{lv} and γ_{sv} are close to each other, Eq. (48) reverts to the geometric mean combining rule. By combining Eq. (48) with Eq. (31), an alternative equation of state for solid–liquid interfacial tensions [125,126] can be written as

$$\gamma_{sl} = \gamma_{lv} + \gamma_{sv} - 2\sqrt{\gamma_{lv}\gamma_{sv}}\left(1 - \beta_1(\gamma_{lv} - \gamma_{sv})^2\right) \tag{49}$$

Combining Eq. (49) with Young's Eq. (1) yields

$$\cos\theta_Y = -1 + 2\sqrt{\frac{\gamma_{sv}}{\gamma_{lv}}}\left(1 - \beta_1(\gamma_{lv} - \gamma_{sv})^2\right) \tag{50}$$

The question then becomes whether this combining rule fits the experimental contact angle patterns shown earlier. Obviously, for a given set of γ_{lv} and θ data measured on one and the same type of solid surface, the constant β_1 and γ_{sv} values can be determined by a two-variable least-square analysis technique [64,123,124]. Starting out with arbitrary values for γ_{lv} and β_1, iterative procedures can be used to identify that pair of γ_{sv} and β_1 values which provides the best fit of the experimental data to the set of experimental γ_{lv} and θ_Y pairs belonging to one and the same solid surface. Fig. 20 shows the best-fitted curves of Eq. (50) onto the experimental contact angle data for several solid surfaces previously considered. It can be seen that Eq. (50) fits these experimental data very well. The results of such a least-square analysis are summarized in Table 6. Since the β_1 values do not

Table 6
γ_{sv} (mJ/m^2) and β (m^2/mJ)^2 values determined by a two-variable least-square fit, for the two equation-of-state formulations

Solid surface/technique	No. of system	Eq. (44)		Eq. (50)	
		β	γ_{sv}	β_1	γ_{sv}
FC-721-coated mica/capillary rise [86]	8	0.000124	11.7	0.000097	11.7
FC-722-coated mica/ADSA-P [80]	17	0.000111	11.8	0.000092	11.6
FC-722-coated silicon wafer/ADSA-P [89]	4	0.000111	11.8	0.000092	11.6
FC-725-coated silicon wafer/ADSA-P [90]	9	0.000114	11.9	0.000092	11.6
Teflon FEP/capillary rise [86]	9	0.000142	18.0	0.000118	17.8
Hexatriacontane/capillary rise [51,97]	4	0.000124	20.3	0.000100	19.7
Cholesteryl acetate/capillary rise [51,98]	4	0.000128	21.5	0.000104	20.9
Poly(propene-*alt*-*N*-(*n*-hexyl)maleimide)/ADSA-P [76,88]	5	0.000122	27.9	0.000109	27.8
Poly(*n*-butyl methacrylate)/ADSA-P [91]	6	0.000124	28.8	0.000108	28.5
Polystyrene/ADSA-P [92]	6	0.000120	29.7	0.000107	29.5
Poly(styrene-*alt*-(hexyl/10-carboxydecyl (90/10)maleimide))/ADSA-P [93]	5	0.000120	30.8	0.000106	30.6
Poly(methyl methacrylate/*n*-butyl methacrylate)/ADSA-P [94]	6	0.000136	34.7	0.000124	34.6
Poly(propene-*alt*-*N*-(*n*-propyl)maleimide)/ADSA-P [76,88]	6	0.000133	36.9	0.000123	36.9
Poly(methyl methacrylate)/ADSA-P [95]	7	0.000113	38.3	0.000106	38.2
Poly(propene-*alt*-*N*-methylmaleimide)/ADSA-P [89]	3	0.000167	43.4	0.000155	43.3

appear to show any dependence on the solid surfaces [125,126], a weighted mean β_1 was calculated. This yields $\beta_1 = 0.0001057$ (m^2/mJ)^2. A comparison between the γ_{sv} values for various solid surfaces obtained from the two equation of state formulations is given in Table 6. It can be seen that the γ_{sv} values obtained from the two formulations (equations) are virtually identical. Although the two relations are very different, Eq. (45) can indeed be obtained from a first-order approximation of a Taylor-series expansion of the adjusting parameter in Eq. (40). A FORTRAN computer program to calculate γ_{sv} from γ_{lv} and θ, using Eq. (50) with $\beta_1 = 0.0001057$ (m^2/mJ)^2, is given in Appendix B.

Since Eq. (46) was formulated here as an expression similar to those of Eq. (36) and Eq. (39), insight about molecular interactions of unlike pairs can be gained; the rationale is as follows. Knowing $\beta_1 = 0.0001057$ (m^2/mJ)^2, the present form of the combining rule for the free energy of adhesion, Eq. (47), can be written as

$$W_{sl} = \left(1 - 0.0000264(W_{ll} - W_{ss})^2\right)\sqrt{W_{ll}W_{ss}} \tag{51}$$

where $\alpha_1 = \beta_1/4 = 0.0000264$ (m^2/mJ)^2. Since $W \propto \varepsilon$ and if $W \approx k\varepsilon$, a combining rule for the energy parameter can be derived:

$$\varepsilon_{sl} = \left(1 - 0.0000264k^2(\varepsilon_{ll} - \varepsilon_{ss})^2\right)\sqrt{\varepsilon_{ll}\varepsilon_{ss}} \tag{52}$$

where k is a proportionality constant.

Although the proportionality constant k is unknown at the moment, Eq. (52)

should, in principle, be able to tell us something about the molecular interactions between unlike solid–liquid pairs. In the study of molecular interactions between solids and liquids through, e.g. the Lennard–Jones solid–fluid potential [45,48,49,114], a combining rule is always required to represent the interactions of unlike pairs of molecules ε_{ij} from those of like pairs, ε_{ii} and ε_{jj}. However, the exact form of the combining rule for solid–liquid energy potential is often uncertain owing to the fact that estimating solid–liquid interfacial tensions directly is a difficult task and hence any specific (proposed) form of the combining rule cannot be easily tested and verified. As Eq. (52) stands, information about unlike molecu-

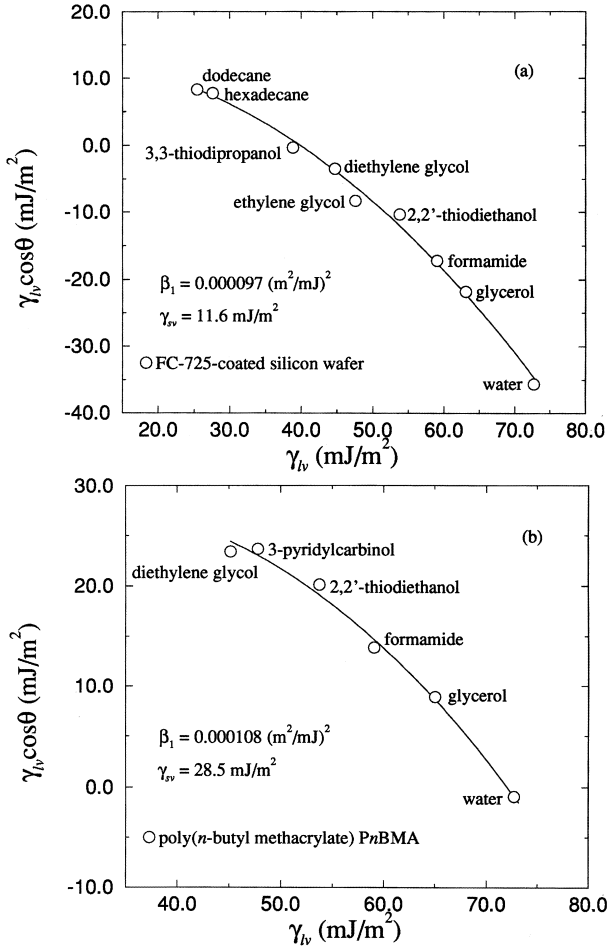

Fig. 20. $\gamma_{lv}\cos\theta$ vs. γ_{lv} for (a) FC-725-coated silicon wafer [90], (b) poly(*n*-butyl methacrylate) P*n*BMA [91], (c) polystyrene PS [92], (d) poly(styrene-*alt*-(hexyl/10-carboxydecyl(90/10)maleimide)) [93], (e) poly(methyl methacrylate/*n*-butyl methacrylate) P(MMA/*n*BMA) [94], and (f) poly(methyl methacrylate) PMMA [95]. All curves are best-fits of Eq. (50) to experimental data.

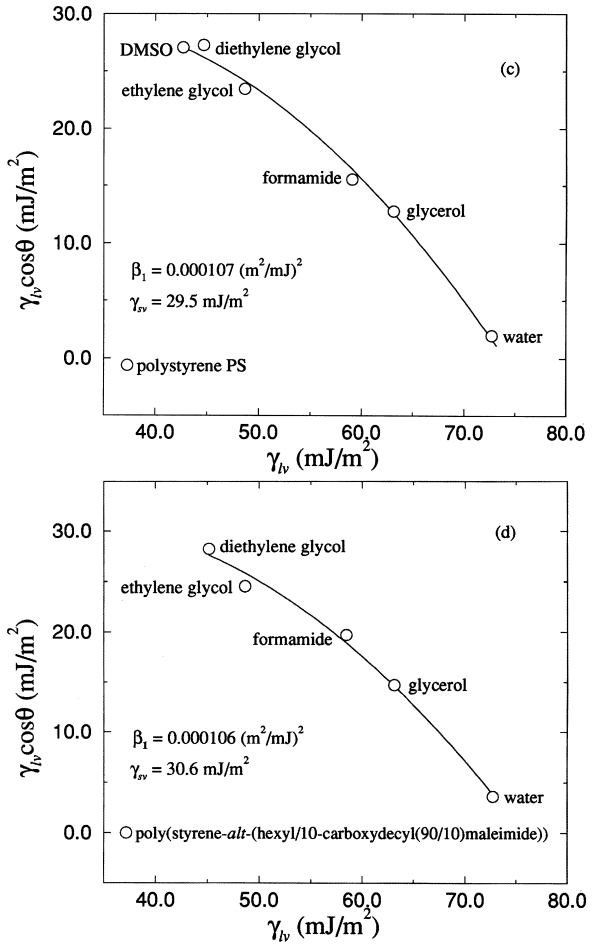

Fig. 20. Continued

lar interactions can be inferred when the proportionality constant k is known. It should be realized that Eq. (46) can be formulated for k to drop out, e.g. by normalization. This procedure should allow the determination of a combining rule for the specific solid–liquid interactions.

3.2.5. Comparison with the original equation of state formulation

The formulation of an equation of state approach is essentially an empirical curve fit to contact angle data. As such there are a variety of ways in which one might proceed. It was decided in the original formulation [12,13] to correlate the data in terms of Good's interaction parameter Φ:

$$\Phi = \frac{\gamma_{sv} + \gamma_{lv} - \gamma_{sl}}{2\sqrt{\gamma_{lv}\gamma_{sv}}} \tag{53}$$

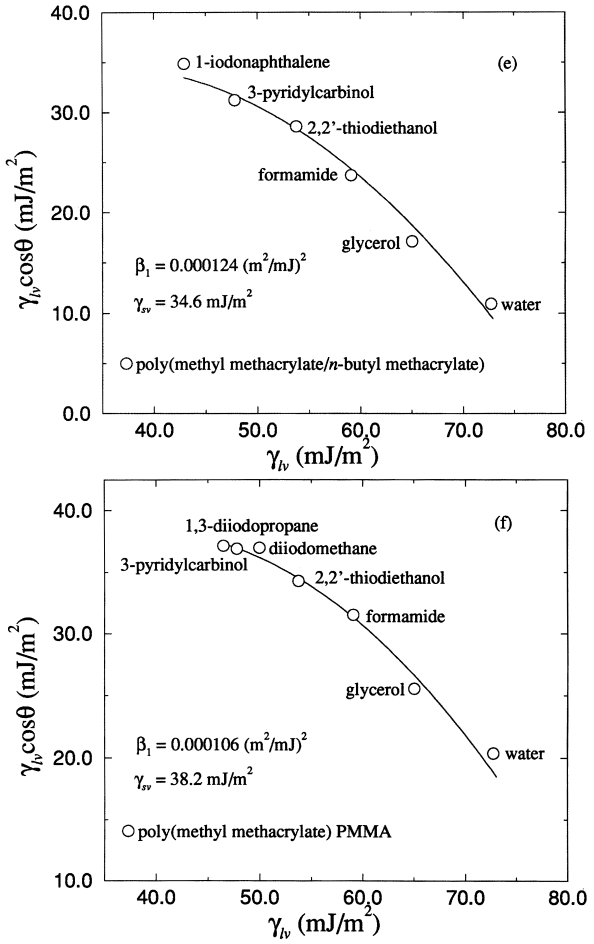

Fig. 20. Continued

The explicit form of such an equation-of-state relation was formulated as

$$\gamma_{sl} = \frac{\left(\sqrt{\gamma_{lv}} - \sqrt{\gamma_{sv}}\right)^2}{1 - 0.015\sqrt{\gamma_{lv}\gamma_{sv}}} \tag{54}$$

Combining Eq. (54) with Young's equation yields

$$\cos\theta_Y = \frac{(0.015\gamma_{sv} - 2.00)\sqrt{\gamma_{lv}\gamma_{sv}} + \gamma_{lv}}{\gamma_{lv}\left(0.015\sqrt{\gamma_{lv}\gamma_{sv}} - 1\right)} \tag{55}$$

It should be noted that Eq. (54) (and hence Eq. (55)) was derived based on

Table 7
Comparison between the three equation-of-state formulations by calculating the γ_{sv} values for hypothetical values of γ_{lv} (mJ/m^2) and θ (degree)

γ_{lv}	θ	γ_{sv} (mJ/m^2)		
		Li et al. [64] Eq. (44)	Kwok et al. [125] Eq. (50)	Neumann et al. [14] Eq. (55)
70.0	20.0	66.1	66.1	66.0
70.0	30.0	61.9	61.8	61.7
70.0	40.0	56.9	56.7	56.5
70.0	50.0	51.5	51.0	50.8
70.0	60.0	45.7	45.1	45.0
70.0	70.0	39.7	39.0	39.1
70.0	80.0	33.6	33.0	33.2
70.0	90.0	27.5	27.0	27.1
70.0	100.0	21.5	21.3	21.1
70.0	110.0	15.8	15.9	15.2
50.0	20.0	47.1	47.1	47.1
50.0	30.0	43.9	43.9	44.0
50.0	40.0	40.0	39.8	40.0
50.0	50.0	35.4	35.3	35.1
50.0	60.0	30.8	30.5	30.2
50.0	70.0	26.0	25.6	25.4
50.0	80.0	21.2	20.8	20.6
50.0	90.0	16.5	16.2	16.2
50.0	100.0	12.2	11.9	12.0
30.0	20.0	28.2	28.2	28.2
30.0	30.0	26.2	26.2	26.2
30.0	40.0	23.6	23.6	23.6
30.0	50.0	20.7	20.6	20.6
30.0	60.0	17.5	17.5	17.5
30.0	70.0	14.4	14.3	14.3
30.0	80.0	11.3	11.2	11.3

extensive contact angle measurements of eight polymer surfaces from Zisman et al. almost 50 years ago. This formulation was first attempted in the 1960s [12] and completed in the 1970s [13]. Note that difficulties may arise for liquids with relatively large liquid surface tensions γ_{lv}, since the denominator of Eq. (55) can become zero. This limitation of the equation of state formulation is due to the use of Good's interaction parameter Φ and is purely mathematical. Physical reasoning has been used to 'mend' Eq. (55), and in practice Eq. (55) is implemented as a computer program [13] (Appendix C) or a set of tables [127]. However, as mentioned, the use of Good's interaction parameter Φ is not the only way to find an explicit expression for the equation of state; two different formulations have been discussed in the previous sections.

It is instructive to compare Eq. (55) with that proposed by Li et al. [14,64], Eq. (44), and the new formulation [125,126], Eq. (50), by calculating γ_{sv}, with hypothetical values of γ_{lv} and θ. Examples of these results are given in Table 7. It is evident

that the three equations yield essentially the same γ_{sv} values. We wish to point out that these results are not trivial. The above three formulations were based on entirely different sets of experimental contact angle data: Eq. (55) was obtained using Zisman's contact angles on eight polymer surfaces [13]; the β in Eq. (44) was calibrated by the contact angles of Li et al. [14,64] on three different solid surfaces; the β_1 in Eq. (50) was obtained from the low-rate dynamic contact angles on the 14 solid surfaces presented in Sections 2.3 and 2.4 [125,126]. It is remarkable that, despite the different formulations and experimental contact angles, Eqs. (44), (50) and (55) yield virtually the same γ_{sv} values, as given in Table 7. For practical purposes, any of the three equations can be used.

3.2.6. Predictive power of the equation of state approach

In this section, the predictive power of the equation of state approach will be illustrated simply by predicting, from a single contact angle measurement, all the other contact angles measured on one and the same solid surface. Since the γ_{sv} values obtained from the three formulations are virtually the same, the choice of any specific formulations becomes irrelevant.

For example, if the surface tension ($\gamma_{lv} = 23.9$ mJ/m^2) and contact angle ($\theta = 67.4°$) of decane on a FC-722-coated mica surface are chosen (from Fig. 7), the equation of state approach [14,64] Eq. (44), yields γ_{sv} value of 11.9 mJ/m^2. From this γ_{sv} value, Eq. (44) can generate a series of contact angles for different

Table 8
Comparison between the measured and predicted contact angles and liquid surface tensions on a FC-722-coated mica

Liquid	θ (degree)		γ_{lv} (mJ/m^2)	
	Measured	Predicted[a] from Eq. (44)	Measured	Predicted[a] from Eq. (44)
Decane	67.36	–	23.88	–
1-Pentanol	72.95	71.4	26.01	26.8
trans-Decalin	73.38	73.4	27.19	27.2
Hexadecane	75.94	74.2	27.62	28.6
1-Decanol	78.84	76.4	28.99	30.4
cis-Decalin	79.56	81.3	32.32	31.3
Ethyl cinnamate	86.54	87.4	37.17	36.6
Dibenzylamine	90.70	91.5	40.80	40.2
Dimethyl sulfoxide	90.95	93.5	42.68	40.4
1-Bromonaphthalene	93.81	95.2	44.31	43.3
Diethylene glycol	94.22	95.6	44.68	43.5
Ethylene glycol	97.87	98.4	47.55	47.0
Diiodomethane	101.18	100.7	49.98	50.5
2,2′-Thiodiethanol	104.56	106.3	56.26	54.4
Formamide	108.49	108.7	59.08	59.0
Glycerol	111.73	113.5	65.02	62.9
Water	118.69	119.3	72.70	71.9

[a] Based on a γ_{sv} value of 11.9 mJ/m^2 calculated from the contact angle of decane.

values of γ_{lv}. These procedures are employed to produce a set of hypothetical contact angles corresponding to the surface tensions of the other liquids on the FC-722 surface. The predicted contact angle results are given in Table 8. In all cases, the predicted and measured contact angles agree well, generally within the usual error limit given in the literature as $\pm 2°$.

Conversely, a series of hypothetical γ_{lv}, values for different experimental contact angle values can also be generated from a single decane contact angle measurement. The predicted γ_{lv} values are also shown in Table 8 for the FC-722-coated surface; it can be seen that the deviations between the predicted and measured values vary from ± 0.1 mJ/m^2 to ± 2.0 mJ/m^2: While these deviations are somewhat outside the experimental error limits, there is no evidence of any systematic variation. Similar calculations can be performed for other solid surfaces, with similar results. From a single contact angle measurement on one and the same solid surface, the equation of state approach [14,64] is capable of predicting the contact angles of different liquids as well as the liquid surface tensions.

4. Evaluation of existing contact angle data

In Section 2.3, we have shown that static contact angles measured by conventional goniometer techniques could be meaningless in the context of Young's equation. By measuring dynamic contact angles at very slow motion of the three-phase contact line using an automated drop shape technique, we obtained a variety of contact angle patterns, which cannot be easily detected by conventional goniometer contact angle techniques and procedures. For example, slip/stick of the three-phase contact line was obtained, where the contact angle increases steadily by as much as 35° at constant three-phase radius. Although such patterns are very interesting, they have to be discarded if the aim is to deduce solid surface tensions: since γ_{lv}, γ_{sv}, and γ_{sl} are material properties and are expected to be constant, Young's equation implies a unique contact angle. Thus, the interpretation of contact angles for solid surface tensions from slip/stick of the three-phase contact line would be meaningless.

Apart from the applicability of Young's equation, several other widely made assumptions are often overlooked. In an example (Fig. 11) shown in Section 2.3.3, the contact angle increases as the drop front advances with essentially constant γ_{lv}. While there is no reason to question the applicability of Young's equation, γ_{sl} is suspected to change: from Young's equation, if γ_{lv} and γ_{sv} are constant, changes in θ must be a consequence of a change in γ_{sl}. While such cases might be very interesting in a different context, they have to be discarded if our goal is to deduce solid surface tension from the simplest possible situations.

The above findings are not readily attainable for static contact angle measurements using conventional goniometer techniques and procedures: goniometer data may contain a mixture of meaningful and meaningless angles for solid surface tensions. If one neglects the goniometer angles shown to be meaningless in the low-rate dynamic contact angle study by, e.g. axisymmetric drop shape analysis —

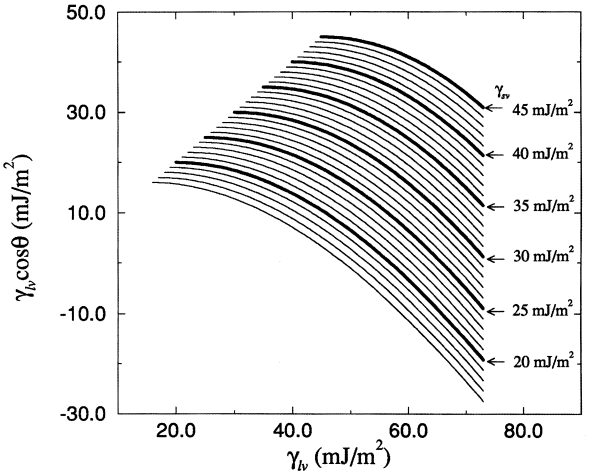

Fig. 21. $\gamma_{lv}\cos\theta$ vs. γ_{lv} generated from the equation of state approach, Eq. (44), from γ_{sv} = 16.0 mJ/m^2 to 45.0 mJ/m^2, in 1.0 mJ/m^2 increments.

profile (ADSA-P), smooth curves emerge in plots of $\gamma_{lv}\cos\theta$ vs. γ_{lv}. This pattern was used to deduce a functional relationship to be used in conjunction with Young's equation for determining solid surface tensions.

Nevertheless, there is an abundance of contact angle data in the literature which were obtained from static measurements, and are hence of unknown status. The question then arises as to whether one should neglect completely the literature contact angle data and repeat all measurements using a dynamic procedure, such as ADSA-P, or whether some of the data can be salvaged. This question will be explored in this section [128], using Zisman's contact angle data on 34 different types of solid surfaces.

The rationale of evaluating literature contact angle data is as follows. After discarding all those measurements which violate the basic assumptions made in all contact angle approaches of current interest [11–17], the low-rate dynamic contact angle measurements yielded contact angles which fell on smooth curves in plots of $\gamma_{lv}\cos\theta$ vs. γ_{lv}, for one and the same solid surface [76,80,88–95]. Assuming that this would also have happened in the systems studied in the laboratory of Zisman [10], we propose to discard those contact angle data which do not sensibly fall on a smooth curve.

The equation of state approach for solid–liquid interfacial tensions [14], i.e. Eq. (44), described in Section 3.2.3 can be used to evaluate these data by generating a series of theoretical constant γ_{sv}, curves, in plots of $\gamma_{lv}\cos\theta$ vs. γ_{sv}. Fig. 21 shows the theoretical curves generated by the equation of state approach, i.e. Eq. (44), from γ_{sv} = 16.0 mJ/m^2 to γ_{sv} = 45.0 mJ/m^2 in 1.0 mJ/m^2 increments; each curve represents a constant γ_{sv} value and hence a hypothetical solid surface. Thus, if goniometer contact angle data are plotted in this graph, it can be decided how well data for any one solid fall onto an individual curve.

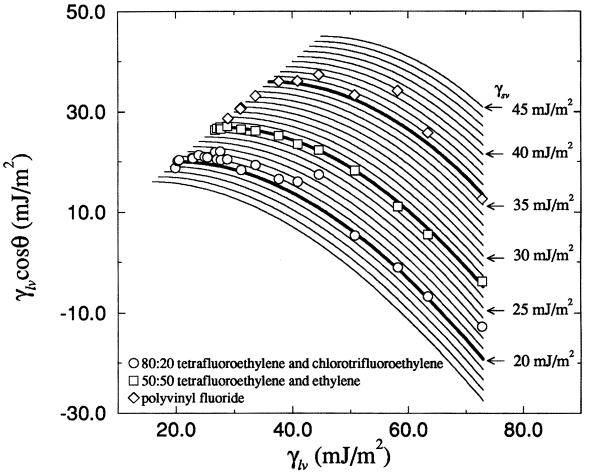

Fig. 22. $\gamma_{lv}\cos\theta$ vs. γ_{lv} for Zisman's data on 80:20 copolymer of tetrafluoroethylene and chlorotrifluoroethylene [129], 50:50 copolymer of tetrafluoroethylene and ethylene [129], and polyvinyl fluoride [130], as well as theoretical constanry, curves from Fig. 21.

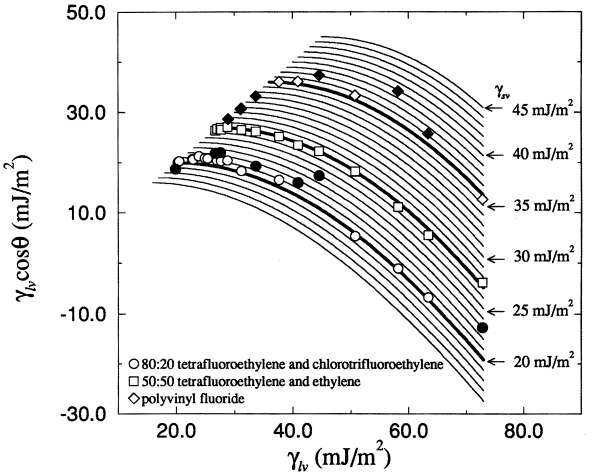

Fig. 23. $\gamma_{lv}\cos\theta$ vs. γ_{lv} for Zisman's data on 80:20 copolymer of tetrafluoroethylene and chlorotrifluoroethylene [129], 50:50 copolymer of tetrafluoroethylene and ethylene [129], and polyvinyl fluoride [130]. Contact angle data which are clearly outside a constant γ_{sv} curve by more than ± 1.0 mJ/m^2 are discarded (solid symbols).

Fig. 22 shows the contact angle data of Zisman et al. for 80:20 copolymer of tetrafluoroethylene and chlorotrifluoroethylene [129], 50:50 copolymer of tetrafluoroethylene and ethylene [129], and polyvinyl fluoride [130] surfaces, as well as the theoretical curves from Fig. 21. In Fig. 22, the data points for the 50:50 tetrafluo-

roethylene and ethylene surface fall consistently close to the theoretical constant γ_{sv} curve of 27.0 mJ/m^2. However, considerable scatter is apparent for the other surfaces. As we have discussed in Section 2.4.1, vapor adsorption of liquids which could cause γ_{sv} to change from one liquid to the next by as low as 1 mJ/m^2 has been considered possible [102]. If ± 1.0 mJ/m^2 is selected as the allowable error, contact angle data which deviate away from a theoretical γ_{sv} curve by more than ± 1.0 mJ/m^2 can be disregarded. It should be noted that this criterion is not an overestimate: the widely-accepted goniometer accuracy of $\pm 2°$ could easily cause the data points in Fig. 22 to vary along the $\gamma_{lv}\cos\theta$ axis by as much as ± 2.0 mJ/m^2. Following the above procedures, it was found that seven of the 22 data for the 80:20 tetrafluoroethylene and chlorotrifluoroethylene surface are clearly outside the error band of ± 1.0 mJ/m^2 and, similarly, six out of 11 data for the polyvinyl fluoride surface; these data are rejected, as shown in Fig. 23 in solid symbols.

In principle, the above procedures can be employed for all other solid surfaces. However, if a large amount of contact angle data and solid surfaces are available, these procedures can be tedious and subjective. For this reason, they were automated by constructing a least-square objective function [123,128] to calculate the deviation of all contact angle data away from a theoretical curve generated by a given γ_{sv} value. The best-fitted constant γ_{sv} curve can then be used to discriminate against data which are clearly above or below the curve within a band, e.g. ± 1.0 mJ/m^2. A FORTRAN computer program which automates these procedures is given in Appendix D.

The computer program given in Appendix D was applied to the goniometer data for the following 34 solid surfaces from Zisman et al.: perfluorocapric acid [131], perfluorolauic acid [131], $C_8F_{17}SO_2N(C_3H_7)-CH_2CH_2OOC-CH=CH_2$ (polymer S) [132], $C_7F_{15}CH_2OOC-C(CH_3)=CH_2$ (polymer A) [132], perfluorocaprylic acid [131], perfluorocaproic acid [131], perfluorovaleric acid [131], perfluorobutyric acid [131], 17-(perfluoroheptyl)-heptadecanoic acid [133], 17-(perfluoropentyl)-heptadecanoic acid [133], perfluorodecanoic acid [134], polytetrafluoroethylene [135], 17-(perfluoropropyl)-heptadecanoic acid [133], paraffin [108], hexatriacontane [108], 17-(perfluoroethyl)-heptadecanoic acid [133], 80:20 copolymer of tetrafluoroethylene and chlorotrifluoroethylene [129], stearic acid [136], *n*-octadecylamine [137], ω-monohydroperfluoroundecanoic acid [138], 60:40 copolymer of tetrafluoroethylene and chlorotrifluoroethylene [129], 50:50 copolymer of tetrafluoroethylene and ethylene [129], polytrifluoroethylene [130], polychlorotrifluoroethylene [129], polystyrene [139], 2-ethylhexanoic acid [140], 2-ethylhexylamine [140], 2-ethylhexanol [140], polyvinylidene fluoride [130], polyethylene terephthalate [139], polyvinylidene chloride [130], polyvinyl fluoride [130], nylon (6,6) [139], and perchloropentadienoic acid [130]. Fig. 24 shows the contact angle data for several solid surfaces, together with the fitted γ_{sv} curves; the rejected angles are given in solid symbols. It can be seen that, disregarding the rejected angles, the experimental data points fall closely to a distinct theoretical γ_{sv} curve for each solid within ± 1.0 mJ/m^2. The contact angles for those pairs falling to ± 1.0 mJ/m^2 on smooth theoretical γ_{sv}, curves are given in Table 9, together with the calculated γ_{sv} values

Table 9
Static contact angles from Zisman et al. which fall within ± 1.0 mJ/m^2 on a fitted γ_{sv} curve

Solid surface	Liquid	γ_{lv} (mJ/m^2)	θ (degree)	γ_{sv} Equation of state, Eq. (44)
Perfluorocapric acid[a] [131]	Octane	21.8	64.5	11.5
	Decane	23.9	69.5	11.3
	Dodecane	25.4	73.0	11.1
	Tetradecane	26.7	75.0	11.2
	Hexadecane	27.6	77.0	11.1
Perfluorolauic acid [131]	Pentamer	18.1	60.0	10.3
	Octane	21.8	65.0	11.3
	Decane	23.9	70.0	11.2
	Di-(*n*-amyl) ether	24.9	68.0	12.2
	Dodecane	25.4	74.0	10.9
	Tetradecane	26.7	78.0	10.4
	Hexadecane	27.6	78.0	10.8
	Polyethylene V-120	27.8	78.0	10.9
	Di-(*n*-decyl) ether	28.4	79.0	10.9
	Benzene	28.9	75.0	12.3
	1,6-Hexamethylene glycol Bis-2-ethylhexanoate	30.2	77.0	12.3
	Pentaerythritol tetracaproate	30.4	80.0	11.5
	Polyethylene SS903	30.4	81.0	11.2
	8-*p*-Tolylnonadecane	30.7	83.0	10.7
	Bis-(2-ethylhexyl) sebacate	31.1	79.0	12.1
	n-Decylbenzene	31.2	83.0	10.9
	9-(α-(*cis*-0,3,3-Bicycloöctyl)-methyl)-heptadecane	31.2	84.0	10.6
	4-Cyclohexyleicosane	31.6	83.0	11.1
	1-Cyclohexyl-2-(cyclohexylmethyl)-pentadecane	32.7	84.0	11.2
	1-α-Decalylhendecane	32.7	84.0	11.2
	9-*n*-Dodecylperhydro-phenanthrene	34.2	86.0	11.2
	1,7-Dicyclopentyl-4-(3-cyclopentylpropyl)-heptane	34.6	86.0	11.3
	1,3-Dicyclopentylcyclopentane	34.6	85.0	11.7
	1,1-Di-(α-decalyl)-hendecane	35.1	88.0	10.9
	Benzylphenyl hendecanoate	37.7	92.0	10.6
	Tetrachlorobiphenyl	44.2	96.0	11.6
	Methylene iodide	50.8	103.0	11.3
$C_8F_{17}SO_2N(C_3H_7)-CH_2CH_2OOC-CH=CH_2$ (polymer S)[a] [132]	Tetramer	17.6	48.5	12.2
	Pentamer	18.1	51.5	12.0
	Hexamer	18.5	54.0	11.8
	Nonamer	19.2	56.5	11.7
	Tridecane	25.9	69.5	12.4
	Tetradecane	26.7	71.5	12.2
	Hexadecane	27.6	73.5	12.1
	Ethylene glyol	47.7	102.5	10.4
	Formamide	58.2	110.5	10.8
	Water	71.9	119.0	11.8

Table 9 (*Continued*)

Solid surface	Liquid	γ_{lv} (mJ/m^2)	θ (degree)	γ_{sv} Equation of state, Eq. (44)
$C_7F_{15}CH_2OOC-C(CH_3)=CH_2$ (polymer A)[a] [132]	Pentamer	18.1	48.5	12.6
	Hexamer	18.5	51.5	12.3
	Nonamer	19.2	53.0	12.5
	Dodecane	25.4	67.0	12.8
	Tridecane	25.9	68.0	12.8
	Tetradecane	26.7	71.5	12.2
	Hexadecane	27.6	73.0	12.2
	Formamide	58.2	109.5	11.2
	Water	71.9	118.5	12.0
Perfluorocaprylic acid[a] [131]	Octane	21.8	60.0	12.5
	Decane	23.9	65.8	12.3
	Dodecane	25.4	68.0	12.5
	Tetradecane	26.7	71.0	12.3
	Hexadecane	27.6	74.0	11.9
Perfluorocaproic acid[a] [131]	Octane	21.8	59.0	12.8
	Decane	23.9	64.5	12.6
	Tetradecane	26.7	68.8	13.0
	Hexadecane	27.6	71.8	12.6
Perfluorovaleric acid[a] [131]	Decane	23.9	70.5	13.3
	Dodecane	25.4	67.5	13.2
	Tetradecane	26.7	65.5	13.3
	Hexadecane	27.6	70.5	13.0
Perfluorobutyric acid [131]	Decane	23.9	61.0	13.5
	Dodecane	25.4	64.5	13.5
	Tetradecane	26.7	67.0	13.5
17-(Perfluoroheptyl)-heptadecanoic acid [133]	Heptane	20.3	52.0	13.4
	Octane	21.8	57.0	13.3
	Decane	23.9	64.0	12.8
	Undecane	24.7	64.0	13.2
	Dodecane	25.4	66.0	13.1
	Tridecane	25.9	68.0	12.8
	Tetradecane	26.7	70.0	12.6
	2-Octanol	26.7	70.0	12.6
	1-Octanol	27.8	68.0	13.8
	Bis-(2-ethylhexyl) phthalate	31.3	78.0	12.5
	Dicyclohexyl	32.8	75.0	14.2
	t-Butylna-phthalene	33.7	78.0	13.6
	Tricresyl phosphate	40.9	90.0	12.5
	Tetrachloro-biphenyl	44.2	93.0	12.7
	Formamide	58.2	105.0	13.2
	Glycerol	63.4	107.0	14.4
	Water	72.8	115.0	14.3

Table 9 (*Continued*)

Solid surface	Liquid	γ_{lv} (mJ/m^2)	θ (degree)	γ_{sv} Equation of state, Eq. (44)
17-(Perfluoropentyl)-heptadecanoic acid [133]	Perfluoroalkane (FCD-330)	20.2	33.0	17.1
	Dicyclohexyl	32.8	72.0	15.2
	t-Butylnaphthlene	33.7	73.0	15.3
	Tricresyl phosphate	40.9	81.0	16.0
	Methylene iodide	50.8	94.0	15.1
	Formamide	58.2	100.0	15.6
	Water	72.8	110.0	17.1
Perfluorodecanoic acid [134]	Perfluorokerosene	18.1	26.0	16.3
	Di(*n*-butyl) ether	22.8	47.0	16.3
	Di(isoamyl) ether	23.0	49.0	16.0
	$H(CF_2)_4CH_2OH$	24.5	55.0	15.5
	Di(*n*-amyl) ether	24.9	54.0	16.0
	Carbon tetrachloride	26.8	60.0	15.6
	$CFCl_2-CF_2-CCl_3$	27.8	56.0	17.4
	sec-Butylbenzene	28.7	65.0	15.2
	Propylbenzene	29.0	59.0	17.2
	Butylbenzene	29.2	63.0	16.1
	Tris-(2-ethylhexyl) Tricarballylate	29.6	65.0	15.7
	1,6-Hexamethylene glycol Bis-2-ethylhexanoate	30.2	66.0	15.7
	t-Butylnaphthalene	33.7	71.0	16.0
	Perchlorocyclopentadiene	37.5	73.0	17.3
	Butylphenylhendecanoate	38.0	76.0	16.5
	Tricresyl phosphate	40.9	82.0	15.6
	Pentamethylene glycol	43.4	82.0	16.8
	Methylene iodide	50.8	90.0	16.9
Polytetrafluoroethylene [135]	Tetramer	17.6	8.0	17.4
	Pentamer	18.1	15.0	17.5
	Hexane	18.4	12.0	18.0
	Hexamer	18.5	19.0	17.5
	Nonamer	19.2	26.0	17.4
	Dodecamer	19.6	29.0	17.3
	Heptadecamer	19.9	30.0	17.3
	Heptane	20.3	21.0	19.1
	Polyethylsiloxane	23.3	43.0	17.6
	Di-(2-ethylhexyl) adipate	30.2	61.0	17.3
	Di-(2-ethylhexyl) sebacate	31.1	62.0	17.6
	Di-(2-ethylhexyl) phthalate	31.2	63.0	17.3
	Carbon disulfide	31.4	62.0	17.8
	t-Butylnaphthalene	33.7	65.0	18.2
	Tricresyl phosphate	40.9	75.0	18.4
	Tetraachlorodiphenyl	44.2	78.0	18.9
	Methylene iodide	50.8	88.0	17.3
	Glycerol	63.4	100.0	18.1
	Water	72.8	108.0	18.3

Table 9 (*Continued*)

Solid surface	Liquid	γ_{lv} (mJ/m^2)	θ (degree)	γ_{sv} Equation of state, Eq. (44)
17-(Perfluoropropyl)-heptadecanoic acid [133]	Perfluoroalkane (FCD-330)	20.2	23.0	18.6
	Bis-(2-ethylhexyl) phthalate	31.3	60.0	18.4
	Dicyclohexyl	32.8	62.0	18.6
	Tricresyl phosphate	40.9	72.0	19.6
	Ethylene glycol	47.7	84.0	18.1
	Methylene iodide	50.8	86.0	18.8
	Water	72.8	106.0	19.4
Paraffin [108]	Std. fluorolube	25.1	38.0	20.2
	Formamide	58.2	91.0	20.1
	Glycerol	63.4	96.0	20.2
	Water	72.8	108.0	18.2
Hexatriacontane [108]	Polymethylsiloxane	19.9	20.0	18.7
	Di(*n*-amyl) ether	24.9	41.0	19.3
	Std. fluorolube	25.1	43.0	19.0
	Di(*n*-heptyl) ether	27.0	45.0	19.9
	Hexadecane	27.6	46.0	20.1
	Di(*n*-decyl) ether	27.7	50.0	19.0
	n-Heptylic acid	28.3	49.0	19.8
	Tri(2-ethylhexyl) tricarballylate	29.6	56.0	18.6
	Pentaerythtitol tetraeaproate	30.4	56.0	19.1
	Trieresyl phosphate	40.9	72.0	19.6
	Formamide	58.2	92.0	19.6
	Glycerol	63.4	97.0	19.7
17-(Perfluoroethyl)-heptadecanoic acid [133]	Dicyclohexyl	32.8	61.0	19.0
	Tricresyl phosphate	40.9	72.0	19.6
	Ethylene glycol	47.7	80.0	19.9
	Methylene iodide	50.8	83.0	20.2
	Formamide	58.2	94.0	18.6
	Water	72.8	105.0	20.0
80:20 Tetrafluoroethylene and chlorotrifluoroethylene [129]	Heptane	20.3	8.0	20.1
	Di(*n*-propyl) ether	20.5	8.0	20.3
	Di(*n*-butyl) ether	22.8	25.0	20.8
	Nonane	22.9	26.0	20.7
	Di(*n*-amyl) ether	24.9	33.0	21.1
	Dodecane	25.4	35.0	21.1
	Di(*n*-heptyl) ether	27.0	41.0	21.0
	Di(*n*-octyl) ether	27.7	43.0	21.0
	Benzene	28.8	45.0	21.3
	Di(2-ethylhexyl) phthalene	31.2	54.0	20.2
	Benzyl phenylundecanoate	37.7	64.0	20.9
	Methylene iodide	50.8	84.0	19.7
	Formamide	58.2	91.0	20.2
	Glycerol	63.4	96.0	20.2

Table 9 (*Continued*)

Solid surface	Liquid	γ_{lv} (mJ/m^2)	θ (degree)	γ_{sv} Equation of state, Eq. (44)
Stearic acid [136]	Octanoic acid	29.2	40.0	23.0
	Nonanoic acid	29.5	43.0	22.4
	Tricresyl phosphate	40.9	65.0	22.5
	Tetrachlorobiphenyl	44.2	70.0	22.4
	Thiodiglycol	54.0	81.0	23.0
	Glycerol	63.4	92.0	22.4
n-Octadecylamine [137]	Di(*n*-butyl) ether	22.8	9.0	22.5
	Nonane	22.9	13.0	22.3
	Decane	23.9	18.0	22.7
	Di(*n*-amyl) ether	24.9	22.0	23.2
	Dodecane	25.4	30.0	22.2
	Tetradecane	26.7	34.0	22.4
	Di(*n*-heptyl) ether	27.0	34.0	22.7
	Hexadecane	27.6	38.0	22.2
	Di(*n*-octyl) ether	27.7	36.0	22.8
	Di(*n*-decyl) ether	28.4	37.0	23.1
	Tri(2-ethylhexyl) tricarballylate	29.6	45.0	21.9
	Hexylbenzene	30.0	39.0	22.3
	1,6-Hexamethylene glycol di-2-ethyl-hexanoate	30.2	44.0	22.6
	Pentaerythritol tetracaproate	30.4	43.0	23.1
	Di(2-ethylhexyl) sebacate	31.1	46.0	22.7
	Di(2-ethylhexyl) phthalate	31.2	49.0	21.9
	Decylbenzene	31.2	44.0	23.4
	α-Methylnaphthalene	36.4	55.0	23.5
	Benzylphenylundecanoate	37.7	58.0	23.2
	Tricresyl phosphate	40.9	65.0	22.5
	Glycerol	63.4	90.0	23.6
	Water	72.8	102.0	21.9
ω-Monohydroperfluoro-undecanoic acid [138]	*n*-Amyl amine	25.2	9.0	24.9
	1,6-Hexamethylene glycol di-2-ethyl-hexanoate	30.2	39.0	24.1
	Di-(2-ethylhexyl) phthalate	31.2	40.0	24.6
	Glycerol	63.4	89.0	24.1
	Water	72.8	97.0	24.9
60:40 Tetrafluoro-ethylene and chlorotrifluoroethylene [129]	Di(*n*-heptyl) ether	27.0	22.0	25.1
	Hexadecane	27.6	24.0	25.2
	Benzene	28.8	25.0	26.2
	t-Butylnaphthalene	33.7	45.0	25.0
	Tricresyl phosphate	40.9	56.0	26.3
	α-Bromonaphthalene	44.6	63.0	25.8
	Glycerol	63.4	87.0	25.2
	Water	72.8	94.0	26.7

Table 9 (*Continued*)

Solid surface	Liquid	γ_{lv} (mJ/m^2)	θ (degree)	γ_{sv} Equation of state, Eq. (44)
50:50 Tetrafluoroethylene and ethylene [129]	Tetradecane	26.7	9.0	26.4
	Di(*n*-heptyl) ether	27.0	9.0	26.7
	Hexadecane	27.6	12.0	27.0
	Di(*n*-octyl) ether	27.7	16.0	26.6
	Benzene	28.8	20.0	27.1
	Di(2-ethylhexyl) phthalate	31.2	32.0	26.8
	t-Butylnaphthalene	33.7	39.0	26.9
	Benzyl phenylundecanoate	37.7	48.0	27.0
	Tricresyl phosphate	40.9	55.0	26.7
	α-Bromonaphthalene	44.6	60.0	27.1
	Methylene iodide	50.8	69.0	27.0
	Formamide	58.2	79.0	26.5
	Glycerol	63.4	85.0	26.4
	Water	72.8	93.0	27.4
Polytrifluoroethylene [130]	Bis-(2-ethylhexyl) phthalate	31.2	22.0	29.0
	Benzyl phenylundecanoate	37.7	44.0	28.5
	Tricresyl phosphate	40.9	49.0	29.0
	Formamide	58.2	76.0	28.0
	Glycerol	63.4	82.0	28.1
	Water	72.8	92.0	28.0
Polychlorotrifluoroethylene [129]	Methylene iodide	50.8	64.0	29.5
	Glycerol	63.4	82.0	28.1
	Water	72.8	90.0	29.2
Polystyrene [139]	Formamide	58.2	74.0	29.2
	Glycerol	63.4	80.0	29.2
	Water	72.8	91.0	28.6
2-Ethylhexanoic acid [140]	Decyl acetate	28.5	2.0	28.5
	Bis-(*n*-butyl)-pyrotartrate	29.3	5.0	29.2
	Bis-(2-ethylhexyl)-β-methyladipate	30.2	14.0	29.3
	1,6-Hexanediol bis-(2-ethylhexanoate)	30.2	10.0	29.7
	Bis-(2-ethylhexyl) tetrahydrophthalate	30.7	14.0	29.8
	Polyethylene SS 906	30.7	23.0	28.3
	Bis-(2-ethylhexyl)-sebacate	31.1	15.0	30.0
	1-Cyclohexyl-2-(cyclo-hexylmethyl)-pentadecane	32.7	27.0	29.3
	9-*n*-Dodecylperhydro-phenanthrene	34.2	32.0	29.4
	1,1-Bis-(α-decalyl)-hendecane	35.1	34.0	29.6

Table 9 (*Continued*)

Solid surface	Liquid	γ_{lv} (mJ/m^2)	θ (degree)	γ_{sv} Equation of state, Eq. (44)
2-Ethylhexylamine [140]	α-Bromonaphthalene	44.6	53.0	30.1
	Methylene iodide	50.8	63.0	29.9
2-Ethylhexanol [140]	Tricresyl phosphate	40.9	37.0	33.5
	Bis-(2-phenylethyl)-β-methyl adipate	41.3	42.0	32.0
	α-Bromonaphthalene	44.6	45.0	33.5
Polyvinylidene fluoride [130]	Benzyl phenylundecanoate	37.7	26.0	34.1
	α-Bromonaphthalene	44.6	42.0	34.7
	Water	72.8	82.0	34.2
Polyethylene terephthalate [139]	Formamide	58.2	61.0	36.2
	Water	72.8	81.0	34.9
Polyvinylidene chloride [130]	Formamide	58.2	61.0	36.2
	Water	72.8	80.0	35.5
Polyvinyl fluoride [130]	Benzyl phenylendecanoate	37.7	17.0	36.1
	Tricresyl phosphate	40.9	28.0	36.4
	Methylene iodide	50.8	49.0	36.6
	Water	72.8	80.0	35.5
Nylon (6,6) [139]	Formamide	58.2	50.0	41.9
	Glycerol	63.4	60.0	40.6
	Water	72.8	70.0	41.7
Perchloropentadienoic acid [130]	Methylene iodide	50.8	34.0	43.1
	Glycerol	63.4	56.0	42.8
	Water	72.8	66.0	44.2

[a] Contact angles were estimated from graphs.

from the equation of state approach [14,64] [Eq. (44)]. It can be seen that the calculated γ_{sv}, values for these surfaces are indeed quite constant. The γ_{sv} values for the 34 solid surfaces obtained from the above least-square fit are summarized in Table 10; the number of contact angles available and being rejected are also shown.

To illustrate the procedures for eliminating contact angles, we reproduced in Fig. 25 the data for the polyvinyl fluoride surface from Fig. 22. For the 11 data in Fig. 25, a best-fitted γ_{sv} value of 36.3 mJ/m^2 was obtained from Eq. (44). Thus, the contact angle which deviates away from a constant γ_{sv} curve generated by this value within a band will be rejected. The first rejected data point is #1 in Fig. 25; a new fitted γ_{sv} value was then obtained from the remaining 10 data. The above

Table 10
Summary of the γ_{sv} (mJ/m^2) values from curve fitting of Eq. (44) for 34 solid surfaces, using contact angle data from Zisman et al.

Solid surface	No. of data		γ_{sv}
	Available	Rejected	
Perfluorocapric acid[a] [131]	5	0	11.2
Perfluorolauic acid [131]	45	18	11.2
$C_8F_{17}SO_2N(C_3H_7)-CH_2CH_2OOC-CH=CH_2$ (polymer S)[a] [132]	19	9	11.4
$C_7F_{15}CH_2OOC-C(CH_3)=CH_2$ (polymer A)[a] [132]	19	10	11.9
Perfluorocaprylic acid[a] [131]	5	0	12.3
Perfluorocaproic acid[a] [131]	5	1	12.7
Perfluorovaleric acid[a] [131]	4	0	13.2
Perfluorobutyric acid [131]	3	0	13.5
17-(Perfluoroheptyl)-heptadecanoic acid [133]	30	13	13.7
17-(Perfluoropentyl)-heptadecanoic acid [133]	17	10	16.2
Perfluorodecanoic acid [134]	88	70	16.4
Polytetrafluoroethylene [135]	56	37	18.0
17-(Perfluoropropyl)-heptadecanoic acid [133]	17	10	19.1
Paraffin [108]	20	16	19.3
Hexatriacontane [108]	35	23	19.6
17-(Perfluoroethyl)-heptadecanoic acid [133]	19	13	19.7
80:20 Tetrafluoroethylene and chlorotrifluoroethylene [129]	22	8	20.2
Stearic acid [136]	18	12	22.6
n-Octadecylamine [137]	38	16	22.6
ω-Monohydroperfluoroundecanoic acid [138]	24	19	24.6
60:40 Tetrafluoroethylene and chlorotrifluoroethylene [129]	17	9	26.1
50:50 Tetrafluoroethylene and ethylene [129]	14	0	26.9
Polytrifluoroethylene [130]	15	9	28.1
Polychlorotrifluoroethylene [129]	9	6	28.9
Polystyrene [139]	7	4	28.9
2-Ethylhexanoic acid [140]	18	8	29.3
2-Ethylhexylamine [140]	13	10	30.0
2-Ethylhexanol [140]	13	11	33.1
Polyvinylidene fluoride [130]	13	10	34.3
Polyethylene terephthalate [139]	7	5	35.2
Polyvinylidene chloride [130]	6	4	35.7
Polyvinyl fluoride [130]	11	7	35.7
Nylon (6,6) [139]	7	4	41.5
Perchloropentadienoic acid [130]	3	0	43.7

[a]Contact angles were estimated from graphs.

procedures were repeated until all (remaining) data points fall to ± 1.0 mJ/m^2 on a smooth γ_{sv} curve, as summarized in Table 11. Details have been given in Appendix D.

For several solid surfaces in Table 10, γ_{sv} values had been obtained from more accurate contact angles. It is, therefore, instructive to compare these values with those determined from the above fitting procedures using Zisman's goniometer data. For example, γ_{sv} values of 28.3 mJ/m^2 and 29.9 $\pm$ 0.5 mJ/m^2 (in Table 4)

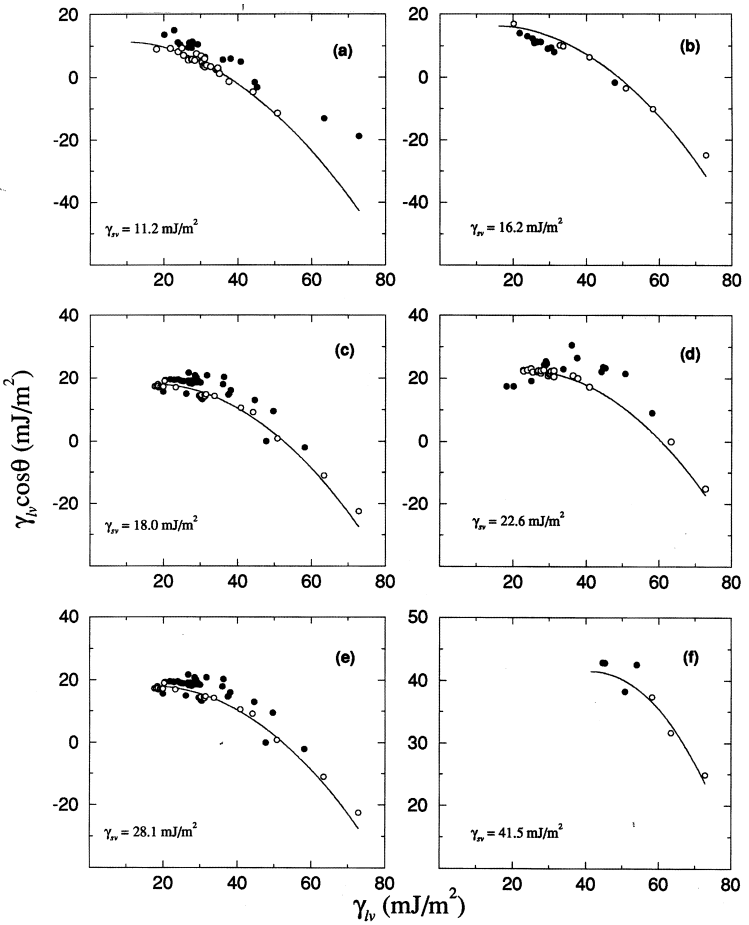

Fig. 24. $\gamma_{lv}\cos\theta$ vs. γ_{lv} for Zisman's data on (a) perfluorolauic acid [131], (b) 17-(perfluoropentyl)-heptadecanoic acid [133], (c) polytetrafluoroethylene [135], (d) *n*-octadecylamine [137], (e) polytrifluoroethylene [130], and (f) nylon (6,6) [139]. Contact angle data are discarded (solid symbols) using the program given in Appendix D. The curves are best-fits of Eq. (44) onto experimental data of γ_{lv} and θ.

had been reported for two different types of polystyrene-coated silicon wafer surfaces [92,141]; they were determined from recent low-rate dynamic contact angles. In view of the difference in polymer properties and molecular weights, a value of 28.9 mJ/m^2 for the polystyrene given in Table 10 is indeed plausible. Furthermore, $\gamma_{sv} = 35.6 \pm 0.4$ mJ/m^2 for polyethylene terephthalate reported elsewhere [64] is again in good agreement with the value of 35.2 mJ/m^2 in Table 10. These findings give confidence in our procedures in deducing solid surface tension values from goniometer contact angles, so that dynamic contact angle procedures by, e.g. ADSA-P do not need to be repeated for the solid surfaces studied by Zisman et al. Thus, contact angles can indeed be used for the

Table 11
Summary of the sequence in rejecting contact angles for the polyvinyl fluroide surface [130] using the program given in Appendix D

Sequence #	Data # (remaining)	Data # rejected	Fitted γ_{sv} (mJ/m^2)
1	1–11	–	36.3
2	2–11	1	36.5
3	3–11	2	36.6
4	4–11	3	36.7
5	5–11	4	36.7
6	5–8,10,11	9	36.2
7	5,6,8,10,11	7	36.1
8	5,6,8,11	10	35.7

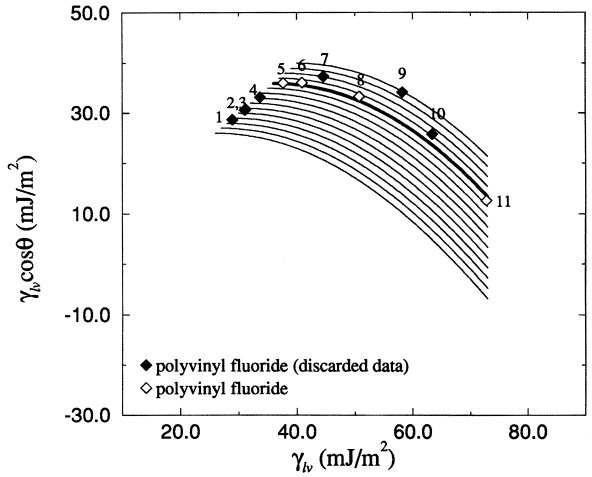

Fig. 25. $\gamma_{lv}\cos\theta$ vs. γ_{lv} for the polyvinyl fluoride [130] surface, reproduced from Fig. 23. The sequence of rejecting data is summarized in Table 11.

determination of solid surface tensions and literature contact angles do not have to be discarded completely.

5. Summary

This study illustrates clearly that obtaining meaningful contact angles for the determination of solid surface tensions depends heavily on how contact angles are measured and whether or not the widely made assumptions have been violated. Experimental procedures and criteria for measuring and interpreting meaningful contact angles have been developed. The discrepancy in the literature in terms of

the contact angle patterns have been explained. A large amount of meaningful contact angle data was also generated on various solid surfaces. Unique experimental curves of $\gamma_{lv}\cos\theta$ vs. γ_{lv} were obtained. The widely used surface tension component approaches [11,15–17] were shown to contradict these experimental contact angle patterns. The new contact angle data established here provide an experimental foundation for future development of the equation of state approach for solid surface tensions; a new formulation of such an approach which allows the determination of solid surface tensions has been developed. Literature static contact angles do not have to be discarded completely and can be used for determining solid surface tensions, with caution.

6. Perspective

A look at the likely future of research on contact angles and surface energetics will benefit from a view back, particularly at persistent obstacles to progress. There are three key attitudes which have hampered progress immensely:

1. Contact angles are simple quantities which can be readily measured and interpreted by anybody, requiring no particular skill, methodology, or knowledge.
2. Contact angle measurements show hysteresis. Hence, experimental contact angles are not equilibrium values, and therefore nothing useful can be learned from contact angle studies.
3. Contact angles contain readily accessible information about intermolecular forces.

All of these propositions are false. With respect to the first proposition, the present study shows how misleading conventional contact angle measurements on sessile drops can be.

The second proposition, while false, is the most difficult to refute. Operationally, the key question is not whether a contact angle is an equilibrium contact angle, but whether it can be used in conjunction with Young's equation. For instance, contact angle hysteresis caused by a modest degree of surface heterogeneity does not make Young's equation inapplicable. Furthermore, it is clear from the systems examined here that contact with a liquid will often affect the solid surface. This does not preclude the possibility that the advancing contact angle is the equilibrium angle; rather this equilibrium cannot be reached from 'the other side', i.e. under receding conditions, because the solid surface is now different. Furthermore, it is difficult to see how the smooth curves of, e.g. Figs. 2 and 7, and Figs. 13–16 could arise if the contact angle data do not contain surface energetic meaning.

Finally, the widely held view expressed in the third proposition is demonstrably false, from curves like those in Figs. 2 and 7, and Figs. 13–16. For a given solid, the contact angle depends only on the liquid surface tension, not directly on the intermolecular forces which give rise to these surface tensions. Referring to the curve for FC-721 in Fig. 2, the fact that methanol falls on the same smooth curve as hexane and decane would imply that the polar component of surface tension of

methanol is zero, i.e. methanol would have to be classified as non-polar, which is clearly absurd.

While the first and third propositions have been dealt with extensively in this study, the answer to the question of contact angle hysteresis in the second proposition would require further study.

7. Future development

The present state of knowledge is well summarized in the equation of state approach outlined above. The approach can be used to good advantage in numerous applications, including interfacial phenomena of powders [25,27]. Nevertheless, there remain many unsolved questions relating to the measurement and interpretation of contact angles.

1. While vapor adsorption does not appear to play a significant role in the contact angle data presented here, it is quite possible that it could enter the picture for more hydrophilic surfaces, particularly if $\gamma_{lv} \approx \gamma_{sv}$ or $\gamma_{lv} < \gamma_{sv}$, i.e. cases which were excluded in the present study. While adsorption may produce contact angle patterns different from those shown in Figs. 2 and 7, and Figs. 13–16, this would not necessarily imply that Young's equation is not applicable or that contact angle approaches might not be feasible. The answer to these questions would require general criteria to distinguish the effect of vapor adsorption on the contact angles from all other effects.
2. Recently, self-assembled monolayers (SAMs) have been widely used to produce surfaces of different chemical compositions and wettabilities. However, it is believed that penetration of liquid into the SAMs is inevitable. Given that two solids having the same solid surface tensions and that a specific liquid may penetrate into one solid but not the other, the contact angles on the two chemically identical surfaces can be different: one would be due to pure energetic effects, and the other to the effects of the changed energetics and liquid penetration. In the latter case, attempts [109] to interpret surface energetics from contact angle approaches naively, e.g. by means of the above equation of state approach, could be misleading (cf. Fig. 19).
3. It is well-known that roughness affects the experimentally observed contact angles. However, there are as yet no general criteria to quantify roughness and at what level of smoothness surface topography has no longer an effect on the contact angle. The answer to such questions will have to involve considerations of line tension [59] and the contortions of three-phase lines.
4. It is still an open question of whether or not β in Eq. (44) and β_1 in Eq. (50) are 'universal' constants, i.e. independent of the solid surface. Such a question can be addressed only after an even larger body of accurate contact angle data on various solids has been generated.
5. While the slip/stick contact angle patterns, e.g. that shown in Fig. 12 and

similar patterns cannot be used to determine surface energetics, they are still very interesting and worth investigating.

6. Routine production of systems which are free of contact angle hysteresis might be considered an important goal. It is firmly believed that all that would be produced is further confirmation of the contact angle story presented here. It is expected that more benefits can be obtained from the much simpler systematic study of receding contact angles of available systems, using concepts and procedures described in Section 2.3.

Acknowledgements

This research was supported by the Natural Science and Engineering Research Council of Canada (Grants: No. A8278 and No. EQP173469), Ontario Graduate Scholarships (D.Y.K.), and University of Toronto Open Fellowships (D.Y.K.).

Appendix A

This FORTRAN program may be used to calculate the solid–liquid γ_{sl} and solid–vapor γ_{sv} interfacial tensions by the equation of state Eq. (44) with $\beta = 0.0001247\ (m^2/mJ)^2$, using Newton's method. The required input data are the liquid surface tension γ_{lv}, and the contact angle θ.

```
      implicit real*8 (a-h,o-z)
10    write(6,*) "Input  gamma LV and the contact angle (deg)"
      read (5,*) glv,theta
      const = 3.141592654/180.0
      a = 0.5d0*(dcos(theta*const) + 1.0d0)
      b = 0.0001247d0*glv*glv
      y = a
20    x = y
      e = dexp(b*(1.0d0 - x*x)**2)
      u = x - a*e
      v = 1.0d0 + 4.0d0*a*b*x*(1.0d0 - x*x)*e
      y = x - u/v
      if (y.lt. 1.0d0) go to 30
      y = a*dexp(b)
      go to 20
30    if (dabs(y - x).lt. 0.00001d0) go to 40
      go to 20
40    gsv = x*x*glv
      gsl = gsv - glv*dcos(theta*const)
      cosin = dcos(theta*const)
      write (6,*) "gamma LY",glv," contact angle",theta
```

```
      write(6,*) "gamma SV",gsv," gamma SL",gsl
      write(6,*) " "
      write(6,*) "Do you want to calculate again (y = 1, n = 0)"
      read(5,*) num
      if (num.eq. 1) go to 10
50    stop
      end
```

Appendix B

This FORTRAN program may be used to calculate the solid–liquid γ_{sl} and solid–vapor γ_{sv} interfacial tensions by the equation of state Eq. (50) with $\beta_1 = 0.0001057\ (m^2/mJ)^2$, using Newton's method. The required input data are the liquid surface tension γ_{lv}, and the contact angle θ.

```
      implicit real*8 (a–h,o–z)
10    write(6,*) "Input gamma LV and the contact angle (deg)"
      read (5,*) glv,theta
      alpha = 0.0001057d00
      b = alpha*glv**2
      const = 3.141592654/180.0
      a = 0.5d00*(dcos(theta*const) + 1.0d0)
      x = 1.0d00
      x1 = x
30    call f(x1,a,g,b,outf)
      call fprime(g,x1,b,outfp)
      x2 = x1 – outf/outfp
      if (dabs(x2 – x1).lt. 0.00001d0 to 40
      x1 = x2
      go to 30
40    gsv = glv*x2*x2
      gsl = gsv – glv*dcos(theta*const)
      write (6,*) "gamma LV",glv," contact angle",theta
      write(6,*) "gamma SV",gsv," gamma SL",gsl
      write(6,*) "Do you want to calculate again (y = 1,n = 0)"
      read(5,*) num
      if (num .eq. 1) go to 10
50    stop
      end
      subroutine f(x1,a,g,b,outf)
      implicit real*8 (a–h,o–z)
      x = x1**2
      g = 1.0d0 – b*(1.0d0 – x)**2
      outf = x1*g – a
```

```
      return
      end
      subroutine fprime(g,x1,b,outfp)
      implicit real*8 (a–h,o–z)
      x = x1**2
      gprime = 4*x*b*(1.0d0 – x)
      outfp = g + gprime
      return
      end
```

Appendix C

This FORTRAN program may be used to calculate the solid–liquid γ_{sl} and solid–vapor γ_{sv} interfacial tensions, by the equation of state Eq. (55). The required input data are the liquid surface tension γ_{lv} and the contact angle θ.

```
      n = 2
1     write(6,*) "Input  gamma lv and contact angle (deg.)"
       read(5,*)glv,angle
       call eqsa(angle,glv,gsv,gsl)
       write(6,*)"gamma – 1v,theta,gamma – sv,gamma – sl"
       write(6,*)glv,angle,gsv,gsl
       write(6,*)" "
       write(6, *)"Do you want to try again, Y = 1"
       read(5,*)nn
       if (nn .eq. 1) goto 1
       stop
       end
       subroutine eqsa(angle,glv,gsv,gsl)
       real angle,glv,gsv,gsl
       thedg = angle
       gaml = glv
       thema = thedg
       if (gaml.lt.50) go to 980
       diff = 0.7*(((gaml/5.) – 9.)**2.) + 3
       delth = abs(90.– thedg)
       call larger(thema,gaml,gams,gamsl)
       go to 983
980   themar = thema*3.14159265/180
       if (thedg.gt.90.) go to 981
       thedg = 180 – thedg
981   therd = thedg*3.14159265/180
       b = 0.015
       cay = sdrt(2.0 + b*gaml*cos(therd))
```

```
      cophi = (sqrt(gaml*27.*b)*(1.0 + cos(therd))/(2.0*(cay**3.0)))
      ang = (sqrt(1.0 - cophi*cophi))/cophi
      phi = atan(ang)
      thibm = (phi + 3.14159265)/3.
      gam = 4.0*(cay*cos(thibm))**2./(3.0*B)
      if (thema.gt.90.) go to 982
      gamsl = gam
      gams = gamsl + gaml*cos(themar)
      go to 983
982   gams = gam
      gamsl = gams - gaml*cos(therd)
983   gsv = gams
      gsl = gamsl
      return
      end
C     ***********subroutine larger***********
      subroutine larger(theta,gaml,gamsv,gamsl)
      real x(150),y(150),sg(150)
      b = 0.015
      h = gaml/2
      i = 1
      x(i) = 90.0
      y(i) = 170.
984   thedg = (x(i) + y(i))/2.
      therd = thedg*3.14159265/180.
      cay = sqrt(2.0 + b*gaml*cos(therd))
      cophi = (sqrt(gaml*27.*b)*(1.0 + cos(therd))/(2.0*(cav**3.0)))
      ang = (sqrt(1.0 - cophi*cophi))/cophi
      phi = atan(ang)
      thibm = (phi + 3.14159265)/3.
      sg(i) = -2.0*gaml*sin(2.*thibm)*(1.-(((4./(b*gaml)) - 2.)/
     +  (1.+ cos(therd))))/(9.*ang) + (4.*gaml*cos(thibm)**2.)/3.
      z = abs(sg(i) - h)
      if (z.le.0.00001) go to 986
      if (i.gt.149) go to 986
      if (sg(i).lt.h) go to 985
      x(i + 1) = thedg
      y(i + 1) = y(i)
      i = i + 1
      go to 984
985   x(i + 1) = x(i)
      y(i + 1) = thedg
      i = i + 1
      go to 984
986   gam = 4.0*(cam*cos(thibm))**2./(3.*b)
```

```
      thddl = 180. − thedg
      thetr = theta*3.14159265/180.
      if (theta.lt.thddl) go to 987
      if (theta.gt.thedg) go to 988
      gamsv = gam + h*(cos(thetr) − cos(therd))
      go to 989
987   theda = 180. − theta
      thedr = theda*3.14159265/180.
      cay = sqrt(2.0 + b*gaml*cos(thedr))
      cophi = (sqrt(gaml*27.*b)*(1.0 + cos(thedr))/(2.0*(cay**3.0)))
      ang = (sqrt(1.0-cophi*cophi))/cophi
      phi = atan(ang)
      thibm = (phi + 3.14159265)/3.
      gamsv = ((2.0*cay*cos(thibm))**2.)/(3.0*b) + gaml*cos(thetr)
      go to 989
988   cay = sqrt(2.0 + b*gaml*cos(thetr))
      cophi = (sqrt(gaml*27.*b)*(1.0 + cos(thetr))/(2.0*(cay**3.0)))
      return
      end
```

Appendix D

The FORTRAN program attached may be used to calculate the solid–vapor interfacial tensions γ_{sv} by fitting goniometer contact angle data to theoretical γ_{sv} curves generated by the equation of state Eq. (44) using $\beta = 0.0001247\ (m^2/mJ)^2$. The required input data are the liquid surface tension γ_{lv} and liquid surface tension times cosine of the contact angle $\gamma_{lv}\cos\theta$. Outputs are contact angles which fall within $\pm 1.0\ mJ/m^2$ to a best-fitted theoretical γ_{sv} curve, the γ_{sv} values corresponding to each data point, and a best-fitted γ_{sv} value to all data.

The program reads experimental pairs of γ_{lv} and $\gamma_{lv}\cos\theta$ from a file and then determines the smallest and largest γ_{sv} values for all data from Eq. (44). For example, in the case of the polyvinyl fluoride surface, the smallest and largest values of γ_{sv} were found to be 28.7 mJ/m^2 (#1 in Fig. 25) and 39.9 mJ/m^2 (#9 in Fig. 25), respectively. They are needed for reasons of procedures to determine the best-fitted γ_{sv} value: it is assumed that the operative γ_{sv} will be somewhere in between these values. A first guess of the γ_{sv} value is obtained by fitting the entire set of experimental data to Eq. (44). This yields a best-fitted γ_{sv} value of 36.3 mJ/m^2, for the 11 data in Fig. 25. As an initial screening, $\pm 10.0\ mJ/m^2$ was selected as a criterion. Thus, data which deviate from $\gamma_{sv} = 36.3 \pm 10.0\ mJ/m^2$ will be discarded first. The criterion is then decreased in $\pm 0.1\ mJ/m^2$ increments, i.e. $\pm 9.9\ mJ/m^2$, $\pm 9.8\ mJ/m^2$, etc. For each increment, contact angle data will be checked and those which exceed the band will be eliminated and a new fitted γ_{sv} value will be obtained from the remaining data. This procedure is repeated until

the band decreases to ± 1.0 mJ/m^2. From the above example, as the band decreases, the first discarded data point is #1 in Fig. 25 and a new fitted γ_{sv} value of 36.5 mJ/m^2 was obtained based on the remaining 10 data. This γ_{sv} value was then used to eliminate contact angles by repeating similar procedures. The sequence of discarding data for the polyvinyl fluoride surface is summarized in Table 11. It turns out that only 4 data fall within ± 1.0 mJ/m^2 on a final best-fitted smooth γ_{sv} curve of 35.7 mJ/m^2. This value is considered as the γ_{sv} value for the polyvinyl fluoride surface.

```
      implicit real*8(a-h,o-z)
      dimension glv(100), ctheta(100), x(100), y(100), t(100)
      dimension diff(100), ndiff(100), sgs(100)
      character*80 name
1     write (6,*) "Input  data file name for gLV and gLV costheta"
      read (5,*) name
      write (6,*) "Input  number of data points, n = ?"
      read (5,*) n
      open (unit = 1, status = 'old', file = name)
      do 5i = 1,n
c     input gamma LV and gamma LV cos theta
      read (1,*)glv(i),t(i)
c     convert gamma LV cos theta to cos theta
      ctheta(i) = t(i)/glv(i)
      x(i) = glv(i)
      y(i) = dlog(dsqrt(x(i))*0.5d0*(1.0d0 + ctheta(i)))
5     continue
      close (unit = 1)
c     check for the lowest value of gSV from data
      sgs(1) = eqs(x(1),ctheta(1))
      gs1 = sgs(1)
      do 55 i = 2,n
      sgs(i) = eqs(x(i),ctheta(i))
      if (sgs(i) .lt. gs1) then
      gs1 = sgs(i)
      end if
55    continue
c     check for the largest value of gSV from data
      sgs(1) = eqs(x(1),ctheta(1))
      gs2 = sgs(1)
      do 51 i = 2,n
      sgs(i) = eqs(x(i),ctheta(i))
      if (gs2 .lt. sgs(i)) then
      gs2 = sgs(i)
      end if
51    continue
```

```
c     best fit based on data
      difmax = 10.0
3     call fitsv(x,y,n,ctheta,gs1,gs2,gsv)
c     eliminate bad data based on fitted gSV
      nd = 0
      do 10 i = 1, n
      diff(i) = dabs(eqs(x(i),ctheta(i)) − gsv)
      if (diff(i) .gt. difmax) then
      nd = nd + 1
      ndiff(nd) = i
      end if
10    continue
      if(difmax .le. 1.05d0) goto 33
      difmax = difmax − 0.1d0
      do 12j = 1,nd
      do 11i = ndiff(j), n
      x(i) = x(i + 1)
      y(i) = y(i + 1)
      ctheta(i) = ctheta(i + 1)
11    continue
      do 14 i = j + 1,nd
      ndiff(i) = ndiff(i) − 1
14    continue
12    continue
      n = n − nd
      goto 3
33    write(6,19)
      do 18 i = 1,n
      write(6,2D)x(i),x(i)*ctheta(i),eqs(x(i),ctheta(i))
18    continue
      write (6,21)gsv
19    format(' ',/,'FITTED RESULTS:',//,5x,'GLV',7x,'GLV COS THETA'+
      4x,'GSV')
20    format(' ',3x,f6.2,8x,f6.2,7x,f6.2)
21    format(' ',/,'THE FITTED GSV = ',3x,f6.2)
      stop
      end
      subroutine fitsv(x,y,n,ctheta,gs1,gs2,gsv)
      implicit real*8 (a−h,o−z)
      dimension ctheta(100), x(100), y(100)
      dimension gs(500), R(500)
c     x = gamma LV
c     b is defined as the beta
      b = 0.0001247d0
10    j = 1
```

```
      gs(j) = gs1
15    do 30 i = 1, n
      p1 = y(i) − dlog(gs(j))* 0.5d0 + b*(x(i) − gs(j))** 2
      p2 = −0.5d0/gs(j) − 2.0d0* b*(x(i) − gs(j))** 2
      p3 = p1* p2
30    p4 = p4 + p3
      R(j) = p4
      if(dabs(R(j)) .lt. 0.000001) go to 100
      p4 = 0.00
      if(j .ne. 1.0) go to 40
      gsa = gs(j)
      Ra = R(j)
      j = j + 1
      gs(j) = gs2
      go to 15
40    if(j .ne. 2.0) go to 50
      gsb = gs(j)
      Rb = R(j)
      if(Ra* Rb .lt. 0.0) go to 45
      go to 10
45    j = j + 1
      gs(j) = 0.5*(gsa + gsb)
      go to 15
50    if(R(j)* Ra .lt. 0.0) go to 60
      gsa = gs(j)
      Ra = R(j)
      j = j + 1
      gs(j) = 0.5*(gsa + gsb)
      go to 15
60    gsb = gs(j)
      Rb = R(j)
      j = j + 1
      gs(j) = 0.5*(gsa + gsb)
      go to 15
100   gsv = gs(j)
      return
      end
      function eqs(glv,ctheta)
      implicit real* 8 (a−h,o−z)
10    a = 0.5d0*(ctheta + 1.0d0)
      b = 0.0001247d0* glv* glv
      y = a
20    x = y
      e = dexp(b*(1.0d0 − x* x)** 2)
      u = x − a* e
```

```
      v = 1.0d0 + 4.0d0*a*b*x*(1.0d0 - x*x)*e
      y = x - u/v
      if (y .lt. 1.0d0) go to 30
      y = a*dexp(b)
      go to 20
30    if (dabs(y - x) .lt. 0.00001d0) go to 40
      go to 20
40    gsv = x*x*glv
      eqs = gsv
      return
      end
```

References

[1] B.V. Derjaguin, V.M. Muller, Y.P. Toporov, J. Colloid Interface Sci. 73 (1980) 293.
[2] K.L. Johnson, K. Kendall, A.D. Roberts, Proc. R. Soc. (London) A324 (1971) 301.
[3] V.M. Muller, V.S. Yushchenko, B.V. Derjaguin, J. Colloid Interface Sci. 92 (1983) 92.
[4] A. Fogden, L.R. White, J. Colloid Interface Sci. 138 (1990) 414.
[5] R.M. Pashley, P.M. McGuiggan, R.G. Horn, B.W. Ninham, J. Colloid Interface Sci. 126 (1988) 569.
[6] H.K. Christenson, J. Phys. Chem. 90 (1986) 4.
[7] P.M. Claesson, C.E. Blom, P.C. Horn, B.W. Ninham, J. Colloid Interface Sci. 114 (1986) 234.
[8] P.M. Pashley, P.M. McGuiggan, R.M. Pashley, Colloids Surf. 27 (1987) 277.
[9] R.M. Pashley, P.M. McGuiggan, B.W. Ninham, D.F. Evans, Science 229 (1985) 1088.
[10] W.A. Zisman, Contact angle, wettability and adhesion, in: Advances in Chemistry Series, vol. 43, American Chemical Society, Washington, DC, 1964.
[11] F.M. Fowkes, Ind. Eng. Chem. 12 (1964) 40.
[12] O. Driedger, A.W. Neumann, P.J. Sell, Kolloid-Z. Z. Polym. 201 (1965) 52.
[13] A.W. Neumann, R.J. Good, C.J. Hope, M. Sejpal, J. Colloid Interface Sci. 49 (1974) 291.
[14] J.K. Spelt, D. Li, The equation of state approach to interfacial tensions, in: A.W Neumann, J.K. Spelt (Eds.), Applied Surface Thermodynamics, Marcel Dekker Inc., New York, 1996, pp. 239–292.
[15] D.K. Owens, R.C. Wendt, J. Appl. Polym. Sci. 13 (1969) 1741.
[16] C.J. van Oss, M.K. Chaudhury, R.J. Good, Chem. Revs. 88 (1988) 927.
[17] R.J. Good, C.J. van Oss, The modern theory of contact angles and the hydrogen bond components of surface energies, in: M. Schrader, G. Loeb (Eds.), Modern Approaches to Wettability: Theory and Applications, Plenum Press, New York, 1992, pp. 1–27.
[18] H.G. Bruil, Colloid Polym. Sci. 252 (1974) 32.
[19] G.D. Cheever, J. Coat. Technol. 55 (1983) 53.
[20] H.W. Kilau, Colloids Surf. 26 (1983) 217.
[21] K. Grundke, T. Bogumil, T. Gietzelt, H.-J. Jacobasch, D.Y. Kwok, A.W. Neumann, Prog. Colloid Polym. Sci. 101 (1996) 58.
[22] E.I. Vargha-Butler, T.K. Zubovits, D.R. Absolom, A.W. Neumann, Dispers. Sci. Technol. 6 (1985) 357.
[23] E.I. Vargha-Butler, E. Moy, A.W. Neumann, Colloids Surf. 24 (1987) 315.
[24] E.I. Vargha-Butler, T.K. Zubovits, D.R. Absolom, A.W. Neumann, Chem. Eng. Commun. 33 (1985) 255.
[25] D. Li, A.W. Neumann, Wettability and surface tension of particles, in: A.W. Neumann, J.K. Spelt (Eds.), Applied Surface Thermodynamics, Marcel Dekker Inc., New York, 1996, pp. 509–556.
[26] S.N. Omenyi, A.W. Neumann, J. Appl. Phys. 47 (1976) 3956.

[27] D. Li, A.W. Neumann, Behavior of particles at solidification fronts, in: A.W. Neumann, J.K. Spelt (Eds.), Applied Surface Thermodynamics, Marcel Dekker Inc., New York, 1996, pp. 557–628.
[28] A.E. Corte, J. Geophys. Res. 67 (1962) 1085.
[29] P. Hoekstra, R.D. Miller, J. Colloid Interface Sci. 25 (1967) 166.
[30] J. Cissé, G.F. Bolling, J. Crystal Growth 10 (1971) 67.
[31] J. Cissé, G.F. Bolling, J. Crystal Growth 11 (1971) 25.
[32] A.M. Zubko, V.G. Lobonov, V.V. Nikonova, Sov. Phys. Crystallogr. 18 (1973) 239.
[33] K.H. Chen, W.R. Wilcox, J. Crystal Growth 40 (1977) 214.
[34] D.W. Fuerstenau, M.C. Williams, Colloids Surf. 22 (1987) 87.
[35] D.W. Fuerstenau, M.C. Williams, Part. Characterization 4 (1987) 7.
[36] D.W. Fuerstenau, M.C. Williams, Int. J. Mineral Process 20 (1987) 153.
[37] D.W. Fuerstenau, M.C. Williams, K.S. Narayanan, J.L. Diao, R.H. Urbina, Energy Fuels 2 (1988) 237.
[38] D.W. Fuerstenau, J. Diao, J. Hanson, Energy Fuels 4 (1990) 34.
[39] S.J. Hemingway, J.R. Henderson, J.R. Rowlinson, Faraday Symp. Chem. Soc. 16 (1981) 33.
[40] R. Guermeur, F. Biquard, C. Jacolin, J. Chem. Phys. 82 (1985) 2040.
[41] B.S. Carey, L.E. Scriven, H.T. Davis, AIChE J. 26 (1980) 705.
[42] E. Moy, A.W. Neumann, Theoretical approaches for estimating solid–liquid interfacial tensions, in: A.W. Neumann, J.K. Spelt (Eds.), Applied Surface Thermodynamics, Marcel Dekker Inc., New York, 1996, pp. 333–378.
[43] H.C. Hamaker, Physica 4 (1937) 1058.
[44] J.N. Israelachvili, Proc. R. Soc. London. A. 331 (1972) 39.
[45] A.E. van Giessen, D.J. Bukman, B. Widom, J. Colloid Interface Sci. 192 (1997) 257.
[46] T.M. Reed, J. Phys. Chem. 55 (1955) 425.
[47] B.E.F. Fender, G.D. Halsey, Jr., J. Chem. Phys. 36 (1962) 1881.
[48] D.E. Sullivan, J. Chem. Phys. 74 (1981) 2604.
[49] D.V. Matyushov, R. Schmid, J. Chem. Phys. 104 (1996) 8627.
[50] T. Young, Philos. Trans. R. Soc. London 95 (1805) 65.
[51] A.W. Neumann, Adv. Colloid Interface Sci. 4 (1974) 105.
[52] D. Li, A.W. Neumann, Thermodynamic status of contact angles, in: A.W. Neumann, J.K. Spelt (Eds.), Applied Surface Thermodynamics, Marcel Dekker Inc., New York, 1996, pp. 109–168.
[53] A. Marmur, Colloids Surf., A 116 (1996) 25.
[54] R.V. Sedev, J.G. Petrov, A.W. Neumann, J. Colloid Interface Sci. 180 (1996) 36.
[55] R.N. Wenzel, Ind. Eng. Chem. 28 (1936) 988.
[56] A.B.D. Cassie, Discuss. Faraday Soc. 3 (1948) 11.
[57] S. Baxer, A.B.D. Cassie, J. Text. Inst. 36T (1945) 67.
[58] A.B.D. Cassie, S. Baxter, Trans. Faraday Soc. 40 (1944) 546.
[59] J. Gaydos, A.W. Neumann, Line tension in multiphase equilibrium systems, in: A.W. Neumann, J.K. Spelt (Eds.), Applied Surface Thermodynamics, Marcel Dekker Inc., New York, 1996, pp. 169–238.
[60] C.J. van Oss, L. Ju, M.K. Chaudhury, R.J. Good, J. Colloid Interface Sci. 128 (1989) 313.
[61] C.J. van Oss, R.J. Good, J. Macromol. Sci-Chem. A26 (1989) 1183.
[62] A.W. Neumann, R.J. Good, Experimental methods, in: R.J. Good, R.R. Stomberg (Eds.), Surface and Colloid Surface, vol. 11, Plenum Press, New York, 1979, pp. 31–91.
[63] J.K. Spelt, E.I. Vargha-Butler, Contact angle and liquid surface tension measurements: general procedures and techniques, in: A.W. Neumann, J.K. Spelt (Eds.), Applied Surface Thermodynamics, Marcel Dekker Inc., New York, 1996, pp. 379–411.
[64] D. Li, A.W. Neumann, J. Colloid Interface Sci. 148 (1992) 190.
[65] D. Li, M. Xie, A.W. Neumann, Colloid Polym. Sci. 271 (1993) 573.
[66] Y. Rotenberg, L. Boruvka, A.W. Neumann, J. Colloid Interface Sci. 93 (1983) 169.
[67] P. Cheng, D. Li, L. Boruvka, Y. Rotenberg, A.W. Neumann, Colloids Surf. 43 (1990) 151.
[68] P. Cheng, Ph.D. Thesis, University of Toronto, 1990.
[69] S. Lahooti, O.I. del Rio, P. Cheng, A.W. Neumann, Axisymmetric drop shape analysis, in: A.W.

Neumann, J.K. Spelt (Eds.), Applied Surface Thermodynamics, Marcel Dekker Inc., New York, 1996, pp. 441–507.
[70] D.Y. Kwok, D. Li, A.W. Neumann, Colloids Surf., A 89 (1994) 181.
[71] C.A. Ward, A.W. Neumann, J. Colloid Interface Sci. 49 (1974) 286.
[72] R. Defay, Etude Thermodynamique de la Tension Superficielle, Gauthier Villars, Paris, 1934.
[73] R. Defay, I. Prigogine, Surface tension and adsorption, A. Bellemans (collab.), D.H. Everett (trans.), Longmans, Green and Co., London, 1954, p. 222.
[74] D. Li, J. Gaydos, A.W. Neumann, Langmuir 5 (1989) 293.
[75] D. Li, A.W. Neumann, Adv. Colloids Interface Sci. 49 (1994) 147.
[76] D.Y. Kwok, T. Gietzelt, K. Grundke, H.-J. Jacobasch, A.W. Neumann, Langmuir 13 (1997) 2880.
[77] D.H. Kaelble, J. Adhesion 2 (1970) 66.
[78] S. Wu, in: L.-H. Lee (Ed.), Adhesion and Adsorption of Polymers, Plenum, New York, 1980, pp. 53–65.
[79] C.J. van Oss, R.J. Good, M.K. Chaudhury, Langmuir 4 (1988) 884.
[80] D.Y. Kwok, R. Lin, M. Mui, A.W. Neumann, Colloids Surf., A 116 (1996) 63.
[81] J.F. Oliver, C. Huh, S.G. Mason, J. Colloid Interface Sci. 93 (1983) 169.
[82] J.F. Oliver, C. Huh, S.G. Mason, Colloids Surf. 1 (1980) 79.
[83] D. Duncan, D. Li, J. Gaydos, A.W. Neumann, J. Colloid Interface Sci. 169 (1995) 256.
[84] A. Amirfazli, D.Y. Kwok, J. Gaydos, A.W. Neumann, J. Colloid Interface Sci. 205 (1998) 1.
[85] D.Y. Kwok, D. Li, A.W. Neumann, Capillary rise at a vertical plate as a contact angle technique, in: A.W. Neumann, J.K. Spelt (Eds.), Applied Surface Thermodynamics, Marcel Dekker Inc., New York, 1996, pp. 413–440.
[86] D.Y. Kwok, C.J. Budziak, A.W. Neumann, J. Colloid Interface Sci. 173 (1995) 143.
[87] K. Grundke, P. Weidenhammer, P. Werner, R. Trinowitz, A. Janke, D.Y. Kwok, K. Pöschel, H.-J. Jacobasch, A.W. Neumann, in preparation.
[88] D.Y. Kwok, C.N.C. Lam, A. Li, A. Leung, A.W. Neumann, Langmuir 14 (1998) 2221.
[89] O.I. del Rio, D.Y. Kwok, R. Wu, J.M. Alvarez, A.W. Neumann, Contact angle measurements by axisymmetric drop shape analysis and an automated polynomial fit program, Colloid Surf. A (1998) in press.
[90] D.Y. Kwok, C.N.C. Lam, A. Li, A. Leung, R. Wu, E. Mok, A.W. Neumann, Measuring and interpreting contact angles: a complex issue, Colloids Surf. A (1998) in press.
[91] D.Y. Kwok, A. Leung, A. Li, C.N.C. Lam, R. Wu, A.W. Neumann, Colloid Polym. Sci. 276 (1998) 459.
[92] D.Y. Kwok, C.N.C. Lam, A. Li, K. Zhu, R. Wu, A.W. Neumann, Polym. Eng. Sci. 38 (1998) 1675.
[93] D.Y. Kwok, A. Li, C.N.C. Lain, R. Wu, S. Zschoche, K. Pöschel, T. Gietzelt, K. Grundke, H.-J. Jacobasch, A.W. Neumann, Low-rate dynamic contact angles on poly(styrene-*alt*-(hexyl/10-carboxydecyl(90/10)maleimide)) and the determination of solid surface tensions. (In press)
[94] D.Y. Kwok, C.N.C. Lam, A. Li, A.W. Neumann, J. Adhes. 68 (1998) 229.
[95] D.Y. Kwok, A. Leung, C.N.C. Lam, A. Li, R. Wu, A.W. Neumann, J. Colloid Interface Sci. 206 (1998) 44.
[96] C.J. Budziak, A.W. Neumann, Colloids Surf. 43 (1990) 279.
[97] G.H.E. Hellwig, A.W. Neumann, 5th International Congress on Surface Activity, Section B, (1968) 687.
[98] G.H.E. Hellwig, A.W. Neumann, Kolloid-Z. Z. Polym. 40 (1969) 229.
[99] H.B. Callen, Thermodynamics and an Introduction to Thermostatistics, 2nd ed., John Wiley and Sons, 1985.
[100] G. Antonow, J. Chim. Phys. 5 (1907) 372.
[101] D. Berthelot, Compt. Rend. 126 (1898) 1857.
[102] R.J. Good, in: K.L. Mittal (Ed.), Adsorption at interfaces, ACS Symposium Series, No. 8, American Chemical Society, D.C., 1975.
[103] D. Li, C. Ng, A.W. Neumann, J. Adhes. Sci. Technol. 6 (1992) 601.
[104] C.D. Bain, E.B. Troughton, Y. Tao, J. Eval, G.M. Whitesides, R.G. Nuzzo, J. Am. Chem. Soc. 111 (1989) 321.
[105] C.D. Bain, G.M. Whitesides, Angew. Chem. Int. Ed. Engl. 28 (1989) 506.

[106] P.E. Laibinis, G.M. Whitesides, J. Am. Chem. Soc. 113 (1991) 7152.
[107] P.E. Laibinis, Ph.D. Thesis, Harvard University, 1991.
[108] H.W. Fox, W.A. Zisman, J. Colloid Sci. 7 (1952) 428.
[109] J. Drelich, J.D. Miller, J. Colloid Interface Sci. 167 (1994) 217.
[110] G.S. Ferguson, G.M. Whitesides, Thermal reconstruction of the functionalized interface of polyethylene carboxylic acid and its derivatives, in: M. Schrader, G. Loeb (Eds.), Modern Approaches to Wettability: Theory and Applications, Plenum Press, New York, 1992, pp. 143–177.
[111] D.Y. Kwok, D. Li, A.W. Neumann, Langmuir 10 (1994) 1323.
[112] W. Wu, R.F. Giese, Jr., C.J. van Oss, Langmuir 11 (1995) 379.
[113] F. London, Z. Phys. Chem. (B) 11 (1930) 222.
[114] G.C. Maitland, M. Rigby, E.B. Smith, W.A. Wakeham, Intermolecular Forces: Their Origin and Determination, Clarendon Press, Oxford, 1981.
[115] A. Dupré, Théorie mécanique de la chaleur, Gauthier-Villars, Paris, 1969.
[116] L.A. Girifalco, R.J. Good, J. Phys. Chem. 61 (1957) 904.
[117] R.J. Good, E. Elbing, Ind. Eng. Chem. 62 (1970) 72.
[118] K.C. Chao, R.L. Robinson, Jr., Equation of State: Theories and Applications, ACS, Washington, D.C., 1986.
[119] J.S. Rowlinson, F.L. Swinton, Liquids and Liquid Mixtures, Butterworth Scientific, London, 1981.
[120] J. Kestin, E.A. Mason, AIP Conf. Proc. 11 (1973) 137.
[121] D. Li, A.W. Neumann, J. Colloid Interface Sci. 137 (1990) 304.
[122] E.W. Swokowski, E.W. Calculus with Analytic Geometry, 2nd ed., Prindle, Weber and Schmidt, Boston, 1979.
[123] C. Lipson, N.J. Sheth, Statistical Design and Analysis of Engineering Experiments, McGraw-Hill Publishing Co., New York, 1973.
[124] J.A. Mann, Jr., in: E. Matijjevic, R.J. Good (Eds.), Surface and Colloid Science, vol. 13, Plenum Press, New York, 1984, p. 213.
[125] D.Y. Kwok, A.W. Neumann, Contact angle interpretation in terms of surface energetics, Colloids Surf. A, submitted for publication.
[126] D.Y. Kwok, Ph.D. Thesis, University of Toronto, 1998.
[127] A.W. Neumann, D.R. Absolom, D.W. Francis, C.J. van Oss, Sep. Purification Methods 9 (1980) 69.
[128] D.Y. Kwok, A.W. Neumann, Re-evaluation of existing contact angle data in terms of surface energetics, Colloids Surf. A, submitted for publication.
[129] H.W. Fox, W.A. Zisman, J. Phys. Chem. 7 (1952) 109.
[130] A.H. Ellison, W.A. Zisman, J. Phys. Chem. 58 (1954) 260.
[131] E.F. Hare, E.G. Shafrin, W.A. Zisman, J. Phys. Chem. 58 (1954) 236.
[132] M.K. Bernett, W.A. Zisman, J. Phys. Chem. 66 (1962) 1207.
[133] E.G. Shafrin, W.A. Zisman, J. Phys. Chem. 66 (1962) 740.
[134] F. Schulman, W.A. Zisman, J. Colloid Sci. 7 (1952) 465.
[135] H.W. Fox, W.A. Zisman, J. Colloid Sci. 5 (1950) 514.
[136] E.G. Shafrin, W.A. Zisman, J. Phys. Chem. 61 (1957) 1046.
[137] E.G. Shafrin, W.A. Zisman, J. Colloid Sci. 7 (1952) 166.
[138] A.H. Ellison, H.W. Fox, W.A. Zisman, J. Phys. Chem. 57 (1953) 622.
[139] A.H. Ellison, W.A. Zisman, J. Phys. Chem. 58 (1954) 503.
[140] H.F. Hare, W.A. Zisman, J. Phys. Chem. 59 (1955) 335.
[141] A. Augsburg, K. Grundke, K. Pöschel, H.-J. Jacobasch, A.W. Neumann, Determination of contact angles and solid surface tensions of poly(4-x-styrene) films, Acta Polymerica, (1998) in press.